Emergence of Cardiac Function and Cell Types During Early Embryogenesis

António M. A. Miranda

Trinity Collge

University of Oxford

A thesis submitted for the degree of

Doctor of Philosophy in Cardiovascular Sciences

August 2017

Acknowledgements

First, I would like to thank Professor David Greaves, the rest of the committee for the DPhil program in Cardiovascular sciences, and the British Heart Foundation for giving me the opportunity to pursue this DPhil and for funding my endeavours.

I would also like to thank Professor Shankar Srinivas for the opportunity to pursue this project and for the supervision provided over the past years. I would also like to thank all the lab members of the Srinivas group, past and present, for all the help provided in one way or another. I would like to give a special thank you to Dr. Richard Tyser, whose support has been invaluable.

Lastly, I would like to thank my mother and sisters for all the encouragement, for believing in me and for being supporting me all these years.

Abstract

The heart is the first organ to form and function during embryonic development. Over the past few years, research on cardiac development has focused on uncovering the genetic mechanism controlling cardiac differentiation and clarifying the embryonic origin of the different cardiac lineages. The study of the physiological mechanisms behind cardiac function has proven instrumental for our understanding of heart disease and the interplay between different cardiac cells. However, there is not an extensive body of literature on the role of physiology on early embryonic development, especially on cardiac development. In this thesis, I present my work on the early stages of heart development, focusing on the events occurring from the formation of the cardiac crescent to the linear heart tube stage.

This thesis is divided in 3 result chapters. In the first result chapter (chapter 3), I present the methods I developed to perform live imaging of mouse embryos, including calcium imaging, and to extract quantitative information.. On the second result chapter (chapter 4), I described the work I performed investigating the physiological mechanisms of early heart development, their role in cardiac differentiation, and a detailed single-cell RNA sequencing analysis of early heart development. On the last result chapter (chapter 5), I explore preliminary data on a potential contribution of endodermal cells to the formation of the heart.

The work presented here has led to the discovery of Spontaneous Asynchronous Calcium Oscillations (SACOs) in the early cardiac mesoderm and a key role for NCX1 in regulating these oscillations and cardiac differentiation. Single-cell RNA sequencing analysis suggests a potential role for *Naca* and *Fbxo32* in regulating early cardiac function. I have also identified potential new markers for both the First

and Second Heart Field. Lastly, I found evidence that the endoderm may be contributing to the Second Heart Field, although the function of these cells is still unclear.

General Index

Figures and Tables Index

Chapter 4 – Characterization of the First Embryonic Cardiac Contractions

Chapter 5 – Examining Endodermal Contribution to Cardiac Development

List of Non-Standard Abbreviations

AVE – Anterior Visceral Endoderm

BPM – Beats per Minute

BSA – Bovine Serum Albumin

CC – Cardiac Crescent

CICR – Ca^{2+} induced Ca^{2+} release

CM – Cardiac Mesoderm

DE – Definitive Endoderm

DIC – Differential Interference Contrast

DVE – Distal Visceral Endoderm

Ec – Endocardium

ECC – Excitation Contraction Coupling

ECM – Extracellular Matrix

EMT – Epithelial to Mesenchymal Transition

EPDCs – Epicardium-derived mesenchymal Cells

ExE – Extraembryonic Endoderm

FEP – Fluorinated Ethylene Propylene

FHF – First Heart Field

HF – Head Folds

KD – Knock Down

KO – Knock-out

LHT – Linear Heart Tube

LPM – Lateral Plate Mesoderm

LSM – Laser Scanning Microscope

LTCC – L-Type Calcium Channels

Myo – Myocardium

NA – Numerical Aperture

OC – Outflow Cap

OE – Overexpression

OFT – Outflow Tract

OPM – Oscillations per Minute

PBS – Phosphate Buffered Saline

PBT – Phosphate Buffered Saline with Triton X-100

PE – Parietal Endoderm

PhE – Pharyngeal Endoderm

PhM – Pharyngeal Mesoderm

PS – Primitive Streak

RNAseq – RNA sequencing

RT-qPCR – Reverse Transcriptase quantitative PCR

SACOs – Spontaneous Asynchronous Ca^{2+} Oscillations

scRNAseq – Single-cell RNA sequencing

SDC – Spinning Disk Confocal

SHF – Second Heart Field

SR – Sarcoplasmic Reticulum

VE- Visceral Endoderm

YS – Yolk Sac

Chapter 1 - General Introduction

1

Table of Contents

Throughout this thesis I will be describing experiments performed to better understand the ontology of heart development. The majority of experiments have been performed with mouse embryos. During this chapter, I will give a brief introduction to mouse as model, early mouse embryonic development and provide a description of heart development, introducing topics relevant for all the subsequent chapters. In all of the results chapters (chapter 3 to 6), I will expand on the topics discussed here, detailing studies which are more relevant to the topics of each chapter.

1.1 – Mouse as a Model Organism

The laboratory mouse, *Mus musculus*, is the most widely used model for mammalian development. The reason why mouse represents an attractive model is because it is easy to handle and has fast development for a mammal, with a gestation period of 18-21 days. After birth, it takes only 3 weeks to wean and 2 to 3 more weeks for males to reach sexual maturity. Furthermore, females usually have a large litter, between 5-16 pups, providing a good number of embryos for experimentation. Another advantage to the mouse model, is it remarkable genetic similarity with humans. The mouse genome is only 14% smaller than the human genome, with 99% of mouse genes having homologues in human and overall genomic similarity of 75% (reviewed in (*1*)). Not only is the percentage of homologue genes very high, but a large proportion of the mouse genome is syntenic with the human genome, with a large proportion of genes in the same relative positions (*2*). There are also a large number of natural occurring mutants and wild-type lines that have been derived from lines bred by mouse fanciers centuries ago (*3*). Besides naturally occurring mutants, radiation and chemicals can be used to randomly induce mutations, and have been particularly

useful in genetic screens (*4, 5*). Mouse genetics has benefitted from well-established tools to produce transgenic animals, be it by random introduction of transgenes in the genome, or by targeted transgenics (*3*). With the advent of CRISPR-CAS9, it has now become easier to make transgenic animals, include compound mutants (*6, 7*). Considering all strategies, there are over 4000 live mouse lines registered in the International Mouse Strain Resource database (http://www.findmice.org/index), with this number increasing many fold by also taking in account the frozen down embryos, ovaries and sperm.

1.2 – Early Mouse Embryonic Development

Mouse embryonic development has been extensively studied, and in general the overall steps are well documented. In placental mammals, pre-implantation development occurs from the moment of fertilisation to the moment the embryo attaches to the endometrium of the mother. Shortly after fertilization, the embryo enters the cleavage, characterised by a series of cell divisions without cell growth. The embryo then undergoes compaction, triggering the signalling events required for the first differentiation event. Between the 16 and 32-cell stage (E2.5-E3.5), the cells establish an outer layer, originating the trophectoderm (TE), and an inner cluster of cells, the inner cell mass (ICM). The trophectoderm forms the placenta and accessory tissues, while ICM cells undergo cell rearrangement to form the pluripotent Epiblast and the Primitive Endoderm (PE). During implantation, around E4.5-E4.75 in mouse, cells of the polar TE, epiblast and of the PE rearrange to form a cylindrically shaped embryo, also known as the egg cylinder (*8*). This cylindrical shape is exclusive to

rodents. Every other amniote, whose embryo development has been studied, develop as a disc.

At the time of implantation, the PE forms the Parietal Endoderm and the Visceral Endoderm (VE, called hypoblast in other amniotes), tissues surrounding the egg cylinder. By E5.5, the VE in the distal part of the embryo (DVE) is morphologically, behaviourally and molecularly different from the rest of the tissue (*9*). Between E5.75 and E6.0, the DVE moves to the prospective anterior, stop moving proximally at border with the Extraembryonic Ectoderm (ExE), where they start moving laterally (*10*). During this process, DVE cells become known as Anterior Visceral Endoderm (AVE). AVE migration is a key step during embryonic development, establishing the rostro-caudal axis of the embryo. This is accomplished through expression of Nodal and Wnt inhibitors, restricting the signals required for the formation of the primitive streak (PS) to the posterior region of the embryo (*11*).

During AVE migration, epiblast cells remain in a pluripotent state. Roughly at the same time that AVE cells move to the anterior side of the embryo, there is also extensive movement of epiblast cells converging to the posterior side of the embryo. At around E6.25, and over a period of 36 hours, the primitive streak forms and begins extends towards the distal tip of the embryo. This lays ground for gastrulation to occur (*12*). During this process epiblast cells lose their pluripotent state and form the 3 primitive germ layers, the ectoderm, the mesoderm, and the definitive endoderm (DE). During gastrulation, cells expressing FGFR1 upregulate SNA1 and undergo epithelial-mesenchymal transition (EMT) are then able to ingress through the primitive streak (*13*). Depending on the time, and location of ingression through the primitive streak, these cells form different tissues. For example, the cardiac mesoderm emerges from the anterior and intermediate primitive streak, while cells that form the node and the

definitive endoderm lineage emerge at the extreme anterior tip of the primitive streak (reviewed in (*12*))

1.3 – Overview of Heart Development

The heart is the first organ to form and function during embryonic development with well-established phases (fig. 1.1). As mesodermal precursors of the cardiac mesoderm come out of the PS, they migrate to the anterior side of the embryos. The bilateral pool or cardiac progenitors then fuses to form the cardiac crescent (CC), the first morphologically distinct cardiac structure, around E7.5. Both sides of the cardiac crescent keep growing as the embryo folds, bringing both sides in contact, fusing to form the linear heart tube (LHT), around E8.0. Up to this point, the heart is bilaterally symmetric, composed mainly of tissue that is going to form the left ventricle, with the prospective right ventricle on rostrally and the prospective atrial tissue caudally. As the LHT keep maturing, the heart twists in order to position the right ventricle and outflow tract (OFT) next to the left ventricle and the atrial precursor tissues rostrally to the ventricles. This process takes around 2 days to complete, until E10.5. From this stage onwards, the chambers start septating, separating the two ventricles and the two atria, forming the 4-chambered heart typical of mammals and birds. The separation of the chambers is mostly complete by the time of birth, with the exception of a hole between the atria, the Foramen Ovale, which closes after birth (*14, 15*). During this time, cells from the cardiac neural crest migrate into the OFT, forming the aorta and the pulmonary trunk (*16*). The most common congenital heart defects occur due errors during the septation of the atria, ventricles and OFT.

	Cardiac Crescent	Linear Heart Tube	Looping Heart	Chamber Formation
Human (40 wks)	Day 19	Day 22	Day 28	Day 32
Mouse (3 wks)	Day 7.5	Day 8.0	Day 9.0	Day 10.0
Chicken (3 wks)	Day 1.0	Day 1.5	Day 2.0	Day 2.5
Milestones	▪ Cardiac Differentiation ▪ Migration to the Midline	▪ First Heartbeat ▪ Anterior-posterior and dorsal-ventral patterning	▪ Early Chamber Formation ▪ Atria Move Above Ventricles	▪ Trabeculation ▪ Cushion Formation ▪ Septation ▪ Early conduction system

Fig. 1.1 – Phases of 4-chambered heart development – In mammals and birds the heart undergoes 4 main morphological changes. It first forms a cardiac crescent, which keeps maturing as the embryo folds until it fuses in the midline to form the linear heart tube. The heart then loops in what to constitutes the first break of left-right symmetry. The heart then starts the septation events, until the 4-chambers are formed. Afterwards, the heart keeps maturing and growing, including after birth (adapted from (*17*)).

The heart is composed of 3 main tissues, the endocardium, the myocardium and the epicardium. As the heart undergoes the morphogenetic events described above, these cardiac tissues undergo several cellular events important for this process. Both myocardial and endocardial cells form roughly around the same time, being present at the cardiac crescent stage, while the epicardium starts developing a later stage, during cardiac looping (*18, 19*).

The myocardium is arguably the most important tissue of the heart. Differences in muscle structure and function in different regions of the heart are crucial for the normal function of this organ. As the heart is developing, the muscle tissue also undergoes a remarkable morphological change. Starting around E8.5, signals from the endocardium activate the deposit of extracellular matrix (ECM) proteins in the myocardium. This ECM deposition creates budding of myocardial tissue in the forming ventricles, leading to the formation of cardiac trabeculae. The trabeculae are thought to be necessary to prevent suction between the walls of the ventricles during cardiac contraction. Trabeculation of the ventricles is well visible by E12.5, however, as the heart continues developing, ECM proteins maintaining the trabeculae are degraded, leading to the collapse of these structures. The collapse of the trabeculae leads to a thickening of the ventricular walls (*20, 21*). The myocardium has also been described as undergoing several functional changes, more precisely changes in proteins of the contractile machinery such as myosin subunits. These functional changes not only happen during embryonic development, but also during the neonatal to adult transition (*22*).

As mentioned above, the endocardium develops side by side with the myocardium. While in the adult heart, the endocardium may not play as much of an important role as the myocardium, this tissue is critical for the proper development of

the heart. It is debated whether endocardial and myocardial progenitors are already determined at the time of gastrulation or if they originate from a common progenitor, which later separates into the two lineages. Evidence from chick and zebrafish embryos suggest the first scenario, while mouse and embryonic stem cell (ESC) models support the latter (fig. 1.2). The endocardium is a hotspot for EMT events that are essential for proper heart morphogenesis. During mouse development, between E9.0 and E9.5, the cardiac jelly (ECM rich cardiac layer) expands, initiating the first step in the formation of the endocardial cushions. EMT of endocardial cells is then required in order to populate these cushions (*18, 23*). As heart development progresses, cells in the endocardial cushions undergo EMT once more to form the atrioventricular (AV) valves as well as the valves of the great vessels. Furthermore, endocardial cushions are also important for septation events. The AV cushions fuse in order to form the AV canals, while cells from the OFT cushions undergo EMT to promote OFT septation in conjunction with cardiac neural crest cells. Lastly, it also has been suggested that endocardial cells can form some coronary endothelial cells (*24, 25*).

The last of the 3 main cardiac tissues is the Epicardium. During embryonic development, this tissue appears to start developing slightly later than the myocardium and endocardium, and while it has been suggested that this tissue may share a common origin with the other cardiac tissues, this relationship is not well understood. Unlike the tissues described above, epicardium development does not involve intricate morphogenetic movements. Nevertheless, this tissue is also critical for proper heart development. The epicardium is an epithelial tissue derived from the proepicardial organ, a vesicular outgrowth closely related to the coelomic mesothelium. During murine development, the proepicardium seems to be visible for the first time between

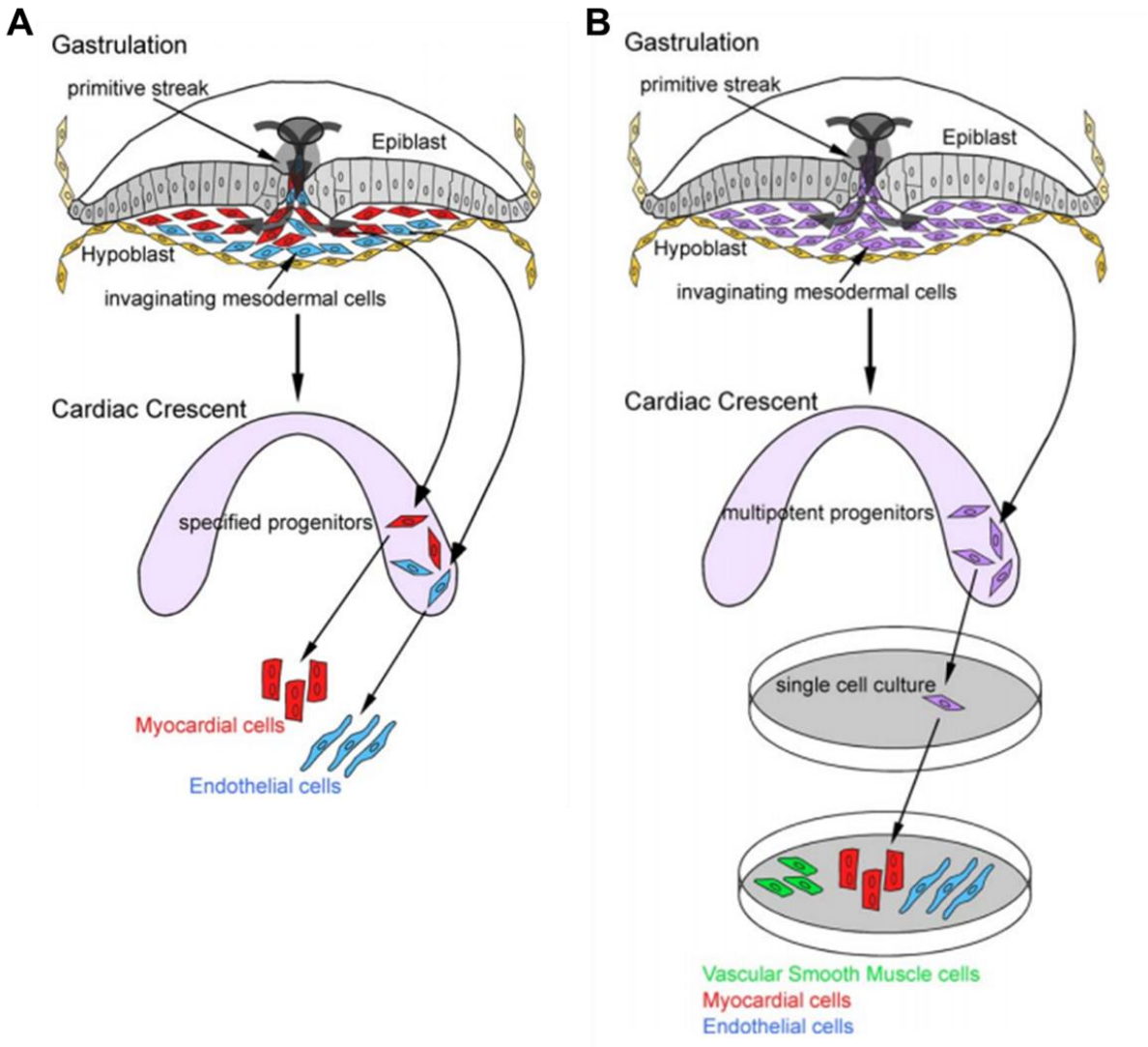

Fig. 1.2 – Two models for the specification of myocardial and endothelial progenitors – Experimental evidence from chick and zebrafish embryos suggest that myocardial and endothelial progenitors are already defined at gastrulation (A). On the other hand, experimental evidence from mouse and embryonic stem cells suggest that mesodermal cells at gastrulation are multipotent progenitors which later differentiate in the progenitors of different cardiac tissues (B). Adapted from (*26*)

E9.5 and E10.0, close to the *sinus venosus*(*27*). Cells from the proepicardium migrate away from this tissue. Depending on the animal model, these cells either attach directly to the cardiac tube or (agnathans) be released as free-floating cells (gnathostomes). Regardless of the mechanisms, these cells eventually cover the whole myocardium (*27*). In the case of the mouse, the free-floating cells eventually aggregate and flatten, with the cells clusters eventually fusing to form a continuous sheet. The cells attach to the myocardium through villous projections during a cardiac contraction (*28*). Epicardial cells also undergo EMT, forming epicardium-derived mesenchymal cells, also known as EPDCs. These cells leave the epicardial epithelium, integrating into the myocardium and differentiating into a wide array of cells. While some controversy exists regarding which cells types EPDCs can form, due to the use of Cre-lines which may not be specific to the epicardium alone and be expressed in other cardiac cells, it has been suggested that these cells can form vascular smooth muscle, fibroblast and endothelial cells such as coronary endothelial cells (*24*).

While heart development is very conserved across species, there are some differences. Unlike the chicken, where there seems to be clearly defined phases of early heart development, in the mouse tube and chamber formation seem to overlap to some extent (*29*). In chick the proepicardium forms only on the right side, as the one in the left undergoes apoptosis (*30*). Unlike mice, the cells of the proepicardium are transferred to the myocardium through bridge between the sinus venosus and the dorsal wall of the ventricle (*28*). Avian ventricles have a network of Purkinje fibres in the atria and associated with the coronary arteries, which is not present in mammalian hearts. Furthermore, avian cardiomyocytes seem to be shorter, which is associated with a slower propagation of the action potential [reviewed in (*31*)].

Throughout the rest of this thesis I will focus on the development of the myocardium. In the next sections I will describe in more detail the molecular and cellular mechanisms involved in the development of this tissue. While I will not go into the detail about the mechanisms of endocardium and epicardium development, it should be noted that the development of these 3 tissues are interdependent on each other, and signalling from both the endocardium and epicardium is necessary for the proper maturation of the myocardium.

1.4 – Molecular Control of Early Cardiac Development

The morphological events mentioned above are tightly controlled at the level of gene expression. The interest in understanding and replicating the molecular pathways involved in cardiac differentiation has led to the discovery of the main signalling cascades, especially which transcription factors are activated during the main steps of this process. When referring to the embryological origins of the gross anatomical structures, two main cellular lineages have been described. These are the first and second heart field. The first heart field has been found to form most of the left ventricle, while the second heart field has been described as originating most of the remaining structures of the heart, However, it should be noted that cells from the first heart field also contributes to the formation of the atria and right ventricle. These two heart fields are established early during heart development, at the cardiac crescent stages (fig. 1.3), differing in terms of position within the embryo, as well as in terms of molecular signature (*32*).

It is widely accepted that all cardiac lineages are derived from the mesodermal germ layer. As mentioned above, cardiac precursor cells are already established

defined at the moment of gastrulation. At this moment, mesoderm cells express *brachyury* (T), a T-box transcription factor and one of the earliest mesoderm markers (*33*). Interestingly, in triploblastic animals (with 3 germ layers), the T protein seems to have a domain which represses endoderm induction, but that does not seem to be the case in all animals (*34*). As mesoderm differentiation progresses, another transcription factor, *eomesodermin* (Eomes) is expressed, leading to the activation of Mesp1 (*35*). Up until Mesp1 expression is established, mesoderm cells are not committed to any particular lineage, however Mesp1+ cells are likely to form cells of the cardiovascular system (*36*), representing the earliest known marker for cardiac differentiation. Furthermore, depending on the timing of Mesp1 expression, these cardiac cells will form different lineages. Cells that first express Mesp1 form the FHF, while the second wave of Mesp1 expressing cells forms the SHF. It should be noted that cardiac progenitor cells only express *Mesp1* while they are migrating towards the anterior region of the embryo, prior to the formation of the cardiac crescent (*37*). It is important to note that Mesp2 works together with *Mesp1* for the migration of the cardiac progenitors to the anterior of the embryo. *Mesp1/2* double knock-out (KO) in mice leads to acardia (failure to form a heart), however this is not necessarily due to inhibition of mesoderm differentiation but to an inability of mesoderm cells to leave the primitive streak (*38*).

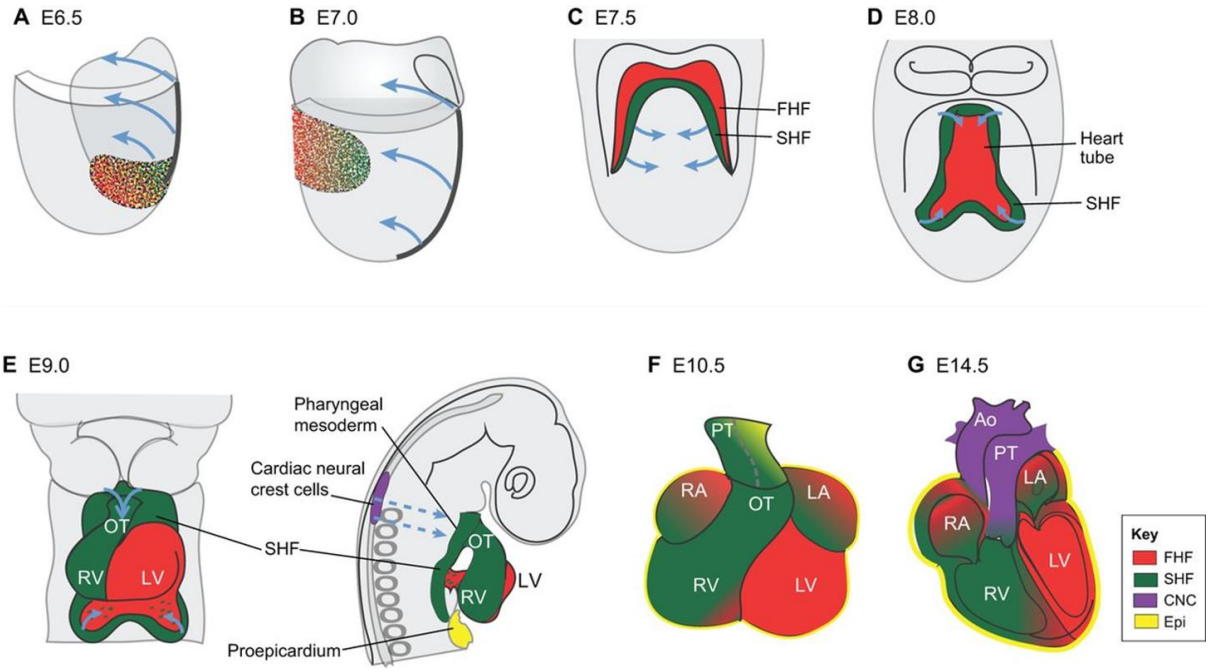

Fig. 1.3 – Schematic of different cardiac lineages – The heart is derived from 4 main tissues: the First Heart Field (FHF, red); the Second Heart Field (SHF, green); the cardiac neural crest (CNC, purple); the proepicardium (Epi, yellow). Taken from (*32*).

As cardiac progenitor cells reach the anterior of the embryo and form the cardiac crescent, cardiac differentiation proceeded through the activation of other transcription factors. One of such transcription factors is *Nkx2.5*. This transcription factor is expressed both in FHF and SHF and has been described as one of the main transcription factors involved in cardiac development. It ought to be noted that both the cardiac-specific and full *Nkx2.5* KO does lead to severe cardiac defects, already visible at the LHT stage, but does not lead to acardia (reviewed in (*39*)).

Another group of transcription factors involved in the specification of the cardiac differentiation program are the GATA transcription factors, especially *Gata4*, *Gata5* and *Gata6*. These 3 GATA transcription factors seem to have overlapping roles during early cardiac development. While the importance of these transcription factors for cardiogenesis has been appreciated for over a decade, only recently the precise molecular pathways have started to be uncovered. Of particular interest, Gata4 has been shown to be required for the inhibition of the canonical Wnt pathway, which is necessary for cardiac differentiation to occur. Similarly to *Nkx2.5*, KO of GATA transcription factors only lead to acardia when gastrulation itself is impaired, otherwise the most serious cardiac defect is *cardia bifida* (*40*).

The transcription factor SRF interacts with both *Nkx2.5* and *Gata4* (*41*), and has been shown to be required for the assembly and maintenance of contractile proteins (*42*). The initiation of the first heartbeats is going to be further explored in Chapter 4. While SRF has been shown to be essential for heart function (*43*), *Srf*-null mice also die due to gastrulation defects (*44*). In fact, the only mutants that lead to acardia are involved either in mesoderm migration, such as the *Mesp1/2* KO mentioned above, or in early mesoderm specification. To the best of my knowledge, once the cardiac crescent is formed, there is no KO that completely stops this process.

Some of the most severe defects relating to cardiac development arise when signalling from the early definitive endoderm is impaired, leading to defects such as cardia bifida. The role of endoderm in heart development will be further discussed in chapter 5.

At the LHT stage, the heart is composed mainly of FHF cells, however as mentioned above, the fully developed heart seems to be composed mainly of SHF cells. It is perhaps not surprising the SHF has been more extensively studied than the FHF. It is debatable how much of a boundary is there between these two heart fields, and whether or not the two heart fields are simply part of a single continuum, with the fate between the two fields being a biproduct of temporal regulation of gene expression. Nevertheless, the SHF is usually considered as a separate pool of cardiac progenitors. The SHF is also derived from MESP1+ cells and between E8.0 – E8.5, makes up a large proportion of the cardiac region (*37*). Localised more dorsally than the FHF, the SHF spans the area between the inflow tract and the subpharyngeal mesoderm (*45*). The marker mostly associated with the expression of Isl-1. While Isl-1 has been the marker most widely used to study the SHF, it should be noted that experiments showed that this gene is actually expressed in all cardiac progenitor cells, including the ones that form the FHF (*32*). By E8.0-E8.5, *Isl-1* expression is downregulated in the FHF, and it is only maintained in the SHF, while *Nkx2.5* remains expressed in both heart fields. This observation is in favour of the hypothesis that it is temporal regulation of gene expression that defines the two heart fields, and not intrinsic differences in gene expression. Many genes have been shown to be important for the development of the SHF, ranging from growth factors such as FGF8 and FGF10 (*46-48*), to transcription factors like TBX1, which regulates the non-canonical planar cell polarity (PCP) Wnt pathway by regulating the expression of Wnt5a, which in turn regulates core PCP components such as VANGL2 (*49*), also important for SHF

development. However, to the best of my knowledge, there are no markers that are exclusive to the SHF and broadly expressed at E8.5 as *Isl-1*. Some genes seem to be expressed in specific domains of the SHF. For example, TBX5 is expressed in the posterior SHF (*50*) and TBX18 is expressed in the lateral region of the posterior SHF (*51*). So far, the only marker that has been described to demarcate these two fields has been HCN4 (*52*), an ion channel typical of pacemaker cells. However, in the chick embryo, it has been described that HCN4+ cells originate outside the cardiac fields (*53*), which could indicate that these cells may not belong to the traditional FHF. Therefore, it is necessary to have a better characterisation of the different cardiac lineages

1.5 – Single-cell RNA sequencing of early embryonic development

Over the past few years, the improvement of sequencing technologies has greatly aided the study of signalling pathways involved in embryonic development. Analysis of whole transcriptomes, or RNA sequencing (RNAseq), under different conditions has been particularly useful. The number of studies where RNAseq has been widely used to identify new candidate genes, required for serval developmental processes, but also to investigate developmental processes on a larger scale. An advantage of RNAseq is that it can be used to not only analyse the most common coding mRNAs in a cell, but also splicing variants and non-coding RNAs. RNAseq has also been widely used in the context of heart development and cardiac differentiation. For example, RNAseq has been used for the identification of long non-coding RNAs (lncRNAs) in the mid-gestation mouse heart (E14.5), and to uncover the differential

expression of these lncRNAs during the foetal-to-adult heart transition (*54*). RNAseq has also been used to study the overall changes in alternative splicing in foetal and adult human hearts (*55*), as well as in Scleraxis KO mutant mouse embryos during cardiac valve development (*56*). While RNAseq has been instrumental in our understanding of developmental biology, it lacks spatial resolution. Some methods have been developed to overcome this limitation such as performing RNAseq on cryosections (*57*), the emergence of single-cell RNAseq (scRNAseq) has been one the greatest advancements in this field.

For scRNAseq, tissues are first dissociated into individual cells, or small clusters of cells, so that they can be sequenced separately. This approach is particularly useful to investigate transcriptional heterogeneity in tissues. In the context of embryonic development, scRNAseq has been especially used to investigate pre-implantation development, including the comparison between murine and human pre-implantation development (*58*). This has led to the discovery that during X-inactivation in humans, unlike mouse, Xist expression is biallelic (*59*). Post-implantation development has also been studied using scRNAseq. Sequencing of E5.5 to E6.5 embryos showed an intermediate population between the mesoderm and definitive endoderm (DE) with markers from both this tissues supporting the idea of a bipotent mesendoderm population that can form both these germ layers (*60*). This study also showed that modulation of Wnt signalling, required for DE formation, is achieved by a close interplay between the mesoderm and the endoderm. The mesoderm has a paracrine function, expressing WNT ligands, while the DE expresses WNT receptors as well as WNT antagonist to fine-tune this signalling pathway (*60*). Cardiac differentiation and heart development have also been studied using scRNAseq. These studies have been performed using both embryonic stem (ES) cells as well as

embryonic and adult murine hearts. For example, scRNAseq of Mesp1+ ES cells at different stages of differentiation has shown this population of cells is very heterogeneous, being constituted by at least 6 subpopulations of cells. Of these 6 subpopulations of cells, 3 represent more uncommitted states, one represents the cardiac lineage, another the hematopoietic lineage and the last a population that the authors hypothesise could either form cardiac or haematopoietic cells, suggesting some plasticity between these two lineages (*36*). In the context of embryonic heart development, scRNAseq has been performed on E8.5, E9.5 and E10.5 for the identification of the Identification of genes differently expressed in different chambers such as *Cav1*, *Nr2f1*, *Tigd2*, *Adm*, *Mpped2*, *Pcsk6*, *Inafm2*, *Hs6st2*, and *Tnc*, as well as new genes involved in cardiac trabeculation related genes such Sorl1, Slit2, Fstl4 and novel endocardium genes *Klhl4* and *Gpr116* (*61*). Another study using scRNAseq of E9.5, E14.5 and post-natal day 0 (P0), P7 and P21 murine hearts, by analysing the expression of cell-cycle related genes has shown that at E9.5 and E14.5, 60% of cardiomyocytes are proliferating, with this number dropping to 20% in the first week of post-natal period, and to 0% by P21 (*62*). Lastly, scRNAseq of embryonic hearts has also shown that in *Nkx2.5* +/- embryos, while not having any overt cardiac defects, cardiomyocytes show a delay in their transcriptomic profile, demonstrating the power of scRNAseq approached in detecting small changes in tissue development (*62*).

1.6 – Thesis Hypothesis and Rationale

This thesis focuses on two main hypotheses: 1) the heart starts to beat earlier than reported and the physiological regulation of this process is an integral part cardiac development; 2) the endoderm can contribute to the heart.

The first hypothesis relates to the development of the FHF. As FHF cells are the first functional cells of the heart, and the best marker for this region is HCN4, a ion channel, a better understanding on which processes are involved in regulating the first heartbeats could provide insights in the development of this heart field.

The second hypothesis is based on the strong interaction between the endoderm and mesoderm during heart development. More precisely, the striking similarity that exists between the markers of the SHF and endodermal markers, raised the hypothesis that endoderm cells could possess some plasticity and be able to form SHF cells.

Chapter 2 – Materials and Methods

2

Table of Contents

2.1 – Animal samples and embryo collection

All mouse experiments were performed according to UK Home Office project license PPL 30/2887 compliant with the UK animals (Scientific Procedures) Act 1986 and approved by the local Biological Services Ethical Review Process. All mice were maintained in a 12-hour light-dark cycle. Noon of the day finding a vaginal plug was designated E0.5. In order to dissect the embryos, pregnant females were killed by rising CO2 concentration and death was confirmed by cervical dislocation, in accordance with the schedule one of the Animal Scientific Procedures Act. The following mouse lines were used: C57Bl/6 (in-house strain); CD1 (Charles River Laboratories); Hhex-GFP (*63*); Ttr-Cre (*64*); ROSA26-EYFP (*65*). Crosses and respective outcomes can be found in table 2.1. Fertilised chicken eggs were purchased from Winter Egg Farm (Herts, UK). Fertilised Japanese quail eggs were purchased from Paslow Common Farm (Essex). Both chicken and quail eggs were kept at room temperature until incubated. Incubation was performed on humidified incubator at 37^{o}C for 44-48 hours according to Hamburgers and Hamilton staging. For all experiments, embryos were dissected in M2 medium (Sigma-Aldrich M7167).

2.2 – Embryo Staging

For all species, different cardiac crescent stages were defined based on the relative dimensions of the cardiac crescent, more precisely the ratio between the length (medio-lateral axis) and the maximum height (rostral-caudal axis). LHT stage was defined as the moment stage where both bulges of the cardiac crescent were

clearly folded and fused.

2.3 – Live imaging

Live imaging of embryos, including Ca^{2+} imaging was performed as described in chapter 3. For mouse embryos, freshly dissected embryos were cultured and imaged in a 1:1 mix of phenol red-free CMRL (PAN-Biotech P04-84600) and Knockout Serum Replacement (Thermo-Fisher 10828010) supplemented with 10 mM L/glutamine (Sigma-Aldrich G7513). To mount the embryos, first two or more parallel lines of vacuum grease, with 2 layers each, are laid down in the coverslip of the MatTek glass bottom dish (MatTek Corporation P35G-1.0-20-C), ideally spaced between each other in order to only fit a single embryo, although this is not critical. The number of parallel lines will depend on the number of embryos one intends to image. Two parallel lines can easily fit at least 5 mouse embryos at E8.0. It is not advisable to use more than 3 parallel lines as otherwise the vacuum grease will limit the volume of media that can be added in the next steps. The next step is to surround the coverslip with 2 layers of vacuum grease in order to be able to add more media to the centre of the dish and eliminate the need to fill the whole bottom of the dish with media. Without these layers of vacuum grease, it is possible to keep a drop of 200 µl of media in the centre of the MatTek by surface tension, but with these 2 layers it is possible to keep a drop of 800 µl. This step is more important for experiments that involve adding pharmacological inhibitors to the media, because it makes it possible to use smaller volumes of the compound. The media should only be added to the dish a few minutes prior to the mounting of the embryos, as the longer the vacuum grease is in contact with media the more difficult it becomes to shape.

Initial characterisation of cardiac contractions was performed using Differential Interference Contrast (DIC) imaging on a Zeiss Spinning Disk Confocal microscope at 37ºC and an atmosphere of 5% CO_2 + Air. Acquisition was performed at 10 frames per second (fps) for up to 20 seconds.

For Ca^{2+} imaging experiments, embryos were loaded with 8 µM of Cal-520 (Abcam ab171868) by incubating the embryos in 1:1 mix of CMRL and Knockout Serum Replacement supplemented with 10 mM L/glutamine with the dye for 15 min in an incubator at 37ºC and a 5% CO_2 + Air atmosphere. The embryos were then transferred to fresh media in a MatTek dish without the dye and imaged. Embryos were imaged on a Zeiss 710 or 880 LSM confocal miscroscope, with a 20× air objective (0.6 NA) with a single optical section every 97 ms (~10 frames per second). Images were captured at 256 × 256 pixel dimensions, with a 2× line step and no averaging to increase the scan speed. For acute inhibition of Ca^{2+} transients (stage 1 to LHT), Ca^{2+} transients were first imaged at baseline, followed by addition of drug-containing media and imaging was performed at 5, 15 and 30 minutes post drug treatment. For inhibitor experiments involving stage 0 embryos, imaging was not performed at the 30-minute time-point due to adverse effects on the embryos. Nifedipine (Sigma-Aldrich N7634) was used at a final concentration of 10 µM, CB-DMB (Sigma-Aldrich C5374) at 20 µM, KB-R7943 (Sigma-Aldrich K4144) at 30 µM , Ryanodine (Tocris 1329) at 100 µM and 2-APB (Tocris 1224) at 200 µM, all diluted in DMSO (Sigma-Aldrich D8418). We found that most drugs had to be used at a higher concentration than previously used in studies involving isolated cells, presumably due to penetration difficulties inherent with using whole embryos. Control experiments for Nifedipine, CB-DMB and KB-R7943 were performed with 0.002% DMSO, and for experiments involving dual inhibition with Ryanodine + 2-APB with 0.6% DMSO.

To image the pharyngeal endoderm, I explanted the pharyngeal region by cutting the embryo directly below and above the outflow tract. I then removed most of the heart, except for around 200 μM of outflow tract close to the pharyngeal endoderm. For live imaging, these explants were imaged at a 512x512 pixel dimension, in the Zeiss LSM 880 confocal microscope with a 40x water immersion objective (1.2 NA) at 10 minutes intervals, with a Z-step of 1.5 μm.

2.4 – Rolling Embryo Culture

Both long-term pharmacological inhibition and DiI labelling, embryos were cultured in a custom table top precision rolling culture system (B.T.C. Engineering, Cambridge) for 12 hours on glass bottles. Embryos were cultured in a mix of 50% CMRL and 50% Knockout Serum Replacement at 37^{o}C and with an atmosphere of 5% CO_2+ Air. For pharmacological inhibition, only embryos at E7.5, prior to cardiac crescent and head fold formation were cultured. For these experiments embryos were cultured in the presence of either in 10 μM Nifedipine, 3 μM CB-DMB or 0.0003% DMSO.

2.5 – DiI Labelling

DiI labelling of embryos was performed using Vybrant DiI Cell-Labelling Solution (Thermo Fisher Scientific V22885). In preparation for DiI labelling, dissected embryos were put in a dish with small semi-circles made of vacuum grease to hold the embryos. For labelling, embryos were held with the cardiac crescent facing down. DiI

was loaded in a heat pulled glass capillary, and released underneath the embryo on small puff. Due to differences in density, the DiI solution floats up before dispersing in the media, labelling the surface of the embryo. The embryos were then washed 3x in clean culture media prior to either live-imaging or rolling culture.

2.6 – Immunostainings

Dissected embryos were fixed for 1 hour at room temperature with 4% PFA in PBS (Alfa Aesar J61899). The embryos were then washed 3x in PBT-0.1% (PBS with 0.1% Triton X-100 (Sigma-Aldrich X100)) for 15 min, permeabilised in PBT-0.25% for 40 min and washed again 3x in PBT-0.1%. The embryos were transferred to blocking solution (5% donkey serum, 1%BSA in PBT-0.1%) overnight (o/n) at 4^{o}C. Primary antibodies (Table 2.2) were then added to the solution and incubated o/n at 4^{o}C. The embryos were washed 3x in PBT-0.1% and incubated o/n 4^{o}C in PBT-0.1% with the secondary antibodies (Table 2.2), then subsequently washed 3x PBT-0.1% for 15 min and mounted in Vectashield mounting media with DAPI (Maravai LifeSciences H-1200) for at least 24 hours at 4^{o}C. Samples were imaged in either a Zeiss 710 or 880 LSM confocal microscope. E8.0 – E8.5 mouse samples were typically imaged with either a 40x oil (1.36 NA) or water (1.2 NA) objective, at a 512 × 512 pixel dimension and tiled 2x2 with a Z-step of 1.5 µm. E12.5 mouse hearts were imaged with either a 10x (0.45 NA) or 20x (0.8 NA) air objective, at a 256 × 256 pixel dimension and tiled 4x4 with a Z-step of 10-12 µm. Chick embryos were image with either 20x air (0.8 NA) or 40x water (1.2 NA) objective, at a 512 × 512 pixel dimension with a Z-step of 10 µm and 1.5 µm respectively. Imaging was performed on a Zeiss 710 and Zeiss 880 microscope. Super-resolution imaging was performed with the Airy Scan on the Zeiss

880 microscope.

For control purposes, at all stages used, all secondary antibodies were tested without primary antibody and all immunostainings were performed with at least two different secondary antibodies.

2.7 – RNA-extraction and qPCR

RNA extraction of whole embryos, embryonic hearts and head folds was performed using an RNeasy Micro Kit (Qiagen 74004) according to manufacturer's instructions: briefly, homogenisation was carried out with a 21G needle and the extract run through an on-column DNase I treatment. In order to collect enough RNA for isolated cardiac crescents and head folds, each sample was composed of 10 individual cardiac crescents or head folds. RNA pellets were dissolved in RNase-free water and the RNA quality and quantity determined by Nanodrop readings at 260, 280 and 230 nm wavelengths. cDNA was generated from 1 µg of RNA using random primers and SuperScript III polymerase (ThermoFisher 18080093). The expression of mRNAs for genes of interest, together with endogenous controls (HPRT, GAPDH (*66*)) was measured in triplicate for each sample by quantitative real-time PCR using SYBR Green (Applied Biosystems 4309155). Each reaction contained: 8 ng cDNA, 0.5 µl of each primer, 6.5 µl water and 12.5 µl 2 x SYBR Green, made up with H2O to a final volume of 22 µl. Primers (Sigma-aldrich, Table 2.3) were either designed using Primer-BLAST (National Center for Biotechnology Information, National Institutes of Health), Primer3 or obtained from PrimerBank. Primers were designed to span exon-intron boundaries, have annealing temperatures around 60 ^{o}C and generate amplicons

between 50 bp - 200 bp. The reaction mixture and samples were loaded into either a MicroAmp Optical 96-Well Reaction Plates (ThermoFisher N8010560) or MicroAmp Fast Optical 96-Well Reaction Plates (ThermoFisher 4346907) and sealed with Optical Adhesive Films (ThermoFisher 4311971). Quantification was performed on a ViiA 7 Detection System (ThermoFisher 4453536) using a PCR programme of 95^{o}C 15 mins followed by 40 cycles of (95^{o}C 15 s melting phase and 60 ^{o}C 1 min annealing and extension). Amplification of a single amplicon was confirmed by obtaining dissociation curve (melt curve) profiles as well as using gel electrophoresis to separate the reaction product. Cycle threshold (Ct) values were generated using Viia7 software. Relative gene expression levels were obtained using the ΔΔCt method, in which expression of each gene of interest was normalised to endogenous controls, and presented as fold change over a reference sample. For time course data fold-change was calculated in relation to the earliest stages, whilst for drug treated experiments fold change was calculated relative to control (DMSO) samples. Non-template controls were performed by replacing cDNA with water to test for non-specific amplification.

2.8 – Statistics

All data involving beat rate and qPCR gene levels was compared using one-way ANOVA followed by a Tukey test for multiple comparisons. In cases where the raw data failed to map to a normal distribution with consistent variance, we applied Taylor's law to choose the best transformation for the data. All data to be analysed passed the Shapiro-Wilk normality test and Bartlett test for homogeneous variances. To compare the number of affected embryos upon acute treatments, a Freeman-

Halton extension of Fisher exact probability test was applied due to a small number of samples.

2.9 – Image Analysis

A variant of absolute image filter was used to visualize and plot measurements of cardiac contractions in the developing cardiac crescent is described in chapter 3. Briefly, pixel displacement, indicative of contractions, was visualized and represented by increased grey levels within the crescent. Change in pixel intensity was assessed in a selected region, to reveal the contraction dynamics. Background Ca^{2+} signal was subtracted from all frames of a given time-lapse using ImageJ. To obtain the profiles for Ca^{2+} transients, regions of interest were plotted using the ratio between observed fluorescent and minimum fluorescent (F/F0) after background subtraction.

2.10 – Cell Collection for Single-cell RNA sequencing

In order to perform single-cell RNA sequencing (scRNAseq) of the developing heart, samples from mouse embryos were collected at E8.0, E8.5 and E12.5. At the cardiac crescent stage (stage 0 to stage 3), after diving the embryos by stage, each embryo was cut through the midline in order to separate the right and left side. The cardiac crescent and overlaying endoderm were then isolated from each half and transferred to a 1.5 ml Eppendorf tube. For embryos at other stages, the whole heart was collected without dividing into left and right sides, Tissue from embryos of the same stage and same side were pooled in the same Eppendorf, each tube containing 2 to 6 samples.

Following the dissection, 500 µl of Accutase Cell Dissociating Reagent (ThermoFisher A1110501) at 37ºC was added to the Eppendorf tubes containing the samples. The sample were then kept at 37ºC and the tubes flicked every 2 minutes, until the tissue is no longer visible. At this point, 500 µl of Fetal Bovine Serum (FBS, ThermoFisher 10500064) was added to the dissociating solution in order to inhibit the reaction. The samples were then centrifuged at 1000 rpm for 1.5 min at 4ºC, followed by removal of the supernatant and resuspension of the cells in 1 ml of a solution consisting of 50% FBS + 50% HBSS. The samples were then kept in ice until collection.

Cell collection was performed on a SH800S Cell Sorter (Sony Biotechnology) using 100 µm microfluidics sorting chips. Prior to collection, each sample was stained with a dead cell marker. For WT samples, cells were stained with a Live/Dead Viability Assay (ThermoFisher L3224) diluted in HBSS 10 min prior to collections, according to manufacturer's instructions. For samples with a transgenic fluorescent reporter, DAPI (ThermoFisher D1306) diluted in HBSS was used to stain dead cells. Cells were also sorted in order to increase the likelihood of collecting individual cells. Cells were collected in 384-wells plates provided by the Wellcome Sanger Institute (WSI) containing lysis buffer and RNA spikes, according to the SmartSeq protocol (*67*). The plates were kept at -80ºC before being sent to the WSI for cDNA amplification and sequencing in a Illumina 10x Genomics sequencing machine.

2.11 – Single-cell RNA sequencing data analysis

Sequencing data was processed using the Cell Ranger 1.1.0 software to align, filter and count unique molecular identifiers (UMIs) per sample. Data was mapped to

the mouse reference genome GRCm38.p4 and the transcriptome annotation from the Ensembl database, version 84 (http://mar2016.archive.ensembl.org/index.html). Data from all samples were consolidated into a single data set using the cellranger aggr program. Cells that expressed <1,000 genes or that had >3% of their transcripts mapped to mitochondrial genes were removed from the dataset. We further removed any cells that expressed both Xist and any of Kdm5d, Eif2s3y, Gm29650, Uty or Ddx3y (genes in the Y chromosome), as these are probably doublets.

The data was normalized for cell-specific biases using a method previously proposed by the Marioni group (*68*) and implemented in the Bioconductor package scran (*69*). To calculate size factors, genes with a mean expression <0.1 were filtered out. The quickCluster function was used to obtain the initial clustering of the cells (method igraph). The estimated size factors were used to normalize all genes expressed in at least one cell. Normalized counts are provided with the ArrayExpress submission.

For downstream analyses, we filtered out all genes with a mean expression <0.01. The distance-to-median method previously proposed (*70*) was implemented, and those with the 20% highest distance-to-median values were called highly variable. All genes from the Y chromosome, Xist, haemoglobin and ribosomal protein genes were removed. Spearman's correlation coefficient was computed from this set of genes and then used to build a distance matrix defined as $\sqrt{((1 - \rho)/2)}$. A t-SNE plot was constructed from the distance matrix, using the Rtsne package (https://github.com/jkrijthe/Rtsne).

To classify cells into different clusters, hierarchical clustering on the distance matrix (hclust function in R, with average method) was used, followed by the dynamic hybrid cut algorithm (dynamicTreeCut package (*71*)) to define clusters

(cutreeDynamic function in R with the hybrid method and a minimum cluster size of 60 cells). Cells that were outliers and could not be assigned to any cluster by the algorithm were removed.

For each cluster, a set of highly variable genes and computed the distance matrix as detailed above was defined. Next, hierarchical clustering and the dynamic hybrid cut algorithm (minimum cluster size of 40 cells) was used to define clusters. In cases in which more than one cluster were identified, a stability analysis was performed by subsampling the number of cells and genes to two thirds of the total and identifying clusters with the same procedure. The Jaccard coefficient was used to assess the similarity of the obtained clusters with the full and subsampled data. This procedure was repeated a hundred times, and clusters with a median Jaccard index of at least 0.5 were split.

Table 2.1 – List of Mouse Crosses

Male	**Female**	**Expected embryo outcome**
C57BL/6	CD1	Mixed background wild-type
Hex-GFP homozygous	CD1	Heterozygous Hex-GFP
Ttr-Cre heterozygous	ROSA26-EYFP homozygous	Ttr-Cre/ROSA26-EYFP ROSA26-EYFP heterozygous

Table 2.2 – List of antibodies used

Primary Antibody	**Company**	**Dilution**
Mouse anti-cTnT	Abcam: ab8295	1:100
Rabbit anti-NCX1	Swant: π11-13	1:200
Rabbit anti-Cav1.2	Santa Cruz: sc-25686	1:100

Goat anti-Nkx2.5	Santa Cruz: sc-8697	1:100
Mouse anti-Myom1	Gift from Dr E. Ehler	1:10
Rabbit anti-Sarcomeric Alpha	Abcam: ab68167	1:100
Rabbit anti-SNAI1	Cell Signaling Technology: 3819S	1:100
Rabbit anti-FGFR1	Novus Biologicals: NB100-2080	1:100
Rabbit anti-FGFR2	Santa Cruz: sc-1226	1:100
Mouse anti-pERK	Cell Signaling Technology: 9106S	1:100
Rabbit anti-Laminin	Sigma: L9393	1:100
Rabbit anti-ZEB1	Santa Cruz: sc-25388	1:100
Rabbit anti-LEF1	Cell Signaling Technology: 2230S	1:100
Rat anti-E-cadherin	Sigma: U3259	1:100
Rabbit anti-N-cadherin	Cell Signaling Technology:	1:100
Rabbit anti-GFP	Life Technologies: A11122	
Secondary Antibodies	**Company**	**Dilution**
Donkey anti-mouse 555	Thermo Fisher Scientific: A-31570	1:100
Donkey anti-Rabbit 647	Thermo Fisher Scientific: A-31573	1:100
Donkey anti-Goat 488	Thermo Fisher Scientific: A-11055	1:100
Donkey anti-Rabbit 488	Life Technologies: R37111	1:100
Donkey anti-Rat 633	Abcam: ab150155	1:100

Table 2.3 – List of primers used

Gene	Forward Primer (5'-3')	Reverse Primer (5'-3')	Amplicon (bp)
Gapdh	AGGTCGGTGTGAACGGATTTG	TGTAGACCATGTAGTTGAGGTCA	101
Hprt	TCAGTCAACGGGGGACATAAA	GGGGCTGTACTGCTTAACCAG	122
Oct-4	TGGAGGAAGCCGACAACAATGAGA	TGGCGATGTGAGTGATCTGCTGTA	148
Brachyury	CATGCTGCCTGTGAGTCATAA	TGTCTGGGAGCCTGGGGTGAT	83
Mesp1	GTCTGCAGCGGGGTGTCGTG	CGGCGGCGTCCAGGTTTCTA	189
Nkx2.5	CTATGCCCTGTCCCTCAGAT	CTCCCGGTCCTAGTGTGGAA	139

Mef2c	ACTGGGAAACCCCAATCTTC	ATCAGACCGCCTGTGTTACC	92
Myh6	GCTGGCTGGAAAAGAACAAG	TCTTGCCTCCTTTGCCTTTA	125
Myh7	ACTGTCAACACTAAGAGGGTCA	TTGGATGATTTGATCTTCCAGGG	91
Tnnt2	CAGAGGAGGCCAACGTAGAAG	CTCCATCGGGGATCTTGGGT	119
Myom1	GGCCATTCGACTCTTGTTCTC	AATACTCAGCGAAATGTGGGC	112
Actn2	GGGCTATGAGGAGTGGCTATT	AGTCCTTCTGCAGCAAGATCT	137
Slc8a1	GGACCAACAGCTGGAGAGAG	GGCAAACAGAACCTTCCAGA	152
Cacna1d	AGAACACCACGATTGCCCTA	CTTCTGGCTCGTCATCTTGC	105
Cacna1c	GGAGGGCGTGCATAAGCATT	AGGAAGAGATACTCCACTCGTTC	160
Cacna1g	TGTCTCCGCACGGTCTGTAA	AGATACCCAAAGCGACCATCTT	184
Cacna1h	CGTGACACTGGGCATGTTC	CCACCATCTTGATAACCATCTCC	106
Ryr2	ATTATGAAGGTGGTGCCGTATCA	TTCCACTCCACGCGACTCTTA	88
Atp2a2	TGGGCAAAGTGTATCGACAG	CAGCAGGAACTTTGTCACCA	108
Sox1	GGCCGAGTGGAAGGTCATGT	TCCGGGTGTTCCTTCATGTG	92
Hcn4	TCATCTCCTCCATCCCTGTC	CTGGCCAGGTCATAGGTCAT	202
Itp3r2	TCATCATCGCCTTGATTCTG	CAGTTCCCTGGGTCTCATGT	170
Camk2d	CTGGCACACCTGGGTATCTT	ATCCCAGAAGGGTGGGTATC	125

Chapter 3 - Establishment of Live Imaging Methods of Early Heart Development

3

Table of Contents

3.1 – Introduction

3.1.1 – Introduction to Microscopy

Being able to visualise biological events has been a constant in biological research for centuries. The invention of the first proper microscope by Antoine van Leeuwenhoek in the 17th century was the beginning of what is now a rich field, with more complex microscopes emerging every year, increasing the range of biological questions that can be investigated. In this chapter, I will introduce these types of microscopy, compare what type of data can be obtained with each in terms of live imaging of mouse embryos, and explain the rationale behind the choice of microscope ultimately used for the experiments in the next result chapters. I will also explore the mounting methods I developed to perform live-imaging of mouse and chick embryos and image analysis methods used to detect cardiac contractions and analyse calcium transients.

When building, or choosing, a microscope there are usually 3 factors that need to be taken in account: resolution, speed and sensitivity. There is no microscope that can excel simultaneously on all of these factors, in order to achieve one, the others need to be compromised to a certain extent. For example, electron microscopy offers very high resolution but it's slow and cannot be done with live samples, while speed in widefield microscopy is limited mainly by the camera but lacks resolution and does not produce 3D images (*72-74*). There are other factors that need to be taken into account when choosing a microscope such as sample size and whether or not the experiment requires live imaging of the samples. Morphogenesis is a highly dynamic process, therefore one of the main challenges in embryology is to capture these processes in

real time, i.e., live imaging. In recent years, many developments have been achieved to improve live imaging methodologies (*75*). When performing live imaging, it is imperative to expose the samples to as little light as possible as to avoid photo-toxicity. As such it is usually preferable to compromise resolution is favour of scan speed. Amniote embryos are in themselves more challenging to culture, are especially sensible to photodamage, and after the first few stages of early development, get too thick to image. These characteristics make amniotes challenging models for live imaging. In this chapter, I will describe the methods I developed to image both mouse and chick embryos using confocal microscopy, mouse embryos in Lightsheet microscopes and explain the image analysis methods necessary to extract quantitative information from these datasets which will be further explored in the remaining result chapters.

3.1.2 – Confocal Microscopy

The main principle behind confocal microscopy is the addition of a pinhole to eliminate out-of-focus light, which is especially problematic in thick samples, offering better resolution than widefield microscopes. Unlike widefield microscopy where the whole sample is bathed with light, confocal microscopes use one or more focused beams of light to illuminate the sample, which allows the acquisition of optical sections that can be used to create a 3D reconstruction of the sample, without the need to physically destroy the sample. While offering better resolution and optical section, illuminating the sample point by point has the disadvantage of requiring longer scanning times that widefield microscopes. There are many variations in confocal microscopy, but these can be divided into 3 main categories: single-photon point-

scanning confocal, multiphoton point-scanning confocal and spinning disk confocal (SDC) (*76*). For the work presented here I used both laser scanning microscopy (LSM), which is a type of single-photon confocal microscopy, and SDC. The main difference between LSM and SCD is that while LSM only has one single pinhole with variable apertures, SDC has a disk with several dozen pinholes of a defined aperture. In the case of LSM a given optical section has to be imaged point by point, with either stage or objective moving in order to scan the whole stack, while in SDC the rotating pinhole disk allows the acquisition of the whole optical section, making it faster and usually more suitable to live-imaging that the LSM. On the other hand, the variable aperture of the LSM pinhole allows more flexibility in order to obtain the desired resolution.

3.1.3 – Lightsheet Microscopy

Lightsheet Fluorescent Microscopy (LSFM) is a modality in microscopy that has gained momentum over the past few years, especially in developmental biology (reviewed in (*77*)). In this methodology, the laser is focused into a single diffraction-limited beam of light that is then scanned to form a sheet that, illuminates only the focal plane of the sample. This property also allows optical sectioning with LSFM, but unlike confocal microscopy which achieves this by illuminating the entire depth of the sample and then blocking the out of focus light through a pinhole aperture, LSFM only illuminates the section of the sample that is being imaged, dramatically reducing the photodamage to the sample. These properties also mean that in comparison with other methodologies for optical sectioning microscopy, LSFM can achieve faster frame rates, which also means less photobleaching and photodamage. The only aspect

where LSFM falls behind in comparison with confocal strategies is on resolution, which is due to the fact that in confocal microscopy, detection of out of focus light is greatly reduced, resolving finer structures. Nonetheless, resolution with LSFM can be improved with deconvolution (*78, 79*). Over the past few years several custom-made variations of LSFM have been developed, varying from number of cameras to how the sample is mounted. In the experiments presented here I used the commercially available Zeiss Z1 Lightsheet microscope.

3.1.4 – Calcium Imaging

The ability of cardiac cells to spontaneously contract is a key biological process that differentiates these cells from other types. The ability to detect and analyse these contractions is essential to assess cardiac differentiation and to provide insights into cardiac physiology (*80, 81*). Every cardiac contraction is preceded by an increase of cytoplasmic concentration of calcium ions (Ca^{2+}), i.e. a Ca^{2+} transient, and while visualising cardiac contractions alone can provide many insights into cardiac function, being able to visualise and/or measure this increase in Ca^{2+} concentration has proven essential to increase our knowledge on cardiac function.

Due to the importance of visualising Ca^{2+} transients, over the years several methods have been, and still are being, developed to enable and improve the visualisation of this process. Ca^{2+} transients were first visualised by using chemical dyes that change their light-emitting properties according to the levels of Ca^{2+} freely available in the cytoplasm and/or in intracellular stores, such as the SR and mitochondria. The first of such dyes was Aequorin, which did not require optical excitation but also could not freely pass through the plasma membrane, requiring

intracellular injections. Nowadays, while there is a wide variety of available dyes, they usually have the same overall composition: a fluorophore such as Rhodamine or Stilbene, a chelator, usually BAPTA, and a conjugated chemical like the AM ester to allow the passage through the plasma membrane (*82, 83*). Besides calcium dyes, genetically encoded calcium indicators have also been developed to facilitate the realisation of experiments that involve the visualisation of calcium transients. Genetically encoded calcium indicators offer several advantages over chemical dyes, as they eliminate variations from differential internalisation of the dye. Genetic indicators are however usually more limited in terms of sensitivity to changes in calcium concentration, emission spectra and their ability to provide ratiometric measurements to have a more quantitative approach to the measurement of calcium concentrations (*84*).

Many of the studies related to the regulation of calcium transients have mainly been performed in isolated adult or foetal myocytes, and occasionally in whole adult hearts. While some studies using embryos have emerged over the past few years, these have focused mainly in anamniote models due to easier culture and imaging conditions. In order to study the interplay between physiology and development in amniotes, I developed and optimized methods to culture amniote embryos, while imaging calcium transients.

3.2 – Results

3.2.1 – Calcium Imaging in Early Amniote Embryos

In order to perform calcium imaging in the early embryonic heart I first dissected E8.5 embryos that already possess strong cardiac contractions, and cultured them in the presence of calcium sensitive dyes. Initially I tested the dyes fluo-8, rhod-2 and fura-2. I first attempted to culture intact embryos in the presence of calcium dyes but that did not allow the proper loading of the calcium dye into the myocardium, and no calcium transients were observed when imaging with the SDC confocal. To overcome this, I next cultured intact embryos in the presence of calcium dye and 0.2% pluoronic acid as it has been performed by others, but this also did not reveal any loading of the dye into the myocardium, assessed with SDC microscopy. Finally, by removing the endoderm and pericardial sac overlaying the myocardium, it was possible to detect fluorescence in the myocardium. This was initially performed in the SDC confocal and later in the LSM and Z1 microscopes. Of the dyes mentioned above, only rhod-2 seemed to be sensitive enough to reliably detect changes of fluorescence in the early developing heart, with imaging settings appropriate for live-cultures. However, when performing these experiments on very early cardiac crescent stages, rhod-2 seemed to not be very reliable. This dye also did not seem to easily work in embryoid bodies. After testing other dyes, such as fluo-3, in embryoid bodies I started performing experiments with Cal-520, and later Cal-590, which were the only dyes that allowed visualisation of calcium oscillations in embryoid bodies and early cardiac crescent stages (fig. 4.6 - B). In the next sections I will discuss calcium imaging in confocal microscopes and in a lightsheet microscope.89

3.2.2 – Imaging Amniote Embryonic Hearts with Confocal Microscopy

Confocal microscopy is a well-established microscopy technique in developmental biology labs. Despite its widespread use, it is often necessary to develop custom culture and mounting methods to image the specific tissues of interest, especially when performing live imaging (*85*). As mentioned above, amniote embryos are particularly difficult to use for live imaging of morphogenesis and as such it is perhaps not surprising that much of the live imaging of heart development comes from imaging zebrafish embryos (*86-90*). Despite all the limitations there are some studies that perform live imaging of chick early heart development, however these usually lack resolution (*91-93*). Mammalian embryos are even more difficult to culture, which is the reason why most heart lineage analysis in mouse embryos relies on Cre-mediated recombination strategies rather than live imaging. In terms of live imaging, only very recently has heart tube morphogenesis been studied (pre print (*94*)). In order to partly fill this gap in knowledge I developed live-imaging methods that can be used to image calcium transients in both mouse and chick embryos and overnight live imaging of mouse embryos at early stages of heart development in inverted microscopes.

An inherent problem with performing live-imaging of post-implantation mouse embryos lies with the difficulty of culturing these embryos. In fact, after E6.5 it is usually advisable to culture mouse embryos using rolling culture systems (*95*). Part of the reason for this particularity of mouse embryos is that embryos at these stages expand significantly due to growth and expansion of the pro-amniotic cavity. Therefore, confining the embryo usually impairs development and while there has been a method

developed to image mouse embryos at these stages, the method is more suitable to image the neural tube and it is not easily applied to heart imaging, involving significant manipulation of the embryo in order to immobilise it.

In order to image the embryos, I initially attempted to immobilise them between finally pulled glass rods. The embryos remained immobilised between the glass rods while the dish remained stationary, however the embryos moved if the dish was perturbed, requiring manipulation of the embryos while the dish is already in the imaging microscope. This makes this method unsuitable for the intended experiments, therefore, to overcome some of the obstacles mentioned above I used inert vacuum grease to immobilise the embryos instead of the glass rods. An advantage of vacuum grease is that besides being easily malleable to confine the embryos it also expands, avoiding some of the issues that arise with embryo confinement. Since both the LSM and SDC used were inverted microscopes I used a MatTek glass bottom dish to mount the embryos, and while the method presented below is optimised for this kind of microscopes it is possible to easily adapt it for upright systems. To mount the embryos, first two or more parallel lines of vacuum grease, with 2 layers each, are laid down in the coverslip of the Mattek dish, ideally spaced between each other in order to only fit a single embryo (fig. 3.1), although this is not critical. The next step is to surround the coverslip with 2 layers of vacuum grease (fig. 3.1) in order to be able to add more media to the centre of the dish and eliminate the need to fill the whole bottom of the dish with media. This step may be skipped in favour of adding a small amount of media (no more than 400 µl) on top of the coverslip, which creates a dome of media kept via surface tension. However, by keeping the media in a dome via surface tension implies that the dish must be carried more carefully. After adding the media and embryos to the dish, there are two main ways to reshape the vacuum grease in order to hold the

embryos in place (fig. 3.1 – A, B). The embryos can either be mounted by moving some vacuum grease in order to create a thin line of vacuum grease over the embryo (fig. 3.1 – A) or by reshaping the vacuum grease on both extremities of the embryos to create wells for the embryos (fig. 3.1 – B). The first method is more suitable for chick embryos, stretched mouse embryos, and when it is necessary to pin the embryos closer to the coverslip. The second method is more suitable when it is necessary to keep mouse embryos completely intact, such as when performing live imaging over several hours, and can also be used to easily position the embryos in any angle.

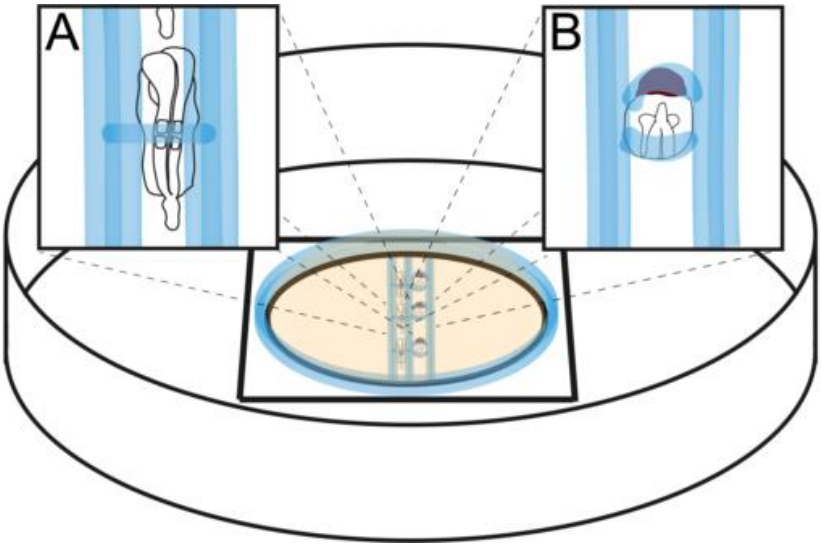

Fig. 3.1 – Mounting method for inverted microscopes - Embryos are mounted between two parallel lines of vacuum grease (in blue). In the case of stretched mouse embryos or chicken embryos an arch of vacuum grease over the centre of the embryos (A) can be used to hold the samples in place. This method was primarily used for calcium imaging. For intact mouse embryos, the vacuum grease is instead moulded around the embryo (B), leaving room for it to expand. This method was predominantly used for overnight live imaging.

After establishing a proper method to mount the embryos I examined which microscope would be more appropriate to image the first cardiac contractions and calcium transients (fig. 3.2). In theory, the SDC would be the most suitable option as it can reach faster frame rates than the LSM. A main difference between the SDC and the LSM used here is that the LSM allows the simultaneously acquisition of several channels, including Differential Contrast Imaging (DIC), while the SDC requires separate acquisition. Using comparable objectives, the SDC did indeed provide faster frame rates, around 30 frames per second (fps) and when comparing just DIC the resolution seems comparable (fig. 3.2 – A, E), which would make the SDC the best option for this kind of experiment. However, the ability to control the aperture did prove useful when performing calcium imaging (Fig. 3.2 – A-C, E) since out of focus light sometimes makes it difficult to detect calcium transients, especially when the change in fluoresce is small. The ability to image the calcium transients simultaneously with DIC imaging, provided by the LSM, is also an advantage because it makes it possible to correlate the propagation of the calcium transients with beating areas, which do not always coincide. When imaging larger samples, such as chick embryos, and using lower magnification, lower numerical aperture objectives (fig. 3.2 – B), the LSM still provides a good option to perform calcium imaging. The frame rates achievable by LSM using a 256x256 frame size (10 fps in the Zeiss LSM710 and 13 fps in the Zeiss LSM 880) are also suitable to visualise the propagation of the calcium transients. It is however possible to reach faster frame rates by acquiring smaller frames, making it possible to image regions with only a couple of cells at speeds that can reach 100 fps (fig. 4.6 – C). As mentioned above, it is also possible to image the embryos from different angles. For example, instead of imaging the mouse embryonic heart it is possible for example to image the embryonic brain (fig. 3.2 – C).

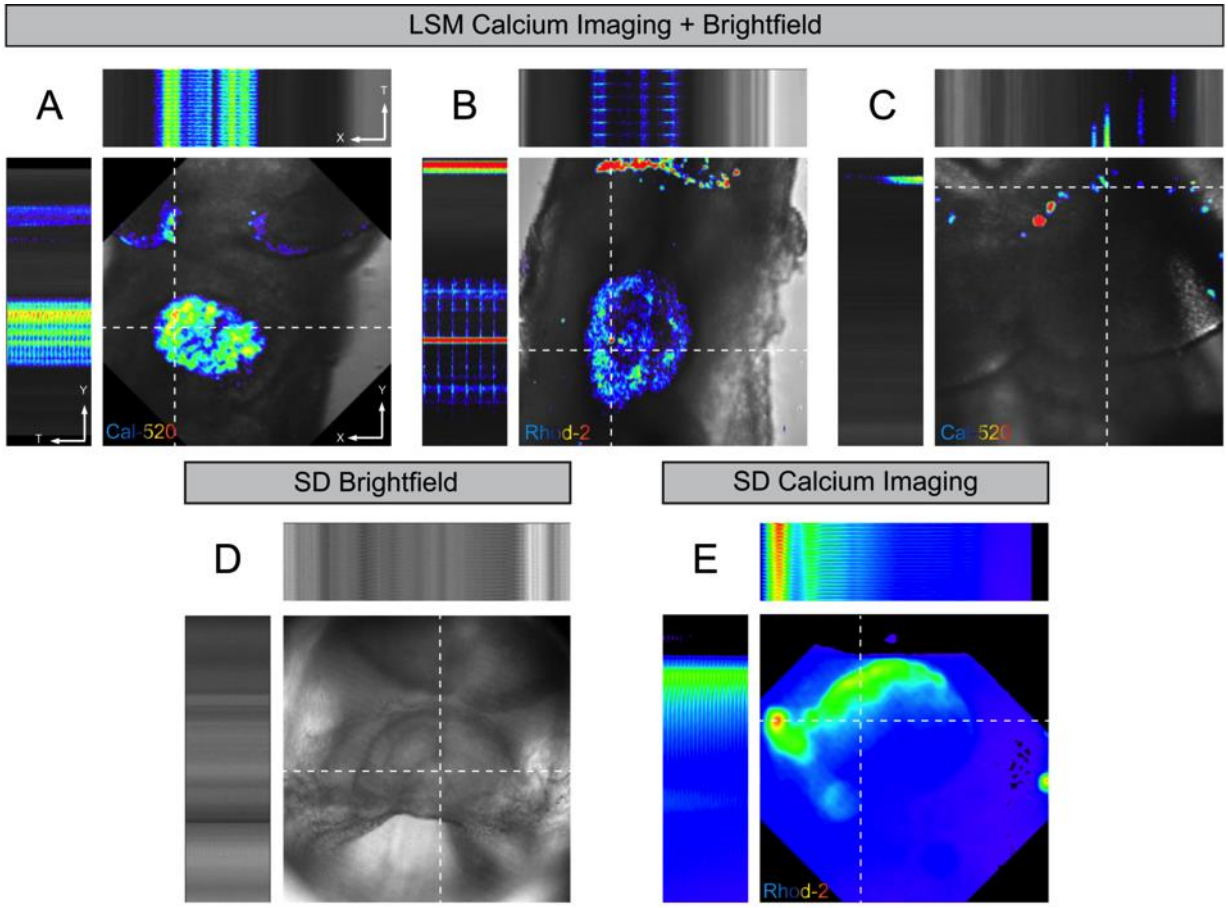

Fig. 3.2 – Calcium imaging in amniote embryos using confocal microscopy – Using the mounting method described in fig. 3.1, embryos were imaged using either a laser scanning confocal microscope (LSM, A-C) or a spinning disk (SDC) confocal microscope (D-E). Using LSM it is possible to simultaneously acquire, at good resolution, calcium transients (rainbow) and brightfield images in the heart of both mouse (A) and chick (B) embryos. It is also possible to orient the embryo to image the brain (C). Using SDC it is not possible to simultaneously acquire more than one channel. The resolution of brightfield (D) images is comparable to the LSM, however there is more background when performing calcium imaging (E). The XT and YT frames represent kymogrpahs, showing intensity changes over the imaging period. Dotted lies represent the lines used to create the kymographs.

3.2.3 – Imaging Mouse Embryos with Lightsheet Microscopy

Since lightsheet microscopy is a technique, which was built mainly for live imaging, I attempted to develop methods to easily image E8.0 mouse embryos in the Z1 lightsheet microscope. A particularity of most lightsheet microscopes is that the sample is hanging in a chamber instead of resting on a dish or coverslip. For this reason, the mounting method explained above cannot be used to image in a lightsheet microscope and new mounting methods had to be devised.

To date, lightsheet microscopy has been used to mainly perform live imaging of zebrafish and drosophila embryos (*77*). The mounting methods used in these papers rely on embedding the sample in agarose inside a capillary tube (*96*), and then extruding the agarose plug in the lightsheet chamber filled with a saline solution. Unfortunately, this method cannot be applied to mouse embryos, because these do not culture well under constraint. In order to be able to use the lightsheet microscope I used instead an FEP tube attached a 1 ml syringe (fig. 3.3 – A)

First the FEP tube was flame sealed in one end of the tube, and was partially filled with agarose. Initially I attempted to mount the embryos without shaping the agarose bed, however with this approach the embryo is not secure and falls on their widest axis. To avert this, upon filling the bottom of the FEP tube with agarose, I inserted a 2 µl pipette tip in the agarose while it solidified. This creates a trough where the embryos could only fall on their thinner axis. Before attaching the FEP tube it is necessary to pierce the syringe above the 0.2 ml mark to allow gas exchange. Once the FEP tube and the syringe are ready they can be held together by slightly melting the interface between the FEP tube and the syringe with heated forceps. The FEP tube, and the syringe can then be filled with culture media and the whole set-up is put

in the incubator in order to equilibrate the FEP tube and the agarose. Prior to imaging the media in the FEP tube should then be changed to new culture media, an embryo can then be dropped through the syringe and can be imaged once it settles on the agarose bed. Lastly, a thin layer of mineral oil is added to the top of the culture media in the syringe in order to prevent evaporation (fig. 3.3 – A). With this set-up, the lightsheet chamber can still be filled with saline solution, however if the chamber is filled with culture media the set-up can be modified by piercing the syringe underneath the 0.1 ml mark in order to allow the media in the chamber to flow into the syringe.

The set-up described above can be used to maintain embryos overnight (fig. 3.3 – B), to image cardiac contractions (fig. 3.3 – C) and calcium oscillations (fig. 3.3 – D). The lightsheet microscope can easily be used at 50 fps, which makes it ideal for calcium imaging. Similarly, to the LSM it is possible to acquire more than one channel simultaneously, but there is no option to acquire DIC images. However, it is possible to acquire a brightfield image by turning on the illumination in the door's webcam and acquiring an image with a far-red filter. Unfortunately, it is not possible to control the webcam's illumination, therefore the light stays on for the whole duration of the experiment, making it unsuitable for live imaging over several hours. In terms of resolution, this microscope provides good results albeit with some out-of-focus light. Even with the lowest 5x objective, this microscope provides good resolution, making it ideal to image large samples or to rapidly image the whole embryo (fig. 3.3 – E, F). At E8.0, the illumination is parallel to the cardiac crescent, which makes it difficult to image the inner most layers of the embryo with good resolution (fig. 3.3 – B).

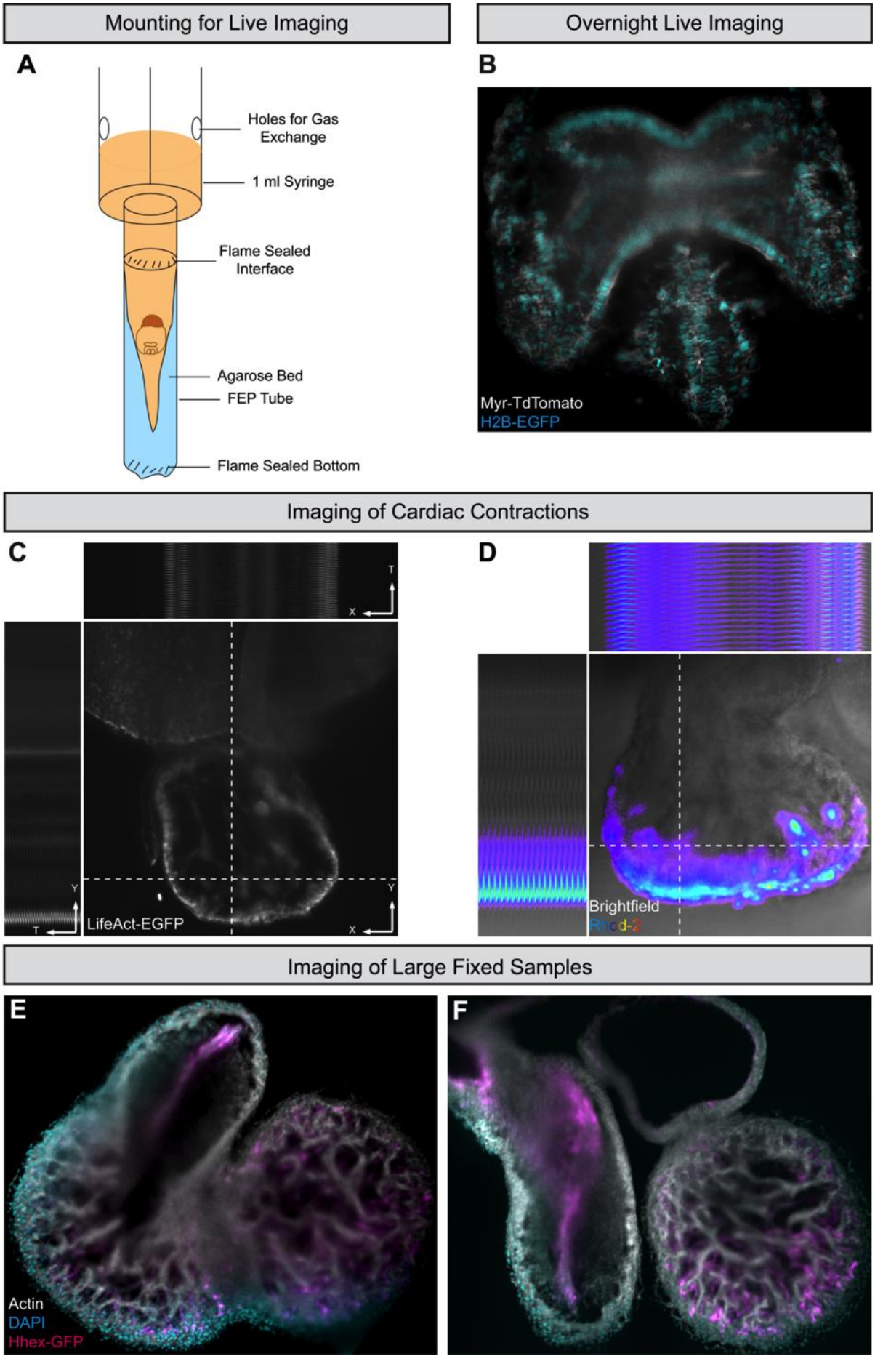
Mounting for Live Imaging
Overnight Live Imaging
A
Holes for Gas Exchange
1 ml Syringe
Flame Sealed Interface
Agarose Bed
FEP Tube
Flame Sealed Bottom
B
Myr-TdTomato
H2B-EGFP
Imaging of Cardiac Contractions
C
T
X
Y
T
Y
X
LifeAct-EGFP
D
Brightfield
Rhod-2
Imaging of Large Fixed Samples
E
Actin
DAPI
Hhex-GFP
F

Fig. 3.3 – Lightsheet Imaging - In order to perform live imaging in the Z1 lightsheet microscope, embryos were mounted using a FEP tube attached to a 1 ml syringe (A). The bottom of the FEP is filled with agarose and a depression is created using a pipette tip, where the embryo can rest. This method can be used to image E7.5-E8.5 embryos both overnight (B: grey – Myr-tdTomato; cyan – H2B-EGFP) and to image cardiac contractions (C: grey – LifeAct-EGFP) and calcium imaging (D). The XT and YT frames represent kymogrpahs, showing intensity changes over the imaging period. Dotted lies represent the lines used to create the kymographs. Using the Z1 lightsheet microscope it is possible to rotate samples to image them from different angles. This is especially useful when imaging larger samples such as E12.5 mouse hearts (E, F – different angles of the same sample. Grey – Actin; Cyan – DAPI; Magenta – Hhex-EGFP)

3.2.4 – Normalising Imaging Data

One of the main advantages of the work presented here is that there is both increased spatial and temporal resolution compared to work previously published on embryonic hearts. However, the methodology presented here does fall behind in terms of quantitative information, especially when compared to well established methodologies such as patch clamping, which allow precise measurements of the changes in calcium concentration inside a cell. To overcome this shortcoming to a certain extent I applied methods developed by other researchers in the department and also created methods to extract quantitative information from recording of beating hearts and calcium transients.

Quantification of cell contraction can be a difficult hurdle to overcome, because the motion of the tissue can displace the sample in unpredictable ways. This is especially problematic with large samples that are not attached to a culture dish. In the case of the embryonic stages used here, it is possible to detect tissue displacement in raw brightfield images of late stage cardiac crescents (fig. 3.4 – A, white arrow), but detecting the first cardiac contractions can be extremely difficult due to small tissue displacement that cannot easily be seen in brightfield images. In order to overcome this problem, Dr. Gil Bub, previously at the Department of Physiology, Anatomy and Genetics, has been developing methods to normalise temporal data from brightfield images in order to quantify contraction of cardiac cells. With the help of Dr. Bub, I employed an absolute difference image filter on brightfield images of mouse embryos between E8.0-E8.5 in order to visualize patterns of cardiac contraction (fig. 3.4 - B). This method calculates pixel intensity at any given timepoint compared to the intensity of the same pixel N frames prior to the current timepoint. N can be changed in order

to optimise the output of specific images, but it is automatically set to maximise local intensity changes, which is usually a value smaller than the period (in frames) between two consecutive contractions (interbeat interval). The result from this process is that the brigthfield image is transformed into a high contrast image, where beating regions within a movie are displayed as cluster of bright pixels, which are easy to visualise (fig. 3.4 – A, red arrow). Dr. Gil Bub included this algorithm in a software package called GView. A similar analysis can be performed using Fiji either by doing the ratio (fig. 3.4 – C) or subtraction (fig. 3.4 – D) of each frame to its previous frame. In this scenario, the given movie is equivalent to a movie that would be obtained if N were equal to 1 using GView, therefore it is not the optimal image processing method. This could be changed by empirically determining the interval between contractions but that can be variable even within embryonic stages, making GView a faster and more reliable approach to detect pixel displacement in samples with little to none information *a priori*.

In terms of semi-quantification, while plotting the intensity profile of raw brightfield images can reveal clear peaks indicative of cardiac contractions, however even at late cardiac crescent stages there is some degree of noise (fig. 3.4 – E). Plotting the changes in intensity using GView gives well-defined peaks (3.4 – F), little noise compared to the brightfield image.

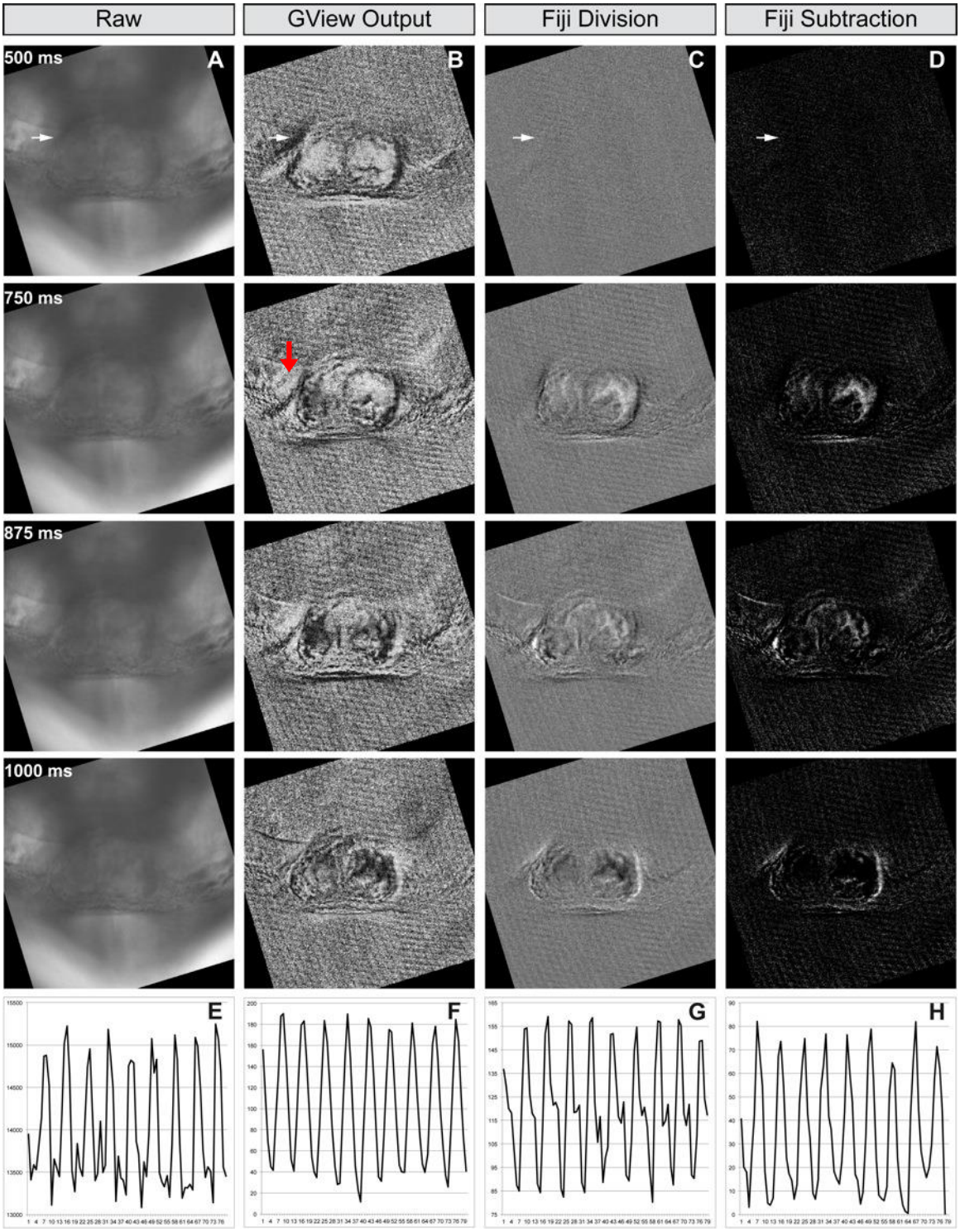

Fig. 3.4 – Pixel displacement analysis – Cardiac contractions are easily detected in brightfield images when the cardiac tissue is overtly displaced (A, region pointed by white arrow), being possible to extract quantitative profiles from the raw image (E). At earlier stages however this displacement is not as obvious, therefore we

applied pixel displacement algorithm developed by Dr. Gil Bub (B) to display moving regions within the embryo. These regions are displayed as high intensity pixels (red arrow). GView calculates the interbeat interval, outputting a profile with less noise (F) than the raw image. Pixel displacement can also be calculated using the “Image Calculator” option from Fiji. In this situation a stack containing timepoints 1 to n-x (n=number of timepoints, x=interbeat interval), can be either divided (C) or subtracted (D) from a stack containing timepoints x to n. x can be considered 1 regardless of the real interbeat interval, but the outputs (G, H) can have more noise than the output obtained from GView. On the other hand the division method using Fiji may create further noise (Fig. 3.4 – G), while the subtraction methods gives well defined plots but slightly more variable (fig. 3.4 – H) than the GView plot.

While quantification of brightfield images can be informative and be used as a surrogate to action potentials (*97*), quantifying fluorescence images of calcium transients is also vital in order to better understand the physiological dynamics of the embryonic heart. Typically, calcium transients are represented by plots, showing the ratio of the fluorescent intensity at any given pixel (F) over the minimum intensity (F0). It is important to note however that this method is usually used when studying individual cells and not whole tissues. A problem that can arise when imaging whole tissues is that F0 becomes somewhat subjective. For any given embryo, F0 can either be the minimum of the whole field of view, which is often 0 as some regions of the embryo do not take in the calcium dye or have very low levels of intracellular calcium, the minimum of the cardiac region which often is also 0, or the minimum for every given pixel. Therefore, in order to apply this method, it would be necessary to extract the intensity profile for any given pixel, identify the minimum value and then normalise the data to that value in order to plot it. Furthermore, using the method described in this chapter to visualise calcium transients there can be regions of high fluorescence intensity (fig. 3.5 – A) due to calcium overload. If the sample is moving the F/F0 method can also show an increase in fluorescence levels due to the samples moving closer to the coverslip (fig. 3.5 – F, notice the gradual increase in local minimums of fluorescence intensity). The drawbacks of this approach are that it is cumbersome to analyse several pixels and that the normalised values cannot be easily transformed back into an image, losing the spatial information.

There are two main methods that can be used to normalise fluorescence intensities for calcium imaging data. The first method is to use a frame where the heart is at a resting phase as baseline and using the image calculator option on Fiji to subtract this frame from all the frames in the stack (fig. 3.5 – B). With this method, the

signal is removed from all the regions where the fluorescence intensity doesn't fluctuate and there is no noise introduced in non-cardiac regions, but there can be edge effects if the sample is undergoing significant movement (fig. 3.5 – B, red arrow). Nevertheless, the overall plot profile is very similar to the F/F0 plot, while eliminating some of the increase in fluorescence due to sample movement (fig. 3.5 – G). The subtraction method also has the advantage of being possible to apply several times in the same movie, i.e., if there is significant movement in the sample, it is possible to eliminate some of these artefacts by choosing a new baseline frame and performing a new subtraction (fig. 3.5 – C), further eliminating fluorescence increase due to sample movement (fig. 3.6 – H).

The second method to normalise all the pixels divide all the frames with the baseline frame and create a 32-bit float output (fig. 3.5 – D, intensity was increased in order to be able to visualise it in the embryo). The advantages of this method are that the edge effect due to sample movement is not as evident as with the subtraction methods (fig. 3.5 – D, red arrow) and that plotting values of any given pixel, the resulting ratios are comparable the ratios obtained with the F/F0 method (fig. 3.5 – I). Some problems with this approach are that often the resulting intensities are relatively dim as it introduces noise to non-cardiac regions, and it does not removed fluorescence increase due to the sample getting closer to the coverslip. Furthermore, a second division further increases the background fluorescence compared to the cardiac region (fig. 3.5 – E), while showing no overall improvement in the plotted values (fig. 3.5 – I).

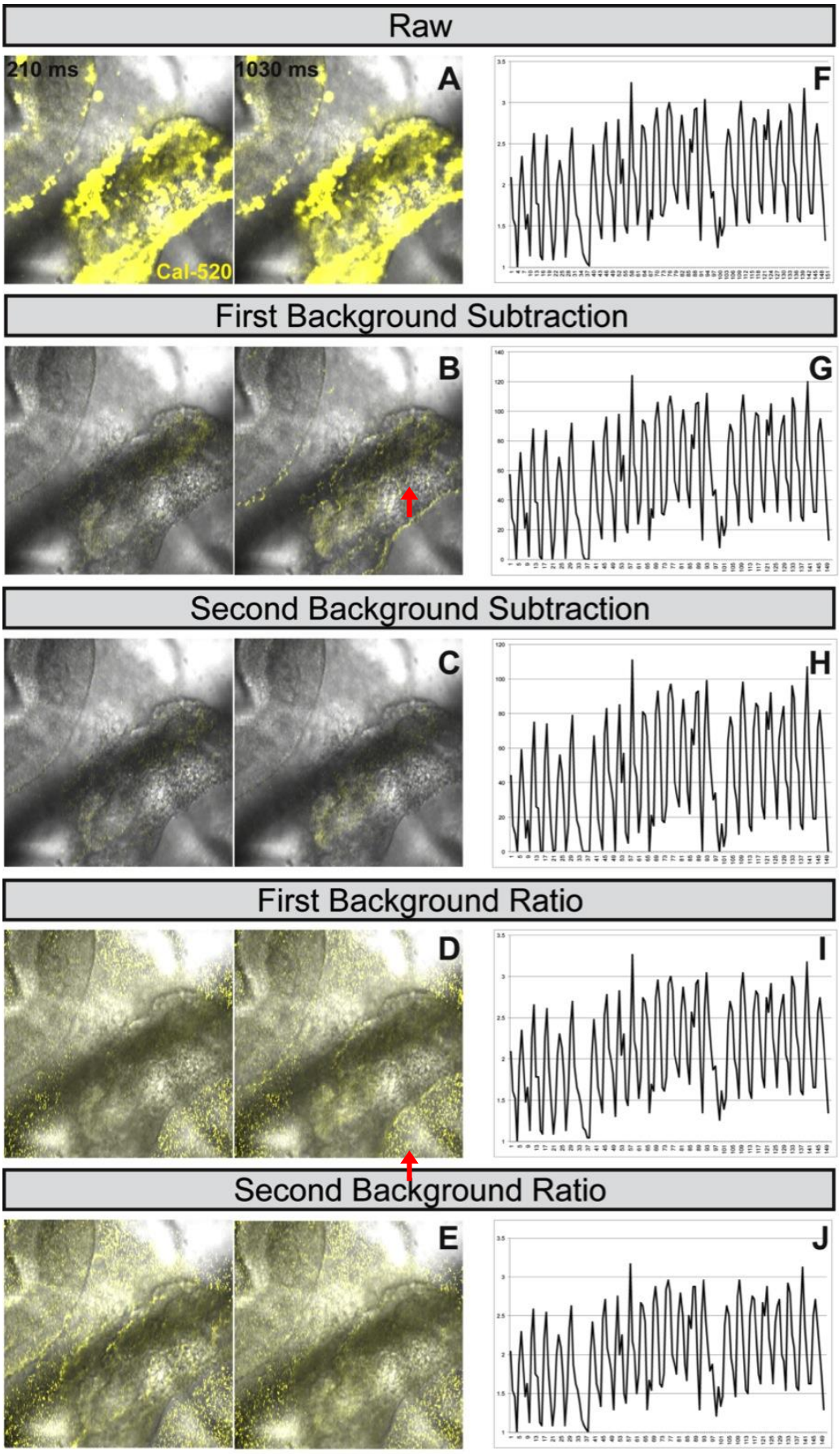
Raw
210 ms
1030 ms
A
Cal-520
F
First Background Subtraction
B
G
Second Background Subtraction
C
H
First Background Ratio
D
I
Second Background Ratio
E
J

Fig. 3.5 – Analysis of calcium transients – Due to the requirement to remove the endoderm in order to image the calcium transients in the cardiac crescent, the cells surrounding the myocardium show calcium overload due to cell death (A). Subtracting the fluorescence in the frame with the heart in resting phase (baseline frame) from all the frames in the stack, makes it possible to remove the signal from any regions that do not have fluctuations in fluorescence (B, C). This can also be achieved by calculating a ratio instead of a subtraction (D, E), however this method increases background fluorescence. In cases where the samples are moving, these methods will show movement artefacts (B, D red arrows), however these can be removed by choosing a second baseline frame (C,E). Traditionally, calcium transients are quantified by using the F/F0 method (F), which needs to be calculated for each pixel. The methods described above don't change the overall profile of the calcium transients (G-J), when compared to the F/F0 method.

3.2.5 – Development of ImageJ Scripts to Automatically Extract Quantitative Information

In order to easily extract quantitative information on the duration of calcium transients and interval between transients, I created a Fiji plugin (fig. 3.6) that automatically extracts several measures from ROIs from either calcium imaging datasets or high contrast images such as the output from the absolute image filter described above. By creating a line over the region intended to analyse, the plugin will create a kymograph, an image with the fluorescence profile over time in all the pixels in the given line (fig. 3.6 – A). Since the plot from the kymograph can be quite noisy, it becomes necessary to clean the data in order to obtain well-defined peaks. The first step to clean the data is to apply a bandpass filter to the kymograph image (fig. 3.6 – B). A bandpass homogenises the frequencies of the images, effectively merging pixels together. For the purpose of this plugin I filtered larger structures down to 50 pixels, small structures down to 2 pixels, and supressed vertical lines. This homogenises the horizontal lines in the kymograph as much as possible, filling some of the gaps in fluorescence. The next step is to apply a Gaussian blur to the bandpass filtered image (fig. 3.6 – C), to further normalise the intensity data. A Gaussian blur essentially outputs a “out of focus” version of the original image. The higher σ is in a Gaussian blur, the blurrier the image, the more the output image resembles background signal. For this plugin I apply a σ=1 for the purpose of keeping some clear signal fluctuation. The final step in order to obtain well-defined fluorescence intensity fluctuations is to subtract the Gaussian blur image from the bandpass filter image (fig 3.6 – D). This subtraction removes all background signal, as well as some real signal, from the bandpass filtered image, which allows the separation of all the intensity peaks. With

the peaks now well defined, the plugin fills the space outside the peaks with black background (fig. 3.6 – E). Drawing a horizontal line through this plot (the position of the line can be adjusted if necessary) and replotting it creates a binary plot (fig. 3.6 – F), which facilitates further analysis. This plot represents frames that are at resting phase with 0 (black) and the frames in activating phases with 255 (white). Using database software such as Excel it is then possible to count the number of consecutive 0s and 255s to estimate the duration of each calcium transient and interbeat interval, in frames. For each measurement, the frame number should be rounded to the closest natural number, to reflect the number of acquired frames.

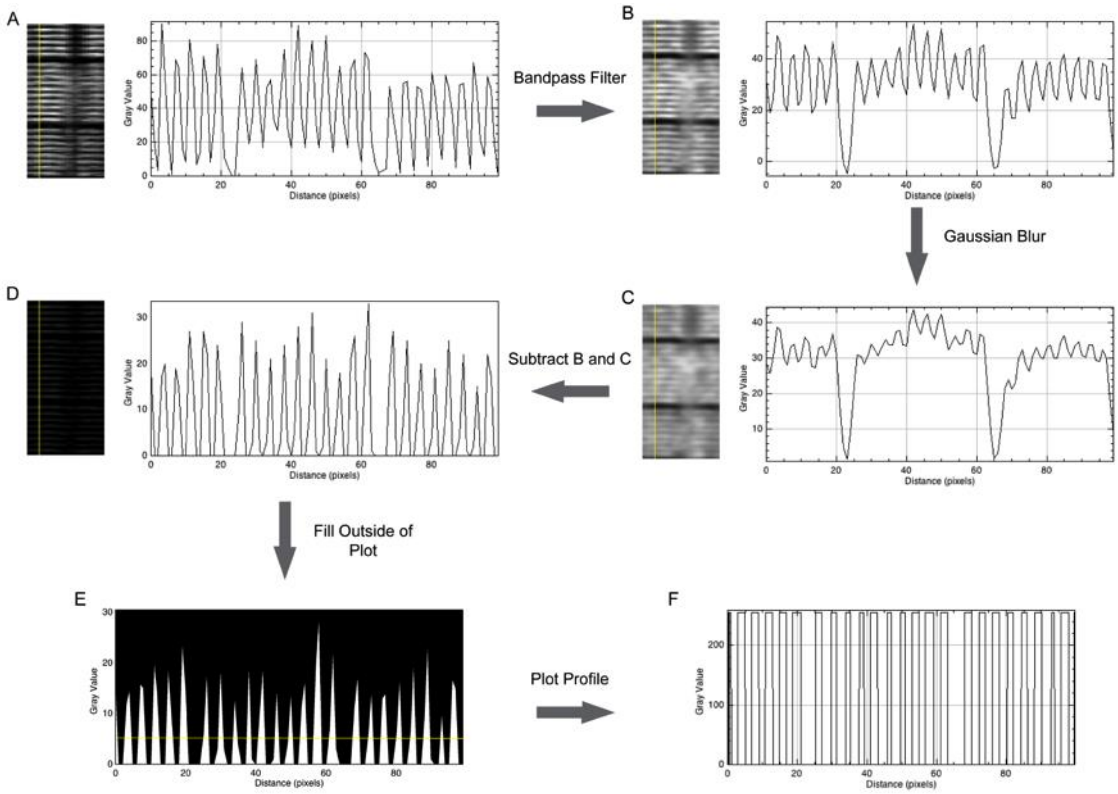

Fig. 3.6 – Automatic extraction of calcium transient duration and interbeat interval – By creating a kymograph using Fiji it is possible to obtain an a single image displaying all the changes in fluorescence over time from a particular region of interest (A). Applying a bandpass filter to this image, supressing vertical lines, eliminates some of the gaps in fluorescence that may be present at each timepoint, while increasing some of the background (B). Passing this second image through a Gaussian blur filter will create a “out of focus” image of the kymograph (C). Subtracting the Gaussian blur image from the bandpass filter image will create a kymograph image with better-defined boundaries (D). Filling the space between the peaks with a different colour such as black (E) and drawing a line across the plot (E, yellow line) makes it possible to create a binary plot (F). The values from the binary plot can then be imported on Excel to easily calculate the average calcium transient and interbeat interval.

Another methodology that is often applied to rhythmic events is calculating the harmonic frequency and harmonic amplitude (*98*). The harmonic frequency is the value of the sine function(s) that define a certain rhythmic event. An event with a perfect periodicity is represented by a harmonic frequency of single sine function. However most rhythmic systems are not perfect and are represented by more complex functions composed of more than one sine, i.e., the more harmonic frequencies the more irregular is the rhythm. Furthermore, each harmonic function will also have different amplitudes, which is a measure of how important that sine function is for the representation of the rhythm. While harmonics is more frequently used in physics, it has been applied to some biological contexts such has somitogenesis (*99*) and to detect arrhythmias (*100*).

While there have been methods developed to extract this information from images, they usually rely on some degree of programming knowledge and are usually developed in MatLab or Python language, which can be difficult to optimise for a lay person. In order to extract this information from cardiac contraction and calcium imaging datasets I developed another Fiji plugin that automatically extracts this information by just drawing a line over the region of interest (ROI). With this plugin it is possible to extract only the harmonics with higher amplitude (can be defined by the user), in order to extract only the harmonic that are more important to represent the periodicity of the cardiac contractions or calcium transients. The more harmonics of high amplitude, the more irregular is the period, and the higher the harmonic frequency, the faster is the rhythm. A region with more than one harmonic of high amplitude can be considered an arrhythmic region.

It is possible to extract the values of harmonic frequencies and amplitudes of any given image or group of images by analysing its Forward Fourier Transformation

(FFT). To achieve this for calcium transient data this plugin also extract the kymograph (fig. 3.7 – A) from a ROI, followed by a Fourier correlation with itself in order to extract the sine profile of the whole kymograph (fig. 3.7 – B). This first sine representation is a very complex representation of the process, as it can be seen by its FFT (fig. 3.7 – C). Ideally a sine representation of a rhythmic event will be represented by only a few values on the central horizontal line of a FFT. To achieve this, the plugin restricts the analysis to the upper or lower boundary of the original sine image, as these regions present low variation (fig. 3.7 – C). The harmonic frequency is given by the distance of the pixels from the central pixel (the FFT displays mirrored quadrants), and the harmonic amplitude is given by the grey value of that pixel. The FFT of this region now shows only one single horizontal line (fig. 3.7 – D), however as it can be seen from its plot, there is a harmonic frequency at almost every pixel, albeit at varied amplitudes (fig. 3.7 – E). Since harmonic frequencies with low amplitude explain only small variations in a rhythmic event, a threshold is applied to isolate the harmonic frequencies with the highest amplitudes (higher than 200 by default). The FFT obtain after the threshold (fig. 3.7 – F) resembles more the profile of a true rhythmic event, with only a few harmonic frequencies, as can be seen from its plot (fig. 3.7 – G).

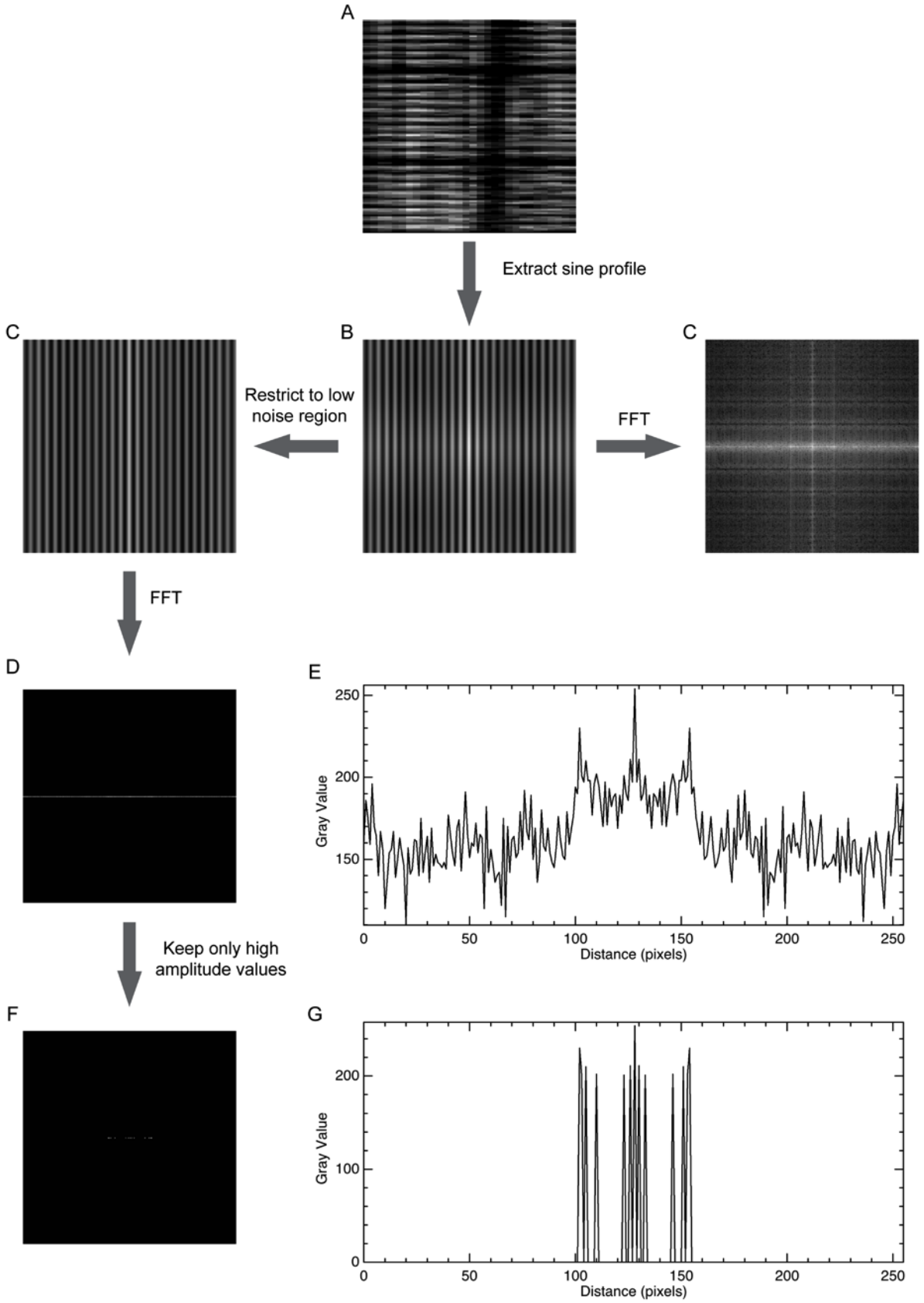
A
Extract sine profile
C
B
C
Restrict to low
noise region
FFT
FFT
D
E
Gray Value
Distance (pixels)
Keep only high
amplitude values
F
G
Gray Value
Distance (pixels)

Fig. 3.7 – Analysis of harmonic frequencies – Images can be mathematically represented by a series of sine functions. By transforming a kymograph image (A) into it's frequency domain, correlating with itself, and transforming the result back into the spatial domain it's possible to obtain a representation of all the sine functions that define the kymograph (B). Using the frequency domain (forward Fourier transformation – FFT) of these sine representations makes it possible to extract the information relating to harmonic frequency and amplitude. A FFT of the complete sine image is too noisy (C) to reliably extract any harmonic information. By restricting the analysis to a single low noise region (the upper and lower boundaries) of the sine representation image (C) it's possible to obtain a cleaner FFT (D). The harmonic frequency is given by the distance from the centre pixel and the harmonic amplitude is given by the grey value (E). The most representative frequencies have higher amplitude. A threshold mask is applied to the FFT image (F) in order to restrict the analysis to frequencies with a amplitude higher than 200 grey values (G).

3.3 – Discussion

During this chapter, I have described the methods I had to develop in order to perform live imaging of E8.0 mouse embryos and chick embryos, as well as some methods to extract quantitative information from calcium transients. Since my DPhil relied heavily on performing live imaging, especially calcium imaging, it was important to establish what would be the best method to optimise the experiments and extract the most usable information possible. When performing live imaging, it is important to strike a balance between speed and resolution. While there have been other studies that have aimed to investigate cardiac physiology in the cardiac crescent and linear heart tube stages of heart development, they have either focused on isolated cells or performed calcium imaging on very small regions in order to perform line scan, which provides very scarce spatial information on the physiological dynamics of these stages. For this purpose, I have performed tests of a Laser Scanning Microscope, Spinning Disk Confocal and a lightsheet microscope (more details on the material and methods chapter).

In term of speed, the lightsheet microscope is the fastest in terms of acquisition of the whole heart, reaching speeds of 50 fps, equating to around 10 frames per beating cycle at the stages I was primarily examining. This is followed by the SDC which can reach speeds of 30 fps, and lastly the LSM which reaches speeds of 10 or 13 fps (depending on the model of the microscope), which equates to 3-4 frames per beating cycle. The LSM can also reach much faster speeds, but this would imply a significant compromise on spatial information by scanning smaller regions and/or reducing the resolution. Therefore, if speed alone was the crucial factor to decide on a microscope to perform these experiments, the lightsheet would be the microscope

of choice, especially considering that movement caused by a beating heart can originate severe imaging artefacts. However, there are other factors to take in account.

One of the main limitations of the lightsheet is that it is optimized to image one single embryos, making it difficult, sometimes impossible, to image more than one embryo in the same experiment. While this can be a drawback, it is somewhat compensated by the ability to rotate the sample on the axis perpendicular to the sheet of light, which allows the imaging of the sample from different angles, maximizing the information that can be obtained in terms of how the whole sample behaves during a particular developmental time. For this reason, the lightsheet microscope is useful when studying the whole embryo or when imaging for long periods of time. My thesis is focused on imaging the heart to study the processes involved in triggering the first heartbeats, therefore imaging other regions of the embryo besides the heart would provide little gain. Most of the long live imaging I performed was on developmental times prior or close to the first heartbeats, therefore artefacts due to movement of the sample are also minimal. The only scenario where movement artefact could be an issue was when performing calcium imaging on beating cardiac crescents, however for these experiments only one optical section was imaged in real time, which eliminates the problem of movement artefacts by sacrificing 3D information to increase speed of acquisition. On the other hand, using the set up described above for inverted microscopes, it is possible to image several embryos in the same experiment, optimizing the number of usable embryos per litter. The inability to image more than one embryo in the same experiment in the lightsheet microscope is also a drawback when it comes to performing pharmacological inhibition of the calcium transients, because the necessary volume of drug for a single embryo would be the same or higher (using media only in the syringe or in the whole chamber respectively) than

what is necessary to use in the confocal microscopes to image 6-10 embryos (the 10 embryos maximum is due to time limitations when performing the protocol of pharmacological inhibition used here).

Finally, in terms of resolution, at similar magnifications, the data obtained from the Z1 Lightsheet and the LSM is very similar when performing calcium imaging, and both allow the simultaneous acquisition of fluorescence and brightfield channels. When performing overnight live imaging the resolution of the LSM is indeed higher than the lightsheet, because it is no longer necessary to compromise resolution for speed. When doing overnight live imaging with the lightsheet is also not advisable to acquire a brightfield channel, because with the microscope used here it would imply leaving the white light on during the whole duration of the experiment. In the lightsheet microscope, because the heart is parallel to the light source, and the light has to travel not only through a large portion of the embryo but also through the agarose, the quality of image decreases when imaging the inner layers of the heart (fig. 3.3 – E, black arrows), which is required for experiments described in chapter 5. The ability to image several embryos in the same experiment, acquire a brighfield image, the higher resolution and the capacity to image fast enough to perform calcium imaging led me to choose the LSM as the microscope of choice to perform the majority of experiments required for my thesis. The only exception was the use of the SDC to acquire brightfield images of cardiac contractions at different stages, which was initiated by Dr. Chiann-Mun Chen and Dr. George Trichas.

In order to extract quantitative information from calcium imaging and brightfield cardiac contraction images I developed two Fiji plug-ins. The first allow the extraction, at any given pixel, of the duration of an event such a calcium transient, as well duration of the period between events. The second plug-in allows the extraction of information

regarding harmonic frequency and amplitude of periodic events. It is important to note that both these plug-ins give approximated values. This is not an issue with images acquired at lower bpms, such as the images obtained at 10 or 13 fps from the LSM, since each event is represented over 4-5 frames, therefore approximations that rely on the detection of number of frames are unlikely to fail because the acquisition itself it is not a precise representation of the event. However, with faster frame rates, since the event has more representative frames, it is more likely underestimate the duration of a transient by a few frames, and at the same time, overestimate the duration of the intervals. While the measurements of harmonic frequency are not affected by frame rate, they are affected by the amount of grey levels. This can make the choice of an amplitude threshold somewhat subjective, hence some variation in the measurements is expected. The amplitude value should then not be used as direct quantitation but only as a measure of how representative of the periodicity within a single embryo a certain harmonic frequency is, i.e., amplitudes from different embryos are not comparable. The advantage of these methods when compared to existing methods is that do not rely on programing knowledge and can be easily applied to any image given with minimal manipulation. It is important to note that the imaging techniques use here are also limited in terms of frame rate, therefore, these quantifications while accurate for the given dataset, may be misrepresenting to a small degree the actual biological event. Nevertheless, it should be possible to apply these methodologies to other types of datasets of periodic events as long as precautions are taken in terms of frame rates and intervals during time-lapses.

For all culture experiments, including the live imaging experiments described in this chapter, the embryos were cultured in a 1:1 ratio of CMRL and Knockout Serum Replacement (KOS). It should be noted that the traditional culture methods of post-

implantation mouse embryos, and especially post-gastrulation embryos, typically involves the use of homemade rat serum, either by itself or mixed with DMEM (*101, 102*). I opted to use KOS instead of rat serum in order to decrease variability inherent to the use of non-standardised substances. Furthermore, the use of serums has been shown to create variability in gene expression when used to culture ESCs (*103*), further demonstrating the importance of developing serum-free alternatives such as the methods developed for mid-gestation mouse embryos (*104*). Therefore, this method represents an update of published culture methods previously used in the lab using CMRL and mouse serum (*105*). While it is not possible to assess the effect of KOS in short term cultures such calcium imaging, after 12 hours of culture, E7.5 embryos develop headfolds, the cardiac crescent and somites, suggesting that KOS does not impact development, with roughly 80% of embryos developing as expected. Further research would have to be performed in order to fully compare the consequences of culturing with serum or KOS, at the level of gene expression, morphology and physiology.

Chapter 4 – Characterization of the First Embryonic Cardiac Contractions

4

Table of Contents

4.1 – Introduction

4.1.1 – First Cardiac Contractions During Embryo Development

As mentioned in Chapter 1, the heart primordium is the first organ to form during embryonic development. One of the defining characteristics of cardiomyocytes it is their ability to spontaneously contract. The observation of the first cardiac contractions has always been a hallmark of heart development studies. Several authors have described the stage of initial cardiac contractions in different species, from the most commonly used models in developmental biology such as mouse (*106*), rat (*107*), chick (*108*) and zebrafish (*109*) to even canids (*110*). Even as early as beginning of the 20th century there has been an interest in establishing when cardiac contractions can be visualised for the first time, how cardiac contractions influence embryo development and vice-versa. Looking at the literature it is evident that the first cardiac contractions can be observed during the transition of the heart primordium to a linear heart tube. Despite this early interest, with the development of modern molecular biology techniques, the focus of research performed in heart development has shifted to understanding the genetic mechanisms involved in heart morphogenesis and the lineage determination of cardiac cells. While lineage and genetic studies are undoubtedly crucial to understand heart development, there is a lack of understanding of the interplay between cardiac function and morphogenesis and how these mechanisms are regulated.

Traditionally, studies regarding the initial cardiac contractions have been performed mainly using chicken embryos and whilst there have been informative papers using mammalian models that have suggested early pacemaker activity on

both sides of the embryonic midline (*111*), as well as spontaneous action potentials in rat (3-somite stage) (*112*) and mouse (3-somite stage) (*113*), these lack spatial and temporal resolution, and do not fully explore the mechanisms behind this process. Despite this interest, due to the used of different models and ways to stage embryos, it is still unclear what is the precise moment when cardiac contractions start. Besides the studies that have aimed to characterise the early cardiac contractions, there have also been recent reports of the implications of the forces created during cardiac contractions for embryonic development, including for the development of the epicardium and for the regulation of gene expression (*114, 115*). Therefore, due to the inherent importance of having beating cardiomyocytes and the apparent role that cardiac forces play in regulating cardiac development, it is important to gain a better understanding on the progression of the embryonic cardiac physiology, how it is regulated and how does it translate do changes in morphogenesis.

In this chapter, I will describe the work I performed together with Dr. Richard Tyser to definitely characterise the onset of cardiac contractions in mouse embryos, including the characterisation of the ion channels and transporters necessary for calcium handling at cardiac crescent stages of heart development and how the inhibition of these proteins impacts the expression of cardiac-related genes

4.1.2 – Cardiac Physiology During Development

In mature cardiomyocytes, coordinated electrical excitation is coupled to physical contraction in a process termed excitation contraction coupling (ECC) (*116*). ECC relies on changes in the intracellular concentration of the second messenger Ca^{2+} via release from the sarcoplasmic reticulum (SR) in a process termed Ca^{2+}

induced Ca^{2+} release (CICR) (*117*). Increases in the concentration of intracellular Ca^{2+} result in cardiomyocyte contraction due to Ca^{2+} binding to troponin and myofilament activation. ECC involves a number of specific proteins including L-type Ca^{2+} channels (LTCC, sarcolemmal Ca^{2+} influx), ryanodine receptors (RyR2, SR Ca^{2+} release), the sarcoplasmic reticulum Ca^{2+} ATPase (SERCA, SR Ca^{2+} uptake) and the Na^{+}/Ca^{2+} exchanger (NCX, Sarcolemmal Ca^{2+} efflux). Targeted disruption of genes encoding ECC proteins in mice has shown that contractile activity of immature cardiomyocytes does not require ECC. Embryonic cardiomyocytes have a less developed SR and T-tubule system as well as an increased requirement for sarcolemmal Ca^{2+} flux (*118, 119*) and whilst they express a variety of ion channels and exchangers present in the adult heart (*120-122*), the expression and activity of these proteins is distinct from that in mature cardiomyocytes (*123*). Using isolated cells as well as genetically manipulated animals, two contrasting mechanisms have been proposed for how Ca^{2+} transients are generated in the developing heart from approximately E8.5 onwards. Early studies suggested that myocyte contraction is triggered by sarcolemmal Ca^{2+} influx through voltage activated Ca^{2+} channels with little or no contribution from the SR (*124, 125*). In contrast, more recently it has been shown that at ~E8.5–9, Ca^{2+} transients originate from the SR, via RyR together with $InsP_3$ channels, to trigger electrical activity as well as contraction (*126-129*). Whilst these studies characterised SR function at ~E8.5–9, they did not investigate how Ca^{2+} transients are regulated at the earliest stages of cardiac crescent development when contraction is initiated, and relied on experiments performed using isolated cells cultured for between 12 to 70 hr (*128, 129*). Thus, there is a lack of cellular resolution *in vivo* and no current mechanistic insight into the onset of Ca^{2+} handling and its impact on differentiation and cardiogenesis.

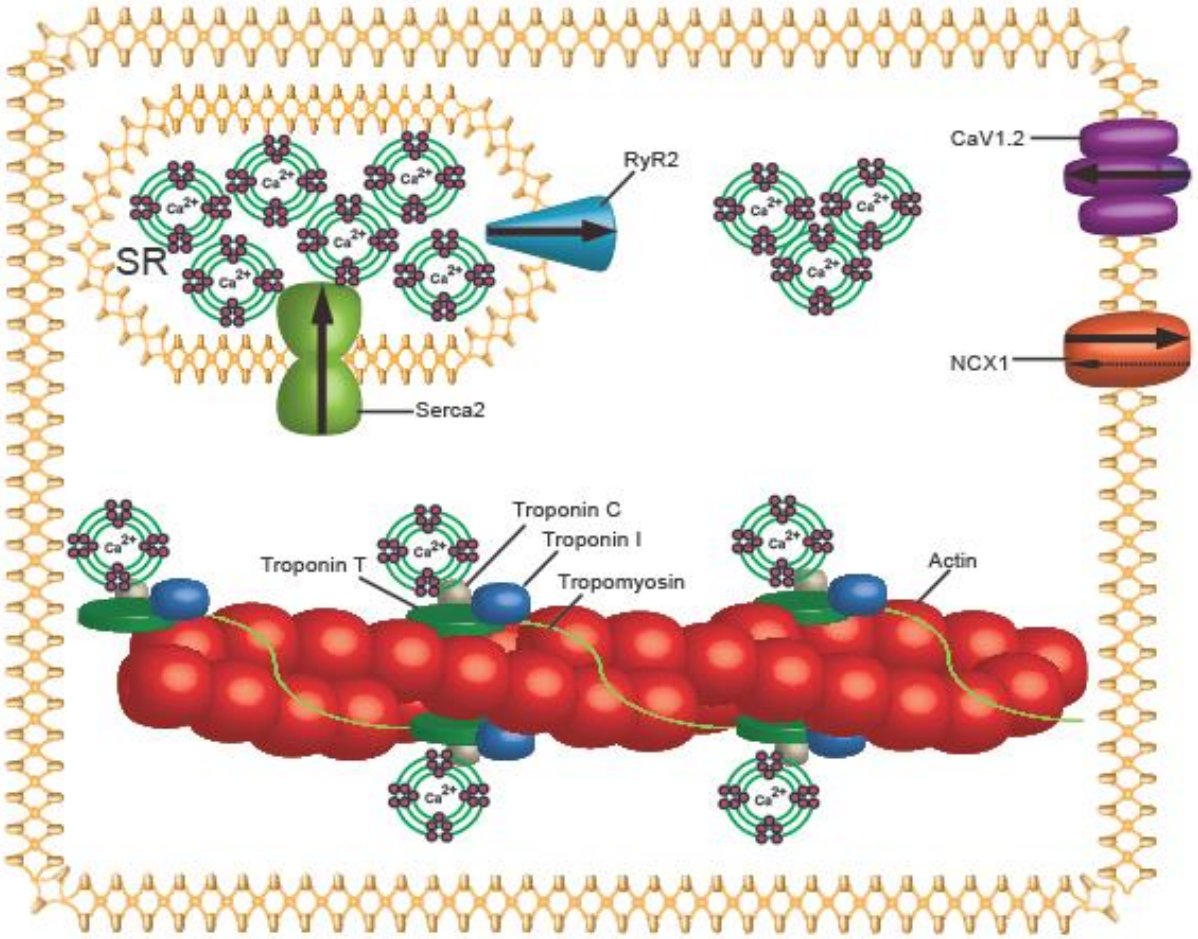

Fig. 4.1 – Schematic of ECC in the cardiac muscle – Calcium ions enter the cell through the L-type calcium channels (composed of CaV subunits). This small increase in calcium leads to the opening of the Ryanodine receptors (RyR) in the Sarcoplasmic Reticulum (SR), promoting the release of calcium ions from this compartment. This calcium ions then bind to the troponin complex, enabling the interaction with myosin heads, causing the actin filaments to slide and the cell to contract. After the contraction, the calcium ions are released from the troponin complex, causing the relaxation of the cell. The ions then enter the SR via SERCA2, with a small amount leaving the cell via the sodium calcium exchanger (NCX). Black arrows represent the direction of calcium movement. It has been proposed that NCX1 may also work in reverse mode to bring a small amount of calcium ions inside the cell.

4.1.3 – Establishment of left-right asymmetry

The establishment of the internal left-right asymmetry is one of the most important, and widely studied mechanisms in development. Asymmetry of internal organs is fundamental for vertebrate life, and dictates organ function itself. While a complete reversal of left-right asymmetry (*situs inversus totalis*) is not lethal, and organisms can lead a normal life, a complete loss of asymmetry (isomerism) is embryonically lethal.

Left-right asymmetry is first established at the level of gene expression shortly after gastrulation, prior to proper, organogenesis, when *Nodal* expression becomes restricted to the left side of the embryo, especially in the lateral plate mesoderm (LPM). This confinement of *Nodal* to the left side of the embryo leads to expression of the transcription factors *Lefty2* and *Pitx2*, stabilising the differential left-right expression in the embryo and effectively establishing the left-right axis (reviewed in (*130*)). Interestingly, the mechanism for establishing the initial *Nodal* asymmetry does not seem to be the same in all species. In mouse, left-right asymmetry arises through leftward liquid flow established by motile cilia in the node, a structure at the distal tip of the egg cylinder (*130*). This nodal flow model seems to be specific to mouse. In chick, a leftward movement of cells seems to occur at the Hensen's node, leading to asymmetric expression of *Shh* (*131*), which does not seem to occur in mouse. Regardless the method of symmetry breaking at the node, there are many unknowns regarding the mechanisms from which these signals at the node are transmitted to other tissues. One of the hypothesis is the transmission of these signals are done through asymmetric propagation of ion channels, such as Ca^{2+}, and in fact several

channels and pumps have been implicated in left-right asymmetry (*132*). The definitive endoderm has also been suggested as a possible signalling centre involved in left-right asymmetries (*133*).

Left-right asymmetry pathway are also essential for heart development, and in fact, cardiac looping is the first morphological symmetry-breaking event in embryonic development. However, left-right asymmetries are not only important for cardiac looping, but mutations in this pathway as been shown to be involved in several other cardiac phenotypes, such aortic arches defects (reviewd in (*134*)). Furthermore, in the adult heart, PITX2 has been associated with atrial fibrillation, and has been shown be activated by TBX5, regulating the expression of ion channels such as *Ryr2* and *Atp2a2* as well as proteins of the contractile machinery (*135, 136*). A study in zebrafish has also purposed a Nodal-independent mechanism during cardiac looping (*137*), suggesting a complex series of regulatory events in the establishment of left-right asymmetry of this organ.

4.2 – Results

4.2.1 – Staging of Early Heart Development

Despite some reports stating otherwise (*106, 113, 122, 138, 139*), it is still commonly thought in the field that the first cardiac contraction can be observed concomitant with the formation of the linear heart tube (*17*). One of the problems with establishing a precise moment for the first cardiac contractions arises with the methodologies used to stage embryos. While more traditional papers provide some degree of morphological description of the heart at the moment that cardiac

contractions can be observed, it has become commonplace to stage embryos using either embryonic day or somite number. Embryonic day is a very broad staging method, it does not take in account intra-litter variability, and perhaps more importantly different genetic backgrounds develop at different rates, making it difficult to compare results obtained from different strains of mice (*127, 139*). The use of somite number offers a more precise method of developmental staging than embryonic day, however it is still variable in its correlation to the overall embryonic stage (*140*), not offering a sufficiently fine-grained proxy for developmental stages of the heart. This can lead to ambiguities, as for example a '3-somite' embryo may refer to an embryo with at early cardiac crescent stage, or at the point where the LHT is practically formed. In order to precisely define the moment where the first cardiac contractions can be observed I created a staging system specific to the early heart, from early crescent to LHT (fig. 4.2) similar to studies at later stages when a more precise morphological characterization was necessary (*141*). I defined four stages (0, 1, 2 and 3) of cardiac crescent development prior to complete fusion of the two bilateral cardiac primordia and formation of the LHT, based on the ratio between width of the cardiac crescent (fig. 4.2 – white dotted line) and maximum height at the bulging regions (fig. 4.2 – green dotted line). Stage 0 hearts are defined as the first discernible crescent structure situated beneath the developing head folds, being the widest (360–390 μm along the medio-lateral axis) and thinnest (70–80 μm along the rostro-caudal axis) of the crescent stages. Whilst no new morphological landmarks emerge by stage 1, this stage is defined as a narrower (300–370 μm) and thicker (75–95 μm) cardiac crescent. By stage 2, folding of the cardiac crescent is evident based on the formation of a trough at the embryonic midline and two lobes on either side. As the embryo transitions to stage 3 this trough becomes less obvious due to the rostral-caudal elongation of the

heart as the LHT begins to form. Transition from stage 3 to the LHT was defined by the complete fusion of the two lobes and loss of the central trough (fig. 4.3).

4.2.2 – Initial Cardiac Contractions

To further characterize the different stages of cardiac crescent maturation, we performed immunostaining for three proteins of the cardiac contractile machinery: sarcomeric α-actinin (α-Act), a protein of the Z-line; Myomesin (Myom), a protein of the M-line and cardiac Troponin T (cTnT), the Tropomyosin binding subunit of the troponin complex (fig. 4.3 and 4.3). At stage 0, cTnT was the most evident contractile protein within the early cardiac crescent, albeit without sarcomeric banding (fig. 4.3 - A). Both α-Actinin and Myomesin appeared in small clusters of cells at stage 0 (fig. 4.3 - A). Sarcomeric banding of these proteins, indicative of contractile capability, is visible within discrete regions within stage 1 and 2 crescents (fig. 4.3 – B, C; fig. 4.3 – B, C). With these stainings it was not possible to say if any particular region within the cardiac crescent is enriched for sarcomeres. By stage 3, sarcomere assembly and myofibrilar banding became uniform and well defined, coincident with coalescence of the bilateral cardiac primordia to the embryonic midline (fig. 4.3 – D; fig. 4.3 – D), similar to the pattern observed at LHT (fig. 4.3 – E; fig. 4.3 – E).

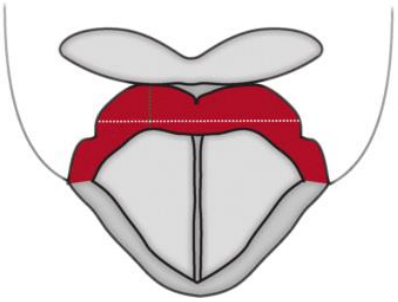

Stage	Width (µm)	Maximum Height (µm)	Width/Height Ratio	Somite Number	Embryonic Day
0	360-390	70-80	4.5-5.5	0-2	E7.75-E8.0
1	300-370	70-95	3.0-4.2	1-3	E8.0-E8.25
2	230-280	95-120	2.0-2.8	2-4	E8.0-E8.5
3	200-230	120-140	1.5-1.8	3-5	E8.25-E8.5

Fig. 4.2 – Staging of early heart development prior to the formation of the Linear Heart Tube – Progression of cardiac crescent development was staged based on the ratio between t the width (white stripped line) and the maximum height (green stripped line) of the cardiac crescent. This method allows staging with more precision was there is a high variation in both somite numbers and within embryonic days. These measurements were derived from 10 embryos per stage.

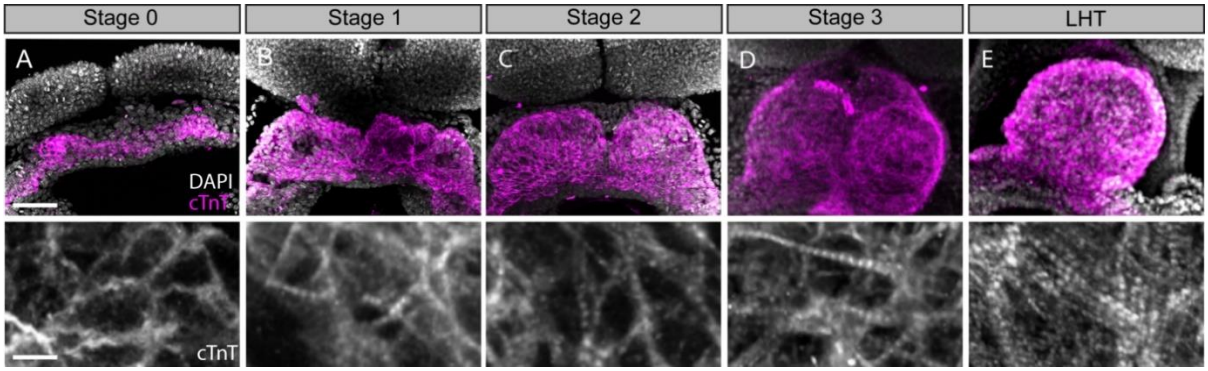

Fig. 4.3 – Confocal imaging of embryos stained for cTnT at different stages of early heart development – Embryos at different stages were stained for cTnT, a component of the troponin complex of the contractile machinery. A functional muscle cell is characterised by the appearance of sarcomeric banding (striated pattern). Sarcomes are detected for the first time on stage 1 embryos (A). Scale bars: top –100 µm; bottom – 10 µm. N=6 per stage. Secondary control can be found in annex 1.

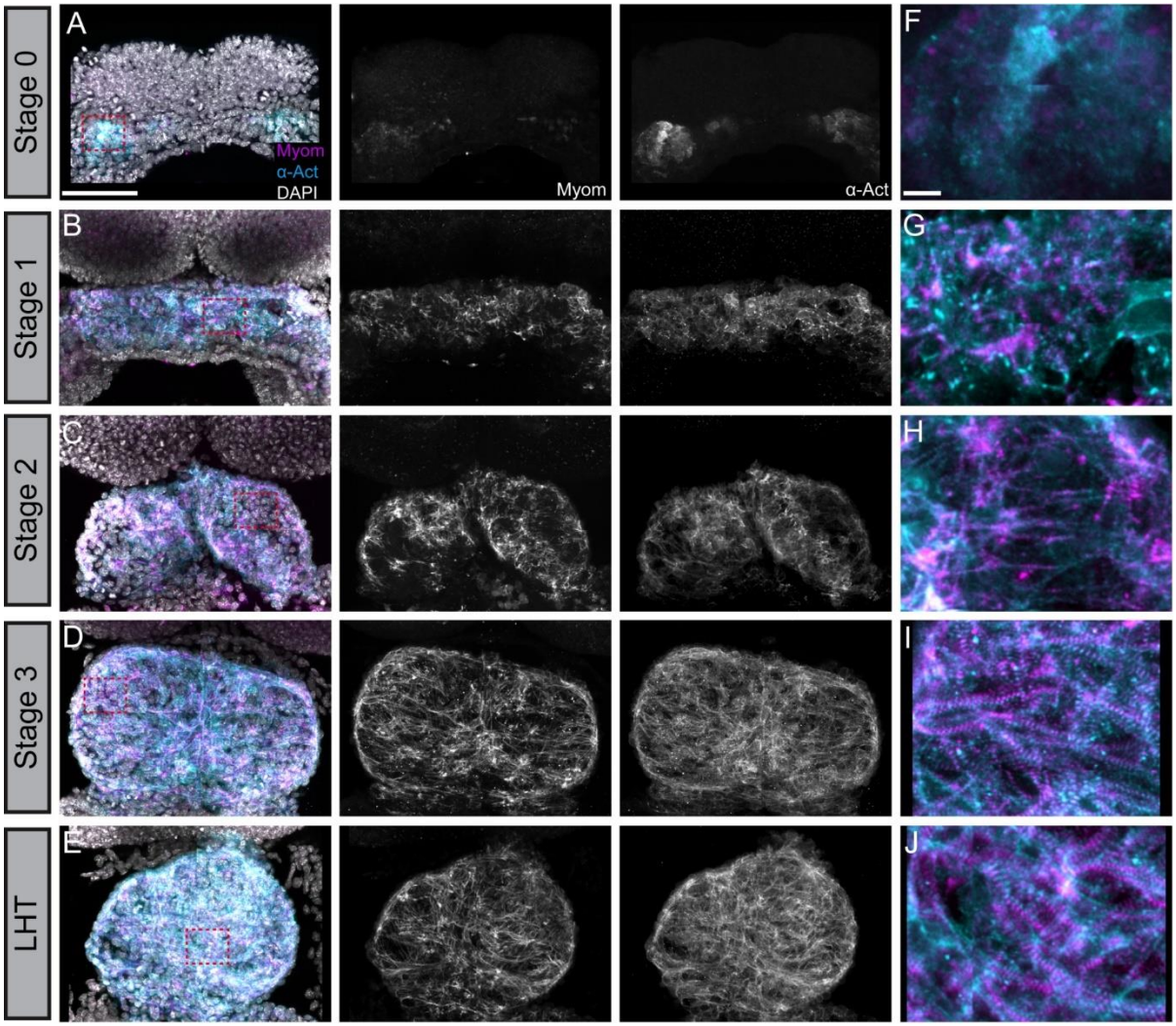

Fig. 4.4 – Confocal imaging of embryos stained for Myomesin and α-Actinin at different stages of early heart development – Embryos at all stages of cardiac crescent development were dual stained from myomesin (magenta), a component of the m-bands of the contractile machinery, and α-actinin (cyan), a component of the z-bands of the contractile machinery. More mature cardiomyocytes display an alternating striated pattern of these proteins. Both proteins are detected at stage 0 in the lateral regions of the cardiac crescent (A, F) but do not show striations. Some striations can be observed at stage 1 (B, G), but become more visible at stage 2 (C, H). Scale bars: A-E – 100 µm; F-J – 10 µm. N=5 per stage.

Coincident with sarcomere formation at stage 1 (fig. 4.3 – B, C; fig. 4.3 – B, G), the first cardiac contractions can be observed at stage 1, by differential interference contrast (DIC) imaging followed by GView analysis (fig. 4.5 – A, red arrows), significantly earlier than previously described (*106, 113*). GView analysis has been explained in chapter 3. Of the embryos analysed at this stage there are no visible contractions in the centre of the cardiac crescent, 3 of which had contractions visible solely on the left side. These foci generally contracted at the same rate, and roughly with the same phase, indicative of either synchronization or a shared intrinsic beat rate for nascent cardiomyocytes (fig. 4.5 - B). This heterogeneity in contracting regions at stage 1 disappears by stage 2, with cardiac contractions observable throughout the whole tissue. At stage 1, cardiac contractions occurred at a frequency of approximately 30 beats per minute (bpm), which increased significantly by stage 3 to around 60 BPM (fig. 4.5 - C). When cultured over a period of several hours, starting at stage 1, it is possible to observe an initial increase in beat rate, reaching a rate above 50 bpm, reflecting approximately the beat rate of freshly dissected embryos at equivalent stages (fig. 4.5 – D, 2,4 and 8 hours). After 12 hours of culture the beat rate significantly drops to rates below 40 bpm, similar to stage 1 and 2 embryos, possibly reflecting abnormal development (fig. 4.5 – D, 13 hours).

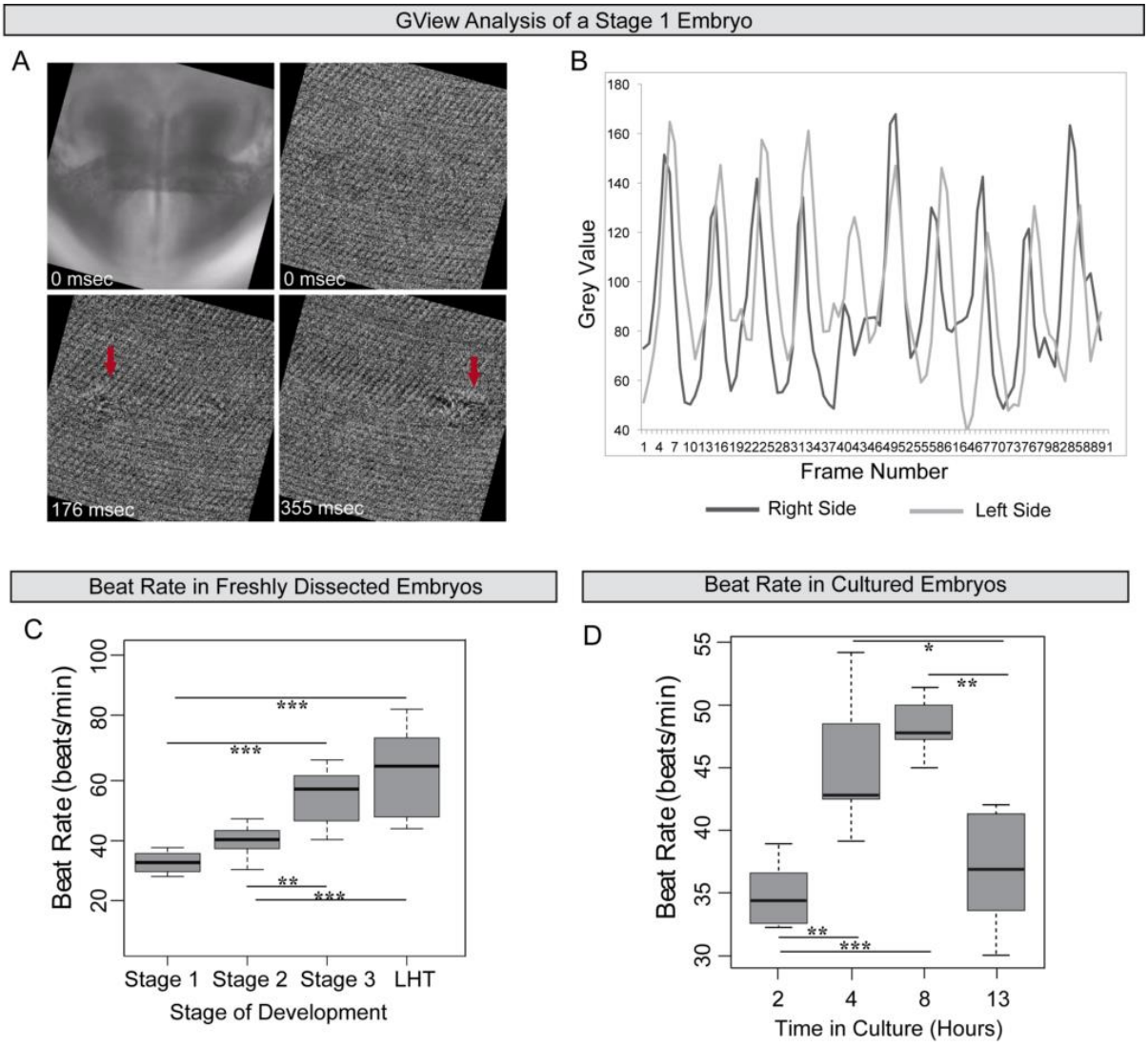

Fig. 4.5 – Imaging and quantification of the first cardiac contractions – Freshly dissected embryos were imaged in a spinning disk confocal using DIC imaging and analysed using GView (A). (B) Representative trace of beating profiles of a stage 1 embryo, showing some degree of synchronisation between the right and left sides of the cardiac crescent. (C) Quantification of beat rate of freshly dissected embryos at different stage of development (Stage 1, n = 12; stage 2, n = 8; stage 3, n = 10; LHT, n = 7). (D) Quantification of changes in beat rate of stage 1 embryos over 13 hours in culture (n = 7). (*p<0.05; **p<0.01; ***p<0.001).

4.2.3 – Calcium Imaging

In order for muscle contractions to occur, Ca^{2+} flux is necessary. To investigate the earliest manifestations of Ca^{2+} handling within the cardiac crescent, I loaded embryos with the fluorescent Ca^{2+} dye Cal-520 followed by live imaging using confocal microscopy. In order to minimize effects that imaging may have on the physiology of the cardiac crescents, the embryos were imaged only for a period not exceeding 20 seconds. I first imaged embryos on stages with overt beating, i.e. stage 1 to LHT. On stage 1 until stage 3 crescents, calcium transients are observable throughout the cardiac crescent propagating laterally (fig. 4.6 – A). As the cardiac crescent starts to fuse to form the LHT, the transients switch from a lateral to a more caudal-rostral propagation, as has been described previously.

Since calcium transients can be observed throughout the tissue at stages with overt beating, I then performed similar experiments at stage 0 embryos in order to try to capture the moment calcium transients are properly established. Unlike the stages analysed previously, at stage 0 calcium transients cannot be observed throughout the cardiac crescent as a propagating wave. Instead, individual cells, or small cluster of cells, sporadically show increase in intracellular calcium (fig. 4.6 – B). We termed these oscillations spontaneous asynchronous Ca^{2+} oscillations (SACOs). SACOs were observed in all stage 0 cardiac crescents imaged (n = 35). Within a single stage 0 cardiac crescent, SACOs displayed a wide range of physiological dynamics (fig. 4.6 – C, C'). Within a cardiac crescent for 1-minute period, cells could display a single SACO (fig. 4.6 – C', green and purple lines), or could show several oscillations (fig. 4.6 – C', red and blue lines). SACOs also varied in duration, however even the fastest SACOs last for a couple of seconds, with fluorescence reaching peak intensity

between 0.79 and 11.9 s and decreasing at a similar slow rate, slower than the propagation of the calcium transients throughout the whole cardiac crescent at stage 1. In fact, at high magnifications it is possible to observe the propagation of the SACOs within an individual cell (fig. 4.6 – C''). During 20 seconds recording periods, we observed only 10.3 ± 0.7 individual SACOs per embryo (n = 35) occurring in different sites. Consecutive SACOs in the same site were rarely observed within the 20 seconds imaging window and, therefore, we conclude that SACOs in individual cells occur at a frequency < 3 opm (oscillations per minute). From the embryos imaged there did not seem to be any sort of pattern in the manifestation of SACOs. It is worth noting after the identification of SACOs at stage 0, a more careful look at data obtained from stages 1 to LHT revealed that some cardiac cells still show SACOs even though a calcium transient is propagating throughout the tissue. Interestingly, at these stages, the calcium transient doesn't seem to propagate thought cells that still show SACOs.

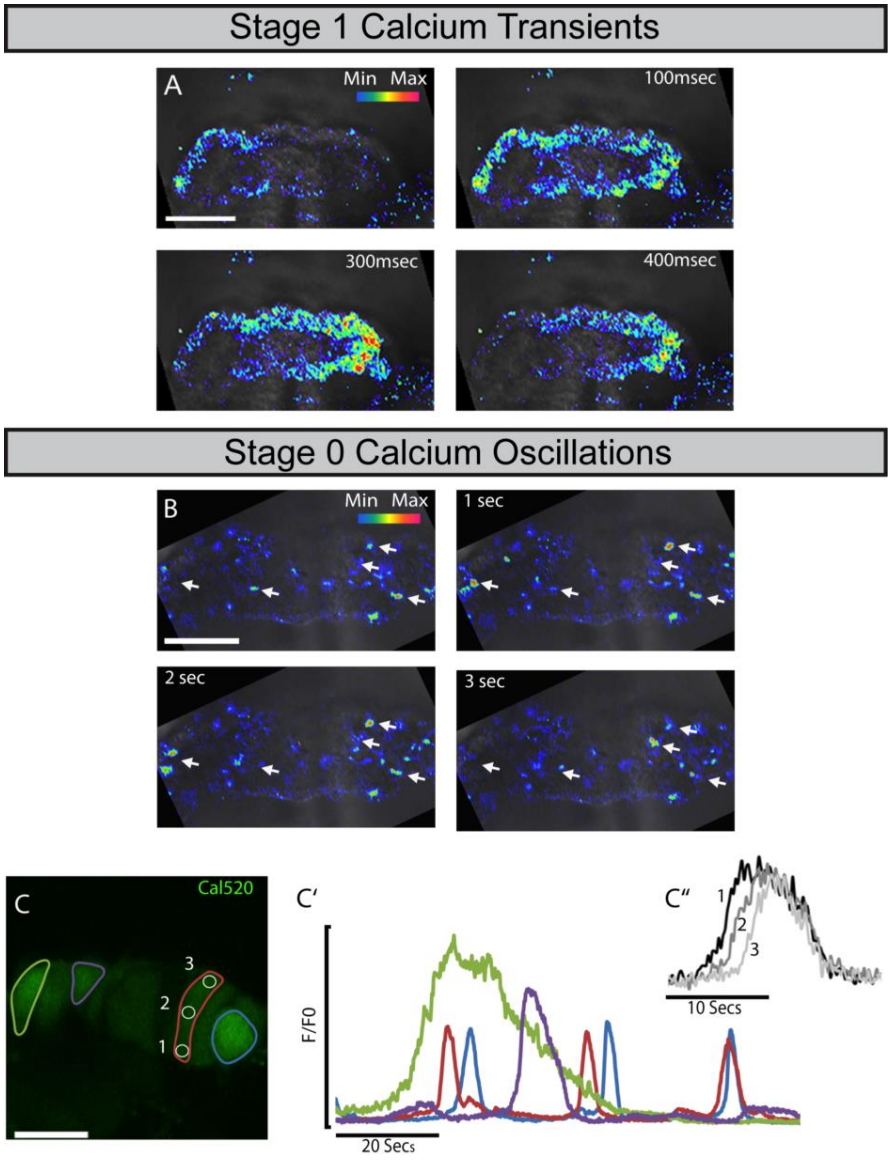

Fig. 4.6 – Calcium Imaging of Stage 1 and Stage 0 mouse embryos – Freshly dissected embryos were stained with cal-520, a calcium dyes, and imaged in a confocal microscope over short periods of time. (A) Representative movie of calcium transients in a stage 1 embryo, showing lateral propagation of the calcium transient. (B) Representative movie of calcium imaging on a stage 0 embryo, showing SACOs (white arrows). (C) Higher resolution imaging of SACOs in a stage 0 embryo, showing variation in the oscillations (C') and propagation within a cell (C''). Scale bars: A-B – 100 µm; C – 20 µm.

To further characterise these stages of heart development, we performed RT-qPCR analysis for key contractile machinery and ECC components (fig. 4.7). The samples used consisted of whole E7.75 embryos as baseline and cardiac mesoderm isolated form all the stages described in fig. 4.2. For components of the contractile machinery, we analysed the gene expression of *Myom1* (encoding Myomesin), *Actn2* (encoding α-actinin) and *Tnnt2* (encoding cardiac Troponin T). *Myom1, Actn2* and *Tnnt2* expression significantly increased between stages 0 and 1 and continued to increase until formation of the LHT (fig. 4.7 – A-C). In fact, there is a statistically significant increase in the levels of *Myom1* and *Actn2* between each cardiac crescent stage, further confirming that the heart development stages defined here truly reflect a gradual increase in cardiac differentiation. ECC components and specifically NCX1, have not previously been implicated in the initiation event of cardiac contraction, nor investigated at the earliest stages of heart development coincident with the onset of beating. In order to gain a better understanding of the physiological mechanisms behind the first cardiac contractions we then assessed the gene expression of the main ECC components, focusing specifically on the sarcolemma components (fig. 4.7 – D, E) *Slc8a1* (encoding NCX1), *Cacna1c* and *Cacna1d* (encoding the LTCC subunits, CaV1.2 and CaV1.3 respectively), and the SR components *Atp2a2* (encoding SERCA2), *Iptr2* (encoding InsP3 type 2 channels) and *Ryr2 (*encoding RyR2) (fig. 4.7 – F-H). Between E7.75 (as defined by the presence of clear head-folds but not a cardiac crescent) and stage 0, *Slc8a1* significantly increased 21x (p-value<0.001), whilst *Cacna1c* revealed a non-significant increase of 2.5 fold (p-value>0.05) and *Cacna1d* a significant 4x increase (p-value <0.01). From stage 1 onwards *Slc8a1, Cacna1c* and *Cacna1d* expression continued to significantly increase until stage 3 (fig. 4.7 – D, E; *Slc8a1*, 234x; *Cacna1c,* 38x; *Cacna1d,* 41x). Between

stage 3 and the LHT, expression of *Slc8a1* and *Cacna1c* was maintained whilst *Cacna1d* significantly decreased (fig. 4.7 – E). Previous studies that aimed to investigate early cardiac physiology have suggested a non-ECC dependent role for the SR during development, implicating both InsP3 and RyR channels (*127-129*). While *Ryr2* significantly increased 30x between E7.75 and stage 0 (p-value<0.001), expression of *Atp2a2* only increased 1.7x (p-value<0.05) and *Iptr2 did not* significantly change (p-value>0.05; fig. 4.7 – F-H).

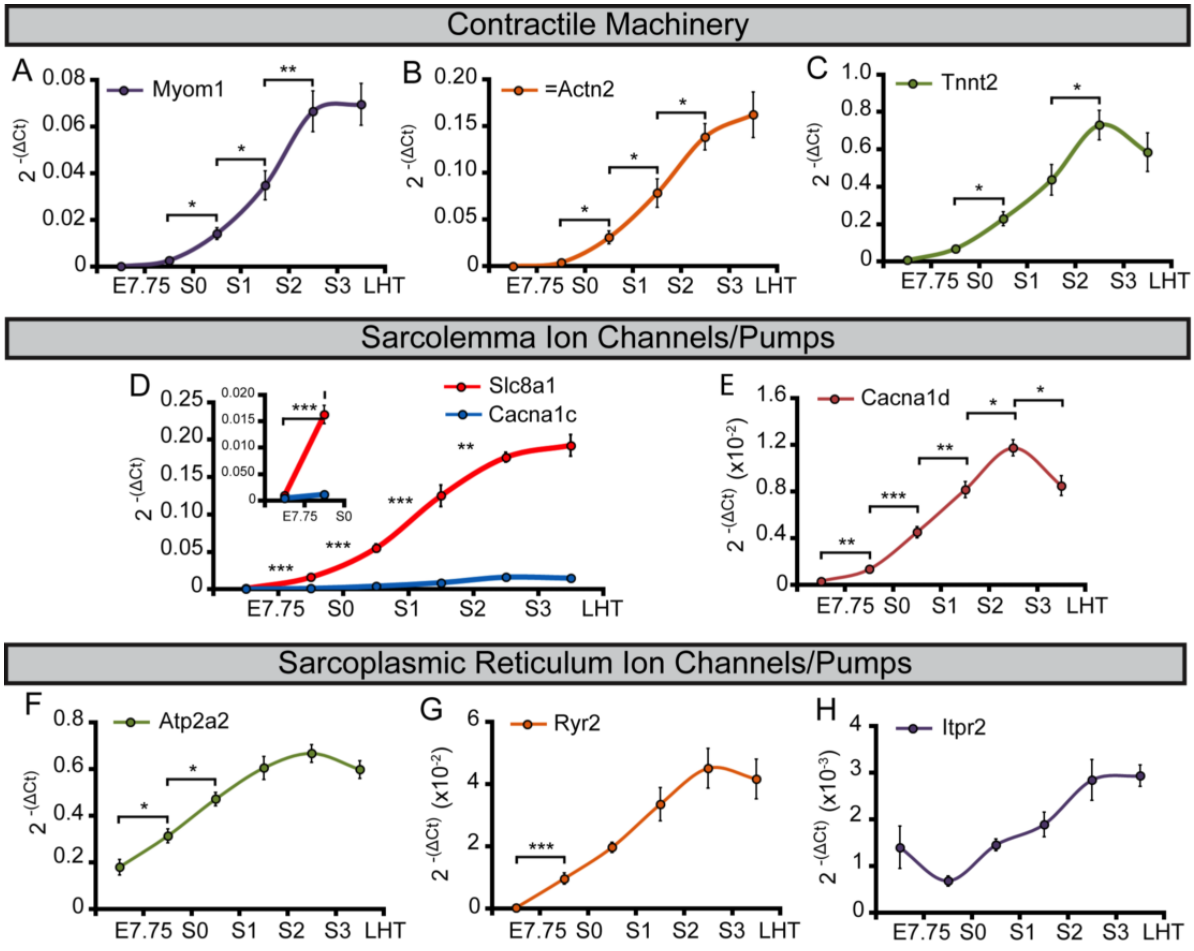

Fig. 4.7 – RT-qPCR analysis of genes required for cardiac contractions – RT-qPCR was performed with E7.75 embryos and mesoderm from all cardiac crescent stages and LHT (n = 5 samples, per stage, each sample composed of 6-10 embryos). RT-qPCR was performed on components of the contractile machinery (A-C), previously shown on immunostainings, sarcolemmal proteins (D-E) and SR proteins (F-H). Slc8a1, encoding for NCX1, shows a drastic increase between E7.75 and Stage 0 (D). (*p<0.05; **p<0.01; ***p<0.001).

Since the sarcolemmal channel genes revealed the most significant increases over the developmental time course, we proceeded to investigate spatiotemporal protein expression of NCX1 and CaV1.2 in embryos (fig. 4.8). At stage 0, NCX1 was clearly detectable within the cardiac crescent (fig. 4.8 - A), whilst CaV1.2 was absent (fig. 4.8 - B). This difference in the protein localization of NCX1 and LTCC was not maintained at later stages with both channels appearing to be localized at the level of the cell membrane within the cardiac crescent (fig. 4.8 - B). Collectively with the gene expression data, these data suggest that NCX1 precedes Cav1.2 within the developing cardiac crescent at stage 0, being present prior to and at the onset of both SACOs and beating, whereas Cav1.2 became upregulated later from stage 1 onwards. Of note, while NCX1 and CaV1.2 signal was detected in other regions of the embryo, notably in the head folds, in contrast to the heart it was not membrane localised in these regions. Furthermore qRT-PCR data for isolated head folds did not reveal any significant increases in *Slc8a1* or *Cacna1c* expression, from E7.75 through to LHT stages (p-value>0.05) even though the head folds were maturing, as shown by morphological changes and expression of the neural ectoderm marker *Sox1* (E7.75 versus LHT, p-value<0.001)

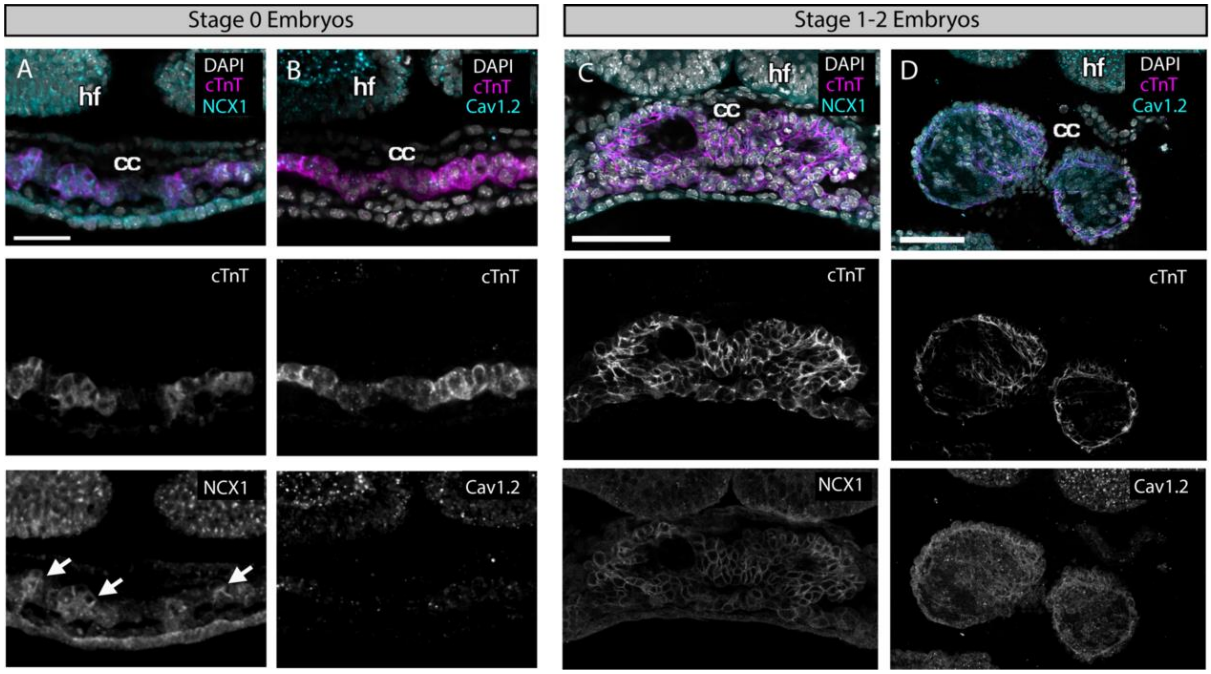

Fig. 4.8 – Confocal imaging of embryos stained for NCX1 and Cav1.2 at different stages of early heart development – Embryos were stained for the sarcolemmal proteins NCX2 and Cav1.2 (LTCC), prior to overt beating (A-B), and when beating is observable (C-D). NCX1 is membrane localised on stage 0 embryos (A, white arrows), however Cav1.2 is only membrane localised at later stages (D). hf = head folds; cc = cardiac crescent. Scale bars = 100 µm.

4.2.4 – Pharmacological Inhibition

To functionally assess the roles of the sarcolemmal and SR channels in establishing and maintaining heartbeat, we employed pharmacological blockade on embryos maintained ex-vivo. For experiments aiming to inhibit NCX1 we used the inhibitors CB-DMB (*142*) or KB-R7943 (*143*), nifedipine to block LTCC (*144*) and Ryanodine together with 2-APB to simultaneously block RyR and InsP3, similar to that described previously (*128, 129*). Treated embryos were imaged for contractile activity by DIC imaging and Ca^{2+} transients were recorded in parallel with confocal fluorescence imaging of Cal-520. Acute treatment (for a maximum of 30 min) with the above-mentioned inhibitors affected the embryos in stage specific manner (fig. 4.9).

Treatment of stage 0 embryos with CB-DMB and KB-R7943 resulted in most cases of a complete abolishment of SACOs after drug application when compared to baseline (fig. 4.9 – A). On the other hand, SACOs were still observable after treatment with Nifedipine (fig. 4.9 – B). Quantification of the number of observable SACOs revealed a 90% decrease upon treatment with CB-DMB and KB-R7943). This was significantly greater than following application of nifedipine to inhibit LTCC, or the DMSO control (CB-DMB, 90% inhibition $\pm$ 6.6, mean $\pm$ SEM, n = 10 embryos, p-value <0.01; KB-R7943, 91% inhibition $\pm$ 7.0, n = 9 embryos, p-value <0.001; nifedipine, 39% inhibition $\pm$ 11.4; n = 8 embryos, p-value=0.44; DMSO, 29% inhibition $\pm$ 7.6, n = 10; fig. 4.9 - E). This data, together with the expression data presented above suggest that NCX1 is a key element in maintaining SACOs at stage 0 embryos. At this stage, the embryos were only treated for a maximum of 15 since at 30 minutes even DMSO treated embryos showed a complete abolishment of SACOs.

Both NCX1 and the LTCC were required for Ca^{2+} transients during stages 1 and 2 (fig. 4.9 – C, D, F), as their inhibition led to an initial confinement of Ca^{2+} transients to one side of the crescent (within approximately 5 min of treatment, which persisted through to 15 min) followed shortly afterwards by complete loss of Ca^{2+} signal in most embryos, although some embryos treated with CB-DMB retained the confinement (fig. 4.9 – C, D). For quantification purposes, inhibition was considered to be any effect on the propagation of the calcium transient and includes both confinement and complete abolishment. At these stages, Nifedipine seems to have a more immediate effect, with a statistically significant effect on calcium transient, with 80% of embryos affected after 15 minutes of treatment (fig. 4.9 – F). Nevertheless, after 30 minutes all treatments, with the exception of DMSO, led to inhibition in 100% of the embryos. At stage 3 and later, only the LTCC was required for Ca^{2+} transient generation, albeit not all embryos at this stage were affected, even after 30 minutes of treatment (fig. 4.9 - G). Treatment with Ryanodine + 2-APB, to assess the contribution of the SR in maintaining calcium transients at these stages, only affected more mature embryos that had already undergone both cardiac looping and embryonic turning (fig. 4.9 – I) and did not prevent Ca^{2+} transients prior to embryonic turning, neither within looping hearts, nor within cardiac crescents at stage 3 and LHT (fig. 4.9 – I). Inhibition of these channels might have led to subtler effects on the calcium transients, however any changes in the amplitude of the calcium transients in the embryos treated with Ryanodine + 2-APB can also be observed in the DMSO control embryos (fig. 4.9 – J).

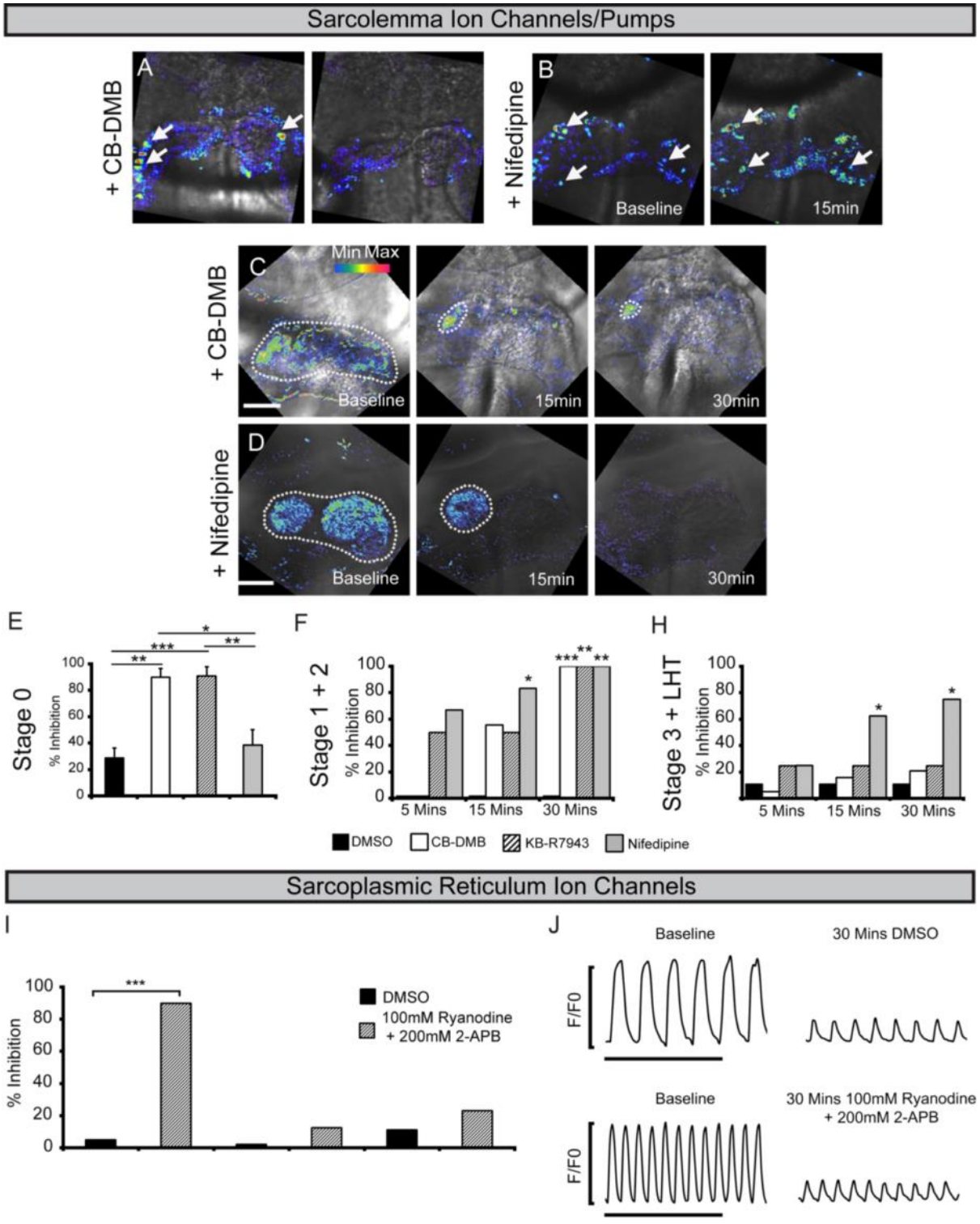

Fig. 4.9 – Acute pharmacological inhibition of sarcolemmal and sarcoplasmic Reticulum components on early stages of heart development – (A) Representative snapshots of stage 0 embryos treated with 20 µM of CB-DMB showing an abolishment of SACOs (white arrows) after 15 minutes when compared to baseline.

(B) Representative snapshots of stage 0 embryos treated with 10 µM of Nifedipine still showing SACOs (white arrows) after 15 minutes of treatment. (C, D) Representative snapshots of stage 1 embryos treated with 20 µM of CB-DMB (C) or 10 µM of Nifedipine (D) at baseline and after 15 and 30 minutes of treatment, showing either a confinement of the calcium transient (C – 15 and 30 minutes, dotted line; D – 15 minutes, dotted line) or a complete abolishment (D – 30 minutes) after treatment. (E-H) Semi-quantitative analysis of inhibition at different stages of cardiac crescent formation upon inhibition with 20 µM of CB-DMB, 10 µM of Nifedipine or 30 µM of KB-R7943. Inhibition was defined as any effect that impairs the propagation of the calcium transient, i.e. a confinement or a complete arrest. Inhibiting NCX (CB-DMB or KB-R7942) has an effect on stage 0 to stage 2. Inhibition of LTCC (Nifedipine) has an effect on stage 1 to LHT. (I, J) Effect of dual inhibition with Ryanodine (for RyR channels) and 2-APB (for InsP3 channels). Inhibition only has an effect of embryos with looping hearts and post embryonic turning (I). Inhibition of SR channels may not lead to a complete abolishment, but instead lead to a decrease in the amplitude of the calcium transients. Inhibition on stage 3 embryos leads to a decrease in amplitude similar to DMSO controls (J). Scale bars = 100 µM. (*$p<0.05$; **$p<0.01$; ***$p<0.001$).

Following the results from the acute pharmacological inhibition of calcium transients at stage 0 we aimed to determine to determine the effect of earlier NCX1 blockade on the subsequent development of the heart. For this purpose, we cultured embryos isolated at E7.25 (the onset of head fold formation and pre-cardiac crescent stage) in the presence of DMSO, CB-DMB or Nifedipine for 12 hr (fig. 4.10) on a rolling culture system. Whilst the embryos remained viable during the culture period, CB-DMB treated embryos in general displayed a delayed development when compared to embryos cultured in other conditions. CB-DMB treated embryos that progressed to similar stages of embryos cultured in other conditions had comparatively reduced expression of cTnT (fig. 4.10 – A). In the case of these embryos however, most cells were still positive for Nkx2.5, suggesting delayed or impaired differentiation likely accounted for the failure of crescent formation under conditions of NCX1 blockade (fig. 4.10 – A). The relative effects of NCX1 and LTCC inhibition on developmental progression and cardiac crescent formation are supported by corresponding gene expression data (fig. 4.10 - B) assessed by RT-qPCR of whole cultured embryos. While *Tnnt2* was down-regulated in both CB-DMB and Nifedipine treated embryos, *Nkx2.5* was only down-regulated in CB-DMB treated embryos.

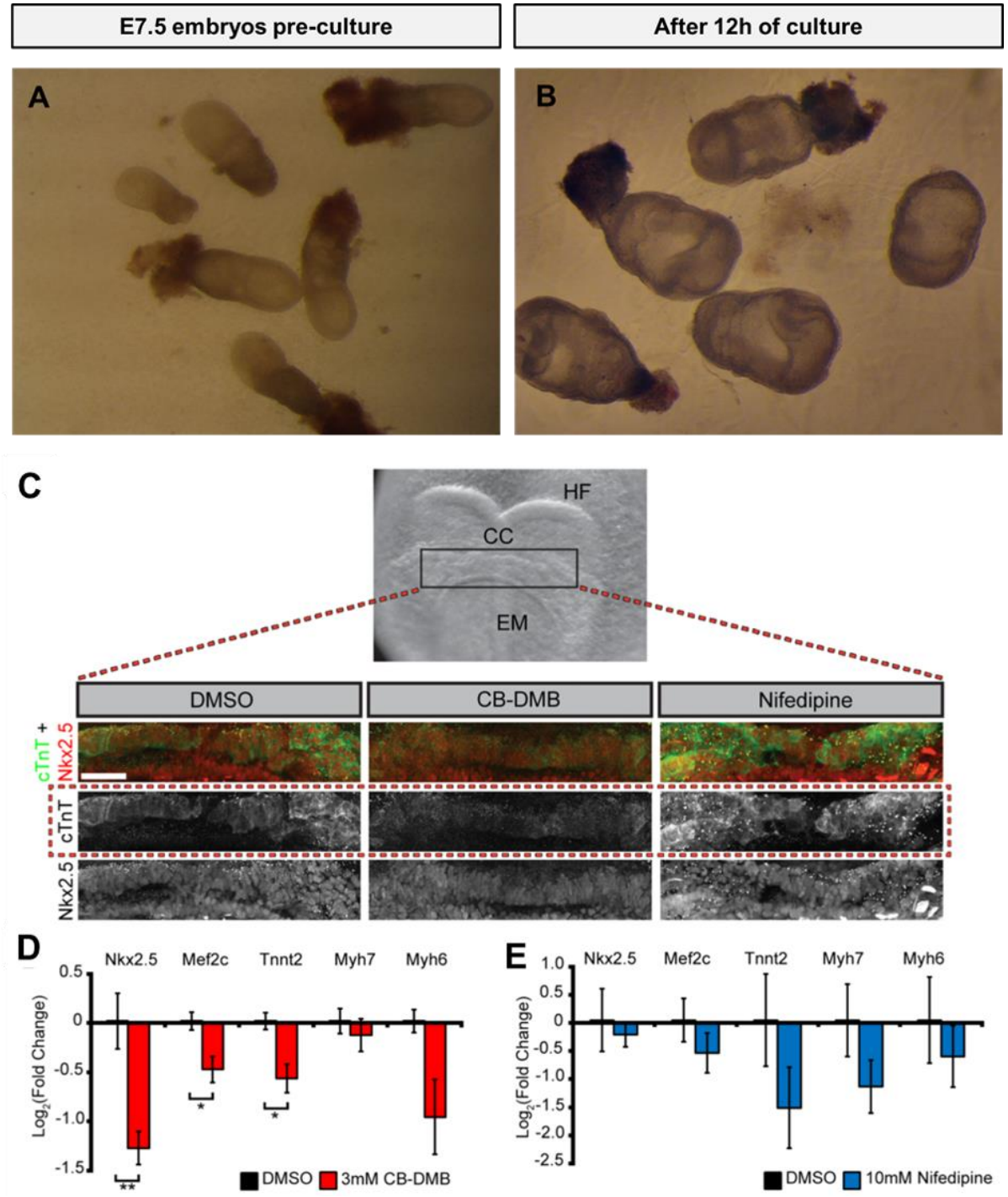
E7.5 embryos pre-culture
After 12h of culture
A
B
C
HF
CC
EM
DMSO
CB-DMB
Nifedipine
cTnT +
Nkx2.5
cTnT
Nkx2.5
D
Nkx2.5
Mef2c
Tnnt2
Myh7
Myh6
Log2(Fold Change)
DMSO
3mM CB-DMB
E
Nkx2.5
Mef2c
Tnnt2
Myh7
Myh6
Log2(Fold Change)
DMSO
10mM Nifedipine

Fig. 4.10 – Effects of overnight pharmacological treatment on heart development – Embryos were treated overnight with either DMSO, 3 µM of CB-DMB or 10 µM of Nifedipine. (A, B) Culture conditions are appropriate for development, as control embryos in DMSO expand and form the headfolds and cardiac crescent as would be expected. (C) Dual immunostaining of post-culture embryos for cTnT and NKX2.5, showing a decrease of cTnT signal and clear membrane localisation (number of affected embryos: DMSO – 1/7; CB-DMB – 7/8; Nifedipine – 1/6). (D, E) RT-qPCR of post-culture embryos, for cardiac transcription factors (Nkx2.5 and Mef2c) and for components of the contractile machinery (Tnnt2, Myh7 and Myh6) (n = 5 samples, 6-10 embryos per sample). HF = head folds; CC = cardiac crescent; EM = embryonic midline (*p<0.05; **p<0.01; ***p<0.001).

4.2.5 – Left-Right Physiological Differences

The role of left-right asymmetries has been extensively studied in heart development and function and Pitx2, the main left-side transcription factor, has been implicated in the regulation of proteins of the contractile machinery. While differential gene expression is established around E7.5, the first morphological evidence of left-right asymmetry is only visible around E8.5, when the heart starts to loop.

A more detailed look at the behaviour of calcium transients in WT embryos shows the possible existence of a left-right bias, prior to morphological symmetry breaking at E8.5. As previously mentioned, prior to the formation of the LHT, calcium transients in the cardiac crescent propagate laterally. Interestingly, the directionality of these transients seems to be stage specific (fig. 4.11 – A). In freshly dissected embryos, at stage 1 the majority show a left-to-right propagation. This behaviour starts to change at stage 2, with some embryos also showing a right-to-left propagation, in a seemingly random distribution. By stage 3, the majority of the embryos show right-to-left propagation, a complete reversal from the initial behaviour. This could be an indication of a physiological break of left-right symmetry prior to any morphological change,

Besides the behaviour described above, the confinement of the calcium transients described previously provides further evidence a left-right difference in the physiology of the cardiac crescent. Unlike the directionality of the calcium transient, it is not possible to analyse confinements at all stages because only treatment with nifedipine has an effect on stage 3 and LHT embryos, and this inhibitor seems to lead to a rapid suppression of the Ca^{2+} transients, without an intermediate confinement stage. Nevertheless, based on experiments where confinement did happen, there seems to bias for calcium transients to be confined to the right side of the cardiac

crescent (fig. 4.11 – B). This indicates that the right side of the cardiac crescent is more resilient to the drug treatment and that the physiology of the left and right side may be different, with the right side possibly working as a pacemaker region.

It has been suggested that the funny current channel HCN4 may be regulated by left-right patterning pathways, being first expressed in the left side but changing to a right-side expression during cardiac looping (*145*). Furthermore, HCN4 is a typical marker pacemaker cells, making it an ideal candidate to investigate the physiological regulation behind the propagation of the calcium transients at cardiac crescent stages. In order to investigate whether the funny current is functional between stage 2 and stage 3, I treated embryos with Ivabradine (*146*), a selective inhibitor of all HCN channels.

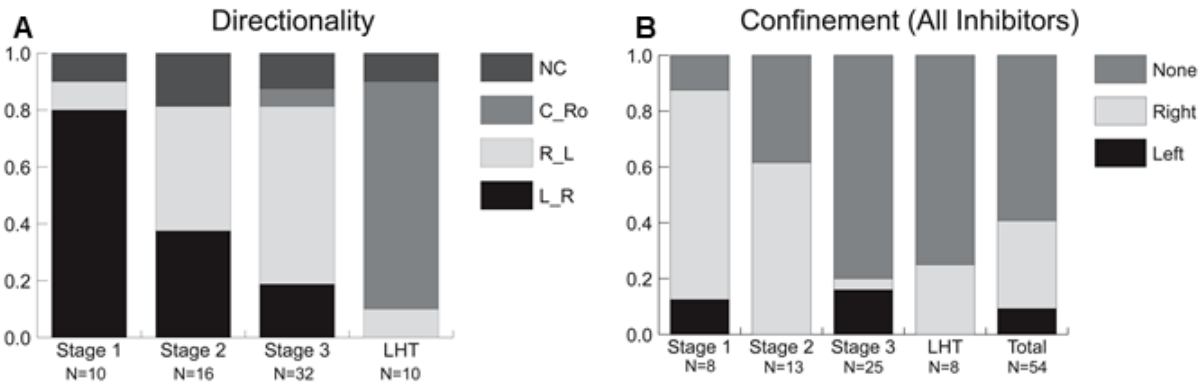

Fig. 4.11 – Left-Right bias in calcium transient behaviour – (A) Calcium transient directionality in freshly dissected embryos stained with the calcium dye cal-520, at different stages of early heart development. NC = not clear; C_Ro = caudal to rostral; R_L = right to left; L_R = right to left. (B) Semi-quantification of side of confinement upon inhibition with either 20 µM CB-DMB, 10 µM Nifedipine, or 30 µM KB-R7943.

Treatment with Ivabradine did not lead to any overt effect on the propagation of calcium transients. However, in some embryos there seemed to be a decoupling of the two sides of the cardiac crescent, with each behaving independently. In order to quantify this behaviour, I used the imageJ scripts described in chapter 3, to extract the duration and interval of calcium transients, as well as information about harmonic frequency and amplitude. (fig. 4.12). In terms of the duration of each calcium transient, in the DMSO controls there is a variation between -20 and 20 milliseconds (fig. 4.12 – A). Upon ivabradine treatment, the duration of the calcium transient increases on both sides. Interestingly, this increase in duration seems to be greater in the left side of the cardiac crescent. This could suggest that the left-side may not have an inherent ability to rapidly propagate the calcium transients, being dependent on the funny current. On the other hand, while the duration of the interval between transients also seems to increase in the ivabradine controls, there does not seem be a left-right difference (fig. 4.12 – B). In terms of the harmonics of this system, upon ivabradine treatment both the harmonic frequencies and harmonic amplitudes are affected. There is a decrease in the harmonic frequency both on both sides of the cardiac crescent, which indicates a slower rhythm (fig. 4.12- C). This decrease in harmonic frequency seems to be higher in the left side of the cardiac crescent, further supporting the hypothesis that the left side is more dependent on the funny current. In terms of harmonic amplitude, under DMSO treatment the amplitude increases on both sides of the cardiac crescent (fig. 4.12 – D). An increase in harmonic amplitude indicates that the sine function is more representative of the rhythm, i.e., the rhythm is more constant. Interestingly, the increase is higher in the right side, which supports the idea that this side is a pacemaker-like region. This is further supported by the effect of the ivabradine treatment. While there still is an increase in amplitude in the left side, albeit smaller,

upon ivabradine treatment there is a decrease of amplitude in the right side. It should be noted these experiments are preliminary, being performed on a limited number of embryos. In order to assess small physiological differences a large number of embryos would be necessary.

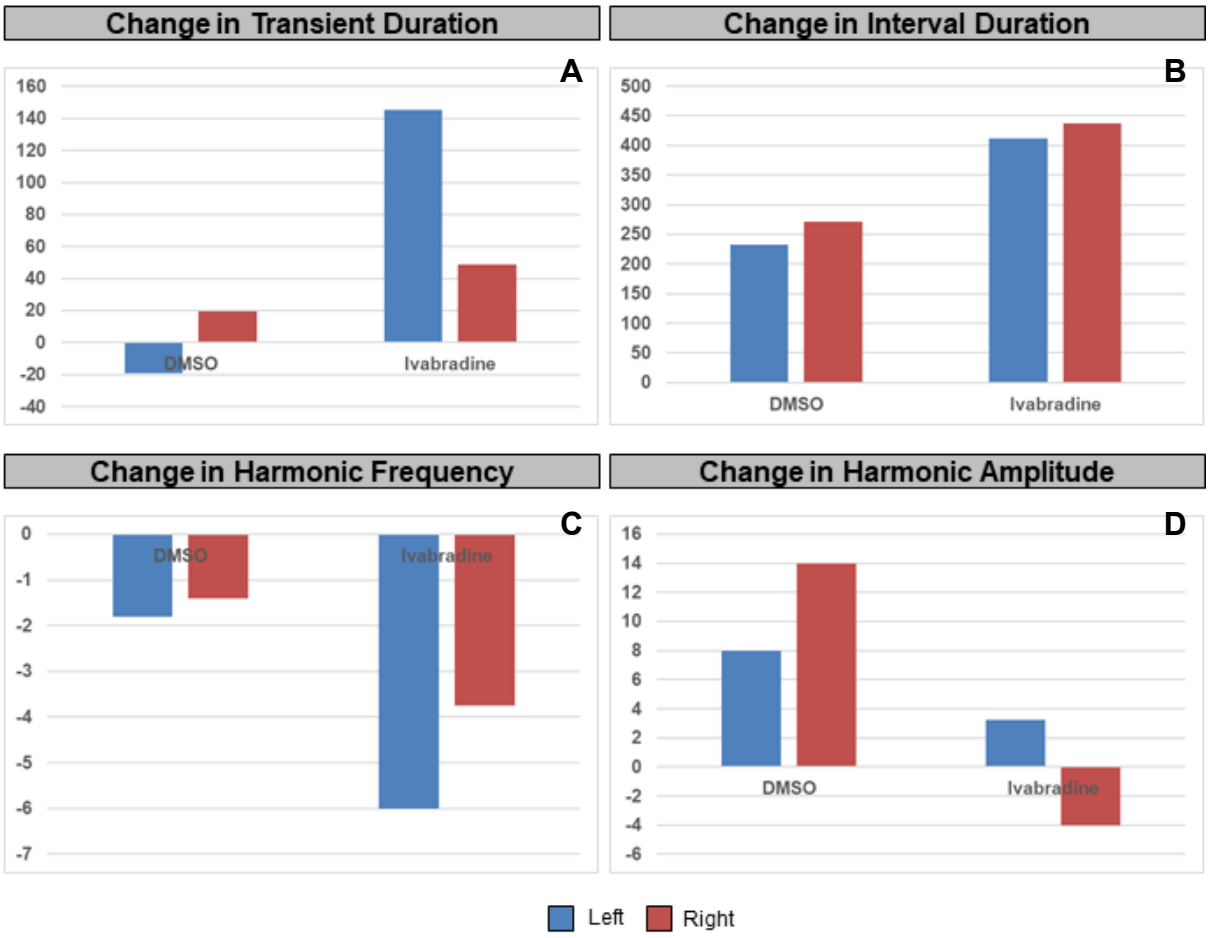

Fig. 4.12 – Quantification of calcium transient behaviour upon ivabradine treatment – Effects on calcium transients upon treatment with 10 µM of Ivabradine, a HCN channel inhibitor, measured by the imageJ scripts presented in chapter 3, on the dynamics of the right (red bars) and left side (blue bars), compared to baseline values. (A) Change on the average duration of each calcium transient (ms). (B) Change on the average duration of each interval between two successive transients (ms). (C) Change in the main harmonic frequency, a measure of rhythmicity. (D) Change in harmonic amplitude of the main harmonic frequency. DMSO n=4, Ivabradine n=3.

4.2.6 – Single-cell RNA sequencing analysis of early heart development

In order to better understand the development of the cardiac crescent and uncover the mechanisms behind the physiological dynamics described above, we performed a detailed scRNAseq analysis. Together with Dr. Richard Tyser, I collected over 5000 cells from WT embryos, from stage 0 to LHT cardiac crescents and overlaying endoderm (manually dissected), separating the left and right sides at the crescent stages, in order to gain more spatial information. These cells were sent to the Sanger Institute in Cambridge for sequencing. Of these cells, 3215 were of good quality after sequencing. Initial processing of sequencing data and clustering of cells was performed by Mr. Teun van den Brand and Dr. Antonio Scialdone from Dr. John Marioni group at EMBL-EBI, Hixton. Clustering of cells by unbiased hierarchical clustering separates the cells in well statistically defined groups, akin to the use of dendrograms in phylogenetics. To better visualise these groups, a graphical representation was performed using tSNE, reducing the dimensionality of the clusters, bringing them closer together. More details can be found Chapter 2.

Hierarchical clustering of sequenced cells based on their whole transcriptome separated the cells into 18 clusters (fig.4.13 – A). While most stages seem to be composed of cells from most of these clusters, the proportions seem to change differently for each stage (fig. 4.13 – B). For example, stage 0 seems to be composed mainly of the turquoise, red and black cluster, while the LHT seems to be composed mainly of the forest green cluster. While this may also give an indication of the biology of each of these clusters it is also important to mention that some differences may also be artefacts derived from manual dissection. Nevertheless, the fact that these cells statistically cluster in 18 different groups based on the whole transcriptome, is

indicative of aremarkable tissue heterogeneity even at early stages of organogenesis. It is important to note the clusters are also composed of a very variable number of cells (table 4.1 – A). The top 10 genes expressed in each cluster can be found in annex 2.

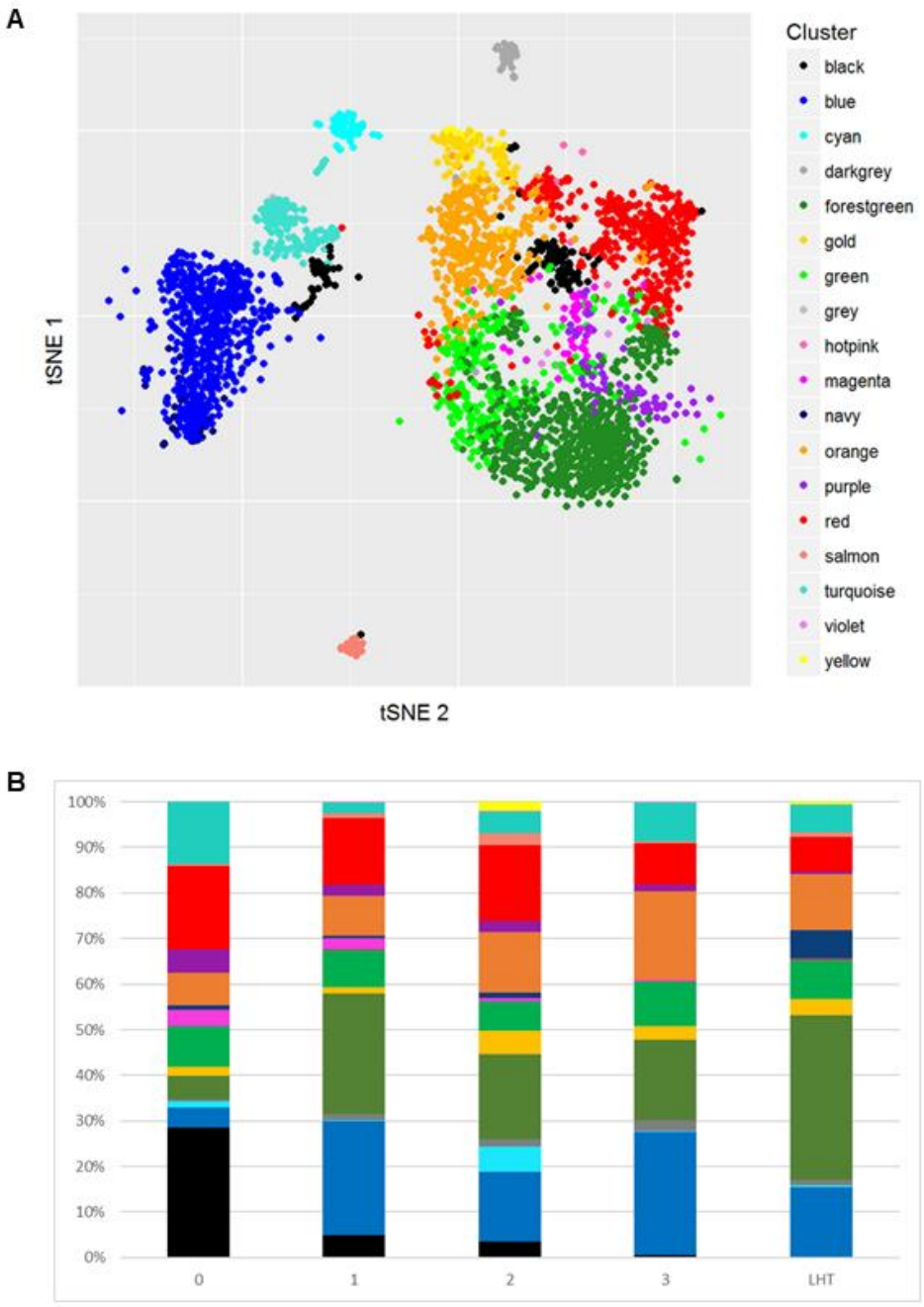

Fig. 4.13 – Clustering of cells based on their whole transcriptome - (A) Graphical representation of clustering analysis using the tSNE method. Different colours represent clusters obtained by hierarchical clustering. (B) Representation of the composition of each stage based on clusters obtained by hierarchical clustering. Different colours corresponf to the coulours of the clusters in A, in the inverse order.

Each cluster is characterised by a set of markers, which are genes within the top 25% highest expression and at least a 3-fold change from the average expression of all clusters. While the list of marker genes is imporant in order to undestand the biology of these clusters, looking for the expression of each individual gene is not an efficient way to determine the tissue identity of these clusters. In order to identify each cluster, I used a tissue database (https://tissues.jensenlab.org/Search). This database identifies provides a list of the most statistically likely tissues based on list of genes. It is important to note that this database deals mainly with adult tissues, however it may serve as a proxy to identify if the cluster is likely to be endodermal, mesodermal or ectodermal. The grey cluster was excluded from any analysis as it is composed by only one cell.

Based on this approach, the list of likely tissues can be extensive, especially when the list of marker genes is large. For this reason I considered only the top tissue when the combined score (based on p-avlue, adjusted p-value and z-score) was higher than 100, or the top 2 when the combined score was lower than 100 and the 2 scores had a close value (Table 4.1 – B). I have also excluded tissues that would be unlikely to be in the embryo at this stage of development (for example, kidney), unless there are no other likely tissues for this stage in development. The cluster with the highest score was the black cluster which was identified as being B-lymphocytes (other types of white blood cells also had a high score in this cluster), which is surprising to find at such an early stage of development. The clustering analysis mentioned above separated in the cells in two main superclusters. The first supercluster is composed mainly by the blue, turquoise and navy clusters, representing a total of 837 cells. The top tissues for these 3 clusters are all tissues of endodermal origin. Of these 3, the Navy cluster had a combined score higher than

100, suggesting that it is the cluster with the best defined transcriptional profile. Which could indicate these are more mature definitive endoderm cells. From here on out, I will be referring this cluster as the endoderm supercluster.

Considering that during the dissection of the cardiac crescents, we aimed to keep both the endoderm as well as the mesoderm, if the supercluster mentioned above has an endodermal signature, it is likely for the remaining supercluster (red, yellow, orange, gold, purple, magenta, violet, green and forest green clusters) to have a mesodermal signature. Indeed, most clusters that make up this supercluster have either a muscle or neural crest signature. Furthermore, the forest green cluster, the cluster with the highest number of cells, has a muscle signature, which indicates this cluster represents the most common cardiac cells at this stage in development, likely the first heart field. Besides the forest green cluster there are 4 other clusters that were identified as being muscle or heart tissue. The green cluster is likely to represent the bulk of the second heart field, of the 5 muscle clusters it the second with the highest number of cells. This is supported by the fact that the SHF shares many markers with endodermal tissues, and the green cluster has also been identified as being gut tissue. This could indicate that the remaining 3 muscle clusters, purple magenta and violet, could represent rare populations of cardiac cells. Of these 3 clusters, the magenta cluster is particularly interesting, as it has been identified as both muscle and several types of neurons. There are a few hypotheses that could explain this observation. First these cells could be ectodermal contamination due to imperfect dissections. Second, these cells could be the precursors for the cells that will innervate the heart. Lastly, these could be cells that are more physiological active.

Table 4.1 – Tissue identity of each identified cluster by tissue database analysis – (A) Number of cells belonging to each cluster. (B) Top tissues obtained from the JASPER analysis of marker genes for each cluster. Combined score is calculated based on the p-value, adjusted p-value and z-score. A combined score higher than 100 (green font) represents good statistical certainty.

A

Cluster	No. Cells
back	149
blue	626
cyan	72
darkgrey	50
forestgreen	665
gold	104
green	270
hotpink	14
magenta	48
navy	43
orange	378
purple	112
red	431
salmon	45
turquoise	168
violet	15
yellow	26

B

Cluster	Top Tissue	Combined Score
black	B-lymphocyte	439.52
blue	Intestine, Gut	54.41, 44.20
cyan	Neural Crest	32.58
darkgrey	Vasculature	177.87
forestgreen	Muscle	208.24
gold	Neural Crest	56.63
green	Gut, Heart	33.11, 20.00
hotpink	Adipose	38.06
magenta	Neurons, Muscle	106-120, 115.78
navy	Gut	118.84
orange	NA	NA
purple	Muscle	353.69
red	Neural Crest	46.34
salmon	Erythroid Cell	145.26
turquoise	Urinary Bladder	22.02
violet	Muscle	184.15
yellow	Neural Crest	43.2

Another surprising finding from this analysis is that there are 4 clusters that have been identified as being neural crest, including the red cluster, which is the 3rd cluster with the highest number of cells. This is unexpected as there have been no reports of cardiac neural crest cells so early in development. However, the score for these clusters are very low, therefore it is not possible to say with certainty that these cells really are neural crest cells. A defining characteristic of neural crest cells is their migratory behaviour, so it is also possible that these cells are not true neural crest cells but cells undergoing EMT, or at the very least, cells with migratory behaviour. That being true, it would be surprising that there would be 4 population of cells with a migratory behaviour in this region of the embryo during this developmental time. Lastly, with this analysis it was not possible to identify the tissue identity of the orange cluster. This cluster only has 18 markers, so it possible that the expression in these cells is very variable, and could represent the least committed pool of cells.

While the previous analysis provides a good starting point to identify the identity of these clusters, it is still incomplete. In order to better understand the pathways that may be regulating each of these clusters, I used the Gene Expression Omnibus (GEO - https://www.ncbi.nlm.nih.gov/geo/) to identify experimental conditions in which the marker genes of each cluster have been shown to either be downregulated or upregulated. This analysis is likely to originate several hits, therefore I only considered the hits with the highest combined score. Since this chapter focus on the development of the cardiac mesoderm, I only performed this analysis for the mesoderm supercluster (Table 4.2), with the exception of the hot pink cluster, which does not seem like a tissue of interest from the previous analysis, and the green cluster, which did not return any significant results.

Table 4.2 – GEO analysis of the mesoderm supercluster – Analysis with the Gene Expression Omnibus of the mesoderm supercluster, based on the list of marker genes of each cluster. This analysis identifies condition, which have been identified to change the expression of a list of genes. This table includes only the top statistically significant hit for each cluster (each colour represents the corresponding cluster). Not all gene changes are displayed on the table.

	Downregulated		Upregulated	
	Eed KO	Hand1, Ccdc80, Lrrn4, Stard8, Msx1, Wnt2, Tmem108, Msx2, Tek, Cfc1	Eed KO	Kitl, Nabp1, Cpa2, Phlda2, Plagl1, Mest, Gata4, Bmp4, Ahnak, Pdgfra
	Ret KO Twist1 OE	Hsd11B2, Au20206, Arg1, Rdh10, Aldh1a2 Pdgfra, Spon1, Mme, 1700017805rik, Ptges	Klf5 KO Nfe2l2 KO	Spon1, Mme, Arg1, Sema3a, Aldh1a2 Pdgfra, Mme, Sema3a
	Hprt KO	Pdgfrb, Mfap4, Foxc2, Fst, Cdh11, Pdlm4	Eomes OE Ezh2 KD Sox2 KO	Foxc2, Efnb1, Mfap4, Col26a1, Ebf2, Six1 Mfap4, Eva1, Frz8, Smoc1, Cdh11. Six1 Mfap4, Eva1, Frz8, Fst, Cdh11, Ebf2
	Hprt KO	Lum, Foxc2, Pdgfrb, Emilin1, Cdh11, Fst	Fli1 KD	Lum, Eya1, Egr1, Ptn, PdgfrB, Plat, Ror1
	Ackr3 KD Naca KO	Tnni1, Actn2, Tnnc1, Acta2, Tnnt2, Myh7, Tnni1, Actn2, Tnnc1, Tnnt2, Myh7, Myl9,	Gata4 KD Hsp90b1 OE	Tnni1, Actn2, Tnnc1, Myl7, Tnnt2, Myh7 Tnni1, Tnnc1, Acta2, Myl7, Myl3, Myh7
	Naca KO	Ttn, Tnni1, Tnni3, Actn2, Tnnc1, Myh6	Gata4 KD Atp1a1 KO	Ttn, Tnni1, Tnni3, Actn2, Tnnc1, Myh6 Myom1, Tnni3, Tnnc1, Myl4, Acta2, Myh6
	Psap KO Ackr3 KD Adora2b KD Lama 2 KD	Hint1, Apoe, Atp5j2, Hint1, Cst3, Tbcb Nexn, Tnnt2, Myl7, Tnni1, Hint1, Gng5 Nexn, Tnnt2, Apoe, Manf, Hint1, Eif3k Nexn, Gng5, Cox4i1, Atp5j2, Atp5g1, Cox7a2	Hsp90b1 OE	Dad1, Tnni1, Myl7, Hint1, Eif3k, Tceb2
	Srf KO Naca KO	Myh6, Myh7, Myom1, Tnnc1, Actc1, Actn2 Myom1, Ttn, Myh6, Myh7, Tnni1, Tnnt2	Gata4 KD Map2k3 OE	Myh6, Myh7, Ryr2, Tnnc2, Tnni1, Tnnc1 Myom1, Myh6, Myh7, Ttn, Atp1b1, HK1

The GEO analysis suggests *Eed* may be the main regulator of the red cluster. Cells where *Eed* was knocked out showing both a downregulation and upregulation of several markers of this cluster. *Eed,* a member of the polycomb group, has been shown to be required for gastrulation movements, with KO embryos failing to form the anterior mesoderm (*147, 148*). This supports the idea that the Jasper analysis identified these cells as being neural crest because they may have an active migratory behaviour, rather than proper neural crest cells. Endothelial specific KO of *Eed* using a Tie2-cre has also revealed that this gene is required for haematopoiesis, with embryos dying by E13.5 (*149*). Since the red cluster is the 3rd largest cluster, it is likely that these could be hematopoietic progenitors.

The orange cluster, which was not possible get a clear tissue identity through JASPER analysis, seems to be regulated mainly by *Ret*, *Twist1*, *Klf5* and *Nfe2l2*. *Ret*, a receptor tyrosine kinase, has been shown to be required for skeletal muscle development (*150*) and haematopoietic stem cell differentiation and function (*151*). *Twist1* is a well-known transcription factor, regulator of EMT. In the context of cardiac development, overexpression (OE) of *Twist1* has been shown to lead to an increased valve cell proliferation (*152*) and to supress neuronal differentiation of neural crest cells (*153*). In the context of development, *Klf5*, a transcriptional activator, has been shown to also be a regulator of haematopoiesis (*154*) and to regulate muscle development by binding to MYOD and MEF2 (*155*). Lastly, not much is known about the transcription factor *Nfe2l2*, except that is important in autophagy and regulate oxidative stress (*156*). Taking this information in account, and that the orange cluster is localised between the red and green/forest green clusters, it is possible that this cluster represents a bipotent population of cells that can differentiate either into the haematopoietic or cardiac lineages.

Hprt KO seems to cause the downregulation of genes present in both the yellow and gold cluster. Unfortunately, the role of *Hprt*, a transferase, during development is not well understood. The main reports for the function of this gene is that it seems required form cAMP/PKA signalling and that it plays a role in neuronal function (*157*). Furthermore, *Eomes* OE, a transcription factor, as well as *Ezh2* Knock-Down (KD), a member of the polycomb group and *Sox2* KO, another transcription factor, seem to cause an upregulation of gold cluster markers. Furthermore, *Flk1* KO, a protein-tyrosine kinase receptor, seems to cause an upregulation of yellow cluster markers. *Eomes* has been shown to induce *Mesp1* and cardiogenesis in embryos (*35*) and ES cells (*158*), but also controls the differentiation of the DE. *Eomes* expression has been shown to be increased in *Hhex* KO (*159*), leading to a repression of DE differentiation into hepatic lineage. *Eomes* has also been shown to be involved in neurogenesis and T-cell differentiation (*160*). *Ezh2* KO has been shown to impair gastrulation (*161*), and has also been shown to impair the formation and maturation of T-cells (*162*). SOX2 is an important factor for neuroectoderm formation, by supressing genes involved in the development of other lineages (*163*). Lastly, FLK is a well-known regulator of endothelial development and vasculogenesis. Interestingly, FLK1 negative mesoderm has been shown to have a higher potential for the erythroid lineage (*164*). Taken together, these results do not provide a clear picture of the identity of the gold and yellow clusters. It is possible that these populations of cells also represent uncommitted populations blood cells.

In terms of the cardiac cluster, composed by the magenta, purple, violet and forest green clusters (also the green cluster, however this did not return any clear results), this analysis reveals a potential complex regulation of cardiac differentiation at this developmental stage. *Naca* KO seems to cause a downregulation of markers

of 3 out of 4 clusters. Targeted deletion of *Naca*, more specifically the skNac isoform, in cardiomyocytes leads to ventricular hypoplasia, causing embryonic lethality by E12.5 (*165*). Since cardiac contractions are required for cardiac hypertrophy, this suggests that Naca may be involved in the regulation of cardiac function. SRF has been shown to be a key regulator of assembly and maintenance of the contractile machinery (*42, 43*). SRF KO, a transcription factor, seems to promote a downregulation of markers of the forest green cluster, but is not statistically significant in the violet and purple cluster. This could suggest that the forest green cluster represents slightly more differentiated cardiomyocytes, while the violet and purple cluster are more primitive cardiomyocytes. Ackr3, an atypical chemokine receptor, and Hsp90b1, a heat-shock protein, also seem to be key regulators of the violet cluster. Ackr3 KO mice die during the first week of postnatal development, with heart defects (*166*). Endothelial conditional KO leads to septal and valve defects (*167*). Hsp90b1 seems to be required for mesoderm induction, as KO mouse embryos die at E7, with either a defect in mesoderm induction or formation of the primitive streak. Hsp90b1 -/- ES cells can form tissues from all 3 germ layers, with the exception of cardiac tissues, suggesting this gene may be especially important for cardiac mesoderm induction (*168*). Interestingly, both Ackr3 and Hsp90b1 seem to be key regulators of magenta cluster markers. This suggests that the violet cluster may represent a bipotent population of cardiac progenitors, able to either form the purple and forest green cluster or the magenta cluster.

Table 4.3 – Top correlated genes with key physiology genes involved in calcium transient regulation at the cardiac crescent stages – Top positively correlated genes with Slc8a1 (NCX1), Cacna1d (Cav1.3) and Cacna1c (Cav1.2). Correlation based on the expression obtained from the scRNAseq data. Genes encoding components of the contractile machinery are highlighted in green and genes encoding channels or pumps are highlighted in orange. Correlations were calculated based on the expression at all stages (top table) and on the expression of stage 0 alone (bottom table).

	Slc8a1		Cacna1d		Cacna1c	
	Gene	Coefficient	Gene	Coefficient	Gene	Coefficient
All Stages	Myh6	0.5173842	Tbx5	0.46353	Hspb7	0.4905375
	Rassf5	0.4810927	Fbxo32	0.4462983	Ttn	0.4495355
	Thbs4	0.4787402	Thbs4	0.4346714	Myh6	0.447773
	Actc1	0.4769627	Atp1b1	0.4327466	Tpm1	0.4410045
	Cdh2	0.4579306	Actc1	0.4299993	Actc1	0.4334731
	Cap2	0.4559621	Csrp2	0.4282175	Actn2	0.4307512
	Emilin2	0.4561303	Ttn	0.4197857	Asb2	0.4296598
	Actn2	0.4525648	Gata4	0.4125637	Apobec2	0.4253877
	Mybpc3	0.4506815	Tpm1	0.4116021	Myl3	0.4243034
	Hspb7	0.4426861	Adora1	0.4059536	Kif26b	0.416262
Stage 0	Ap3m1	0.7079527	Clasp2	0.6031052	Hspb7	0.644009
	Tspan18	0.6996222	Churc1	0.5881121	Tmem163	0.63201
	Smyd1	0.68607	Senp3	0.5729532	Ctnnb1	0.608407
	Ncoa5	0.678918	Itm2c	0.5608015	4930512H18Rik	0.6111774
	Ppp1r14c	0.6586338	Nr1h2	0.560469	Ndrg3	0.5985023
	Mybpc3	0.6478031	Helz	0.553745	Ube2z	0.579292
	Trac	0.6434519	Pcnt	0.520713	Ctdsp1	0.5768315
	Msn	0.6397585	Tchp	0.5149152	Tmod1	0.5848898
	Cap1	0.6350352	Ckb	0.4727487	Atp2a2	0.5763885
	Ugp2	0.6313335	Ubl3	0.4701698	Acta1	0.5805794

A key unanswered question from the experiments exposed in this chapter is how the physiological mechanisms are regulated, and what is the pathway that leads to the establishment of the first heartbeats. In order to uncover the potential key components of these processes, I investigated which genes better correlate with molecules responsible for regulating the cellular physiology analysed previously in this chapter, Slc8a1 (NCX1), Cacna1d (CaV1.3) and Cacna1c (Cav1.2) (Table 4.3).

When this analysis was performed with all stages in consideration, it is possible to see that the majority of genes that correlate with Slc8a1 and the LTCC are genes of the contractile machinery (green rows), and not with other physiology related genes (orange rows). However, there is a high degree of variability in the top correlated genes, suggesting a high heterogeneity in the physiology of this system. The fact that not many physiology genes correlate with each other, also points out to complex regulatory mechanism. These differences in the top correlating genes is even more striking if only stage 0 is considered for the analysis, with the top 10 correlating genes of each condition being unique. As mentioned previously in this chapter, Slc8a1 seems to be the most important regulator of SACOs at stage 0, and it is critical for further heart development. Interestingly, at stage 0, one of the top correlating genes with Slc8a1 is Smyd1. This gene has been shown to participate in similar pathways to Naca (*165*), further supporting a key role for this pathway in early cardiac function and development.

As mentioned previously, there is some indication that the left-right patterning pathway may also be involved in the establishment of the early cardiac physiology. To investigate whether there are any striking left-right differences that may explain the physiological dynamics described in this chapter, I used the scRNAseq data to look for genes with an expression correlated with Lefty2, a well-known regulator of left side

identity, on all clusters, at all stages. I obtained the top 10 positively correlated genes as potential left-side markers, as well as the top 10 negatively correlated genes as potential right-side markers (Table 4.4). The top positively correlated genes all have a stronger correlation than the negatively correlated genes, suggesting that left-side is better defined at this stage in development.

The top positively correlated genes are known left side genes such as Pitx2 and Lefty1. There are no physiology related genes in the top left side genes, A potential drawback with this approach is that this analysis was performed with all clusters and all stages, however this does indicate that there isn't an overt left-side specific physiological mechanism. Interestingly, left-right differences are not observable on all clusters. For example, Lefty2 left side expression seems to be high mainly in the green, magenta and orange cluster (fig. 4.14 – A). Lefty2 expression in the gold cluster seems to be non-existent in the left side, but there seem to expression in the right side (fig. 4.14 – B), suggesting a complex regulation of lateral asymmetries. In terms of the non-traditional left side genes such as Crtac1 and Ntrk1, the higher expression in the left side seems to be subtler (fig. 4.14 – C, E) than the expression of Lefty2.

Table 4.4 – Top 10 positively and negatively correlated genes with Lefty2 expression – Positively (left column) and negatively (right column) genes with Lefty2, based on the expression patterns obtained on the scRNAseq data.

Positive Correlations		Negative Correlations	
Gene	**Coefficient**	**Gene**	**Coefficient**
Pitx2	0.6967282	Cldn6	-0.2527626
Lefty1	0.6912378	Ap1m2	-0.2496648
Nodal	0.589705	Cldn7	-0.2475198
Crtac1	0.4758375	Epcam	-0.2439706
Ntrk1	0.4388082	Gfpt2	-0.2433605
Sema3a	0.42155	Slc2a1	-0.2396165
Col5a1	0.36316	Cdh1	-0.2392266
Igfbpl1	0.3512371	Gprc5c	-0.2253349
Bcat1	0.3470556	Esrp1	-0.2227266
Aplnr	0.3470002	Prss8	-0.2224447

As mentioned above, the right-side genes have lower correlations than the left side genes. Furthermore, most identified right-side genes are expressed solely on the endoderm supercluster. The exceptions to this are Slc2a1 and Gfpt2. Slc2a1 encodes for a glucose transporter and expression seems to be ubiquitous both in the left and right side (fig. 4.15 – A, B). While there seems to be a slight increase of the expression of this gene on all clusters in the right side (fig. 4.2 – B), the magenta cluster has a more skewed expression, with cells with lower levels of expression. This could mean that these cells may have a slightly better control of their glucose levels on the right side. Gfpt2 also seems to be expressed at high levels in most clusters (fig. 4.15 – E, D), and generally higher in the right side. Interestingly, the expression seems to be non-existent in the dark grey and purple clusters. It is important to note that both the magenta and purple clusters are likely to represent cardiac muscle cells, therefore these genes could be an indication that different populations of cardiomyocytes already have left-right differences at this stage in development.

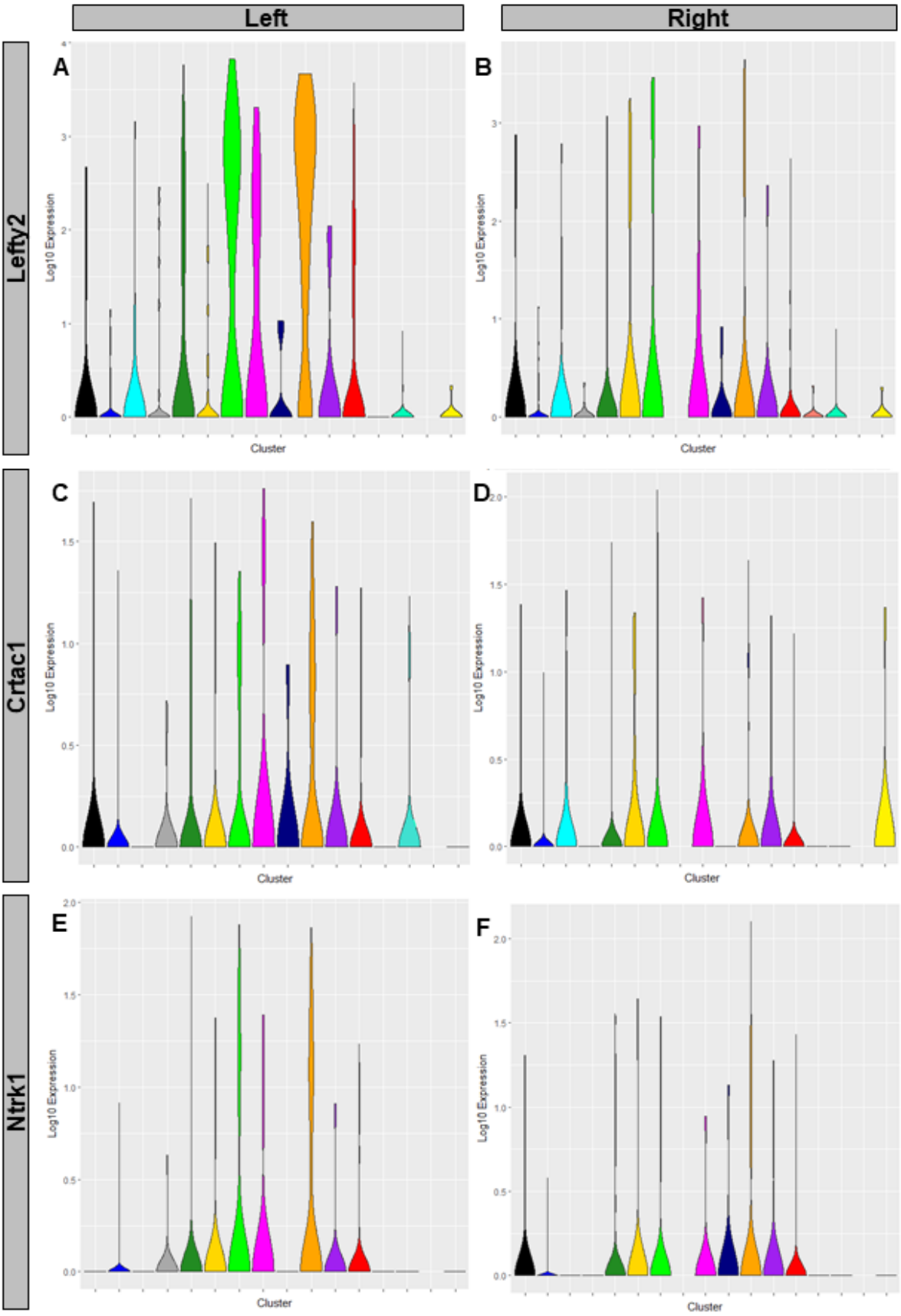
Left
Right
Lefty2
Crtac1
Ntrk1
A
B
C
D
E
F
Log10 Expression
Cluster

Fig. 4.14 – Expression of left side genes in different clusters – Expression pattern of Lefty2 (A, B) and identified “left” genes, Crtac1 (C, D) and Ntrk1 (E, F), on individual clustters of manually dissect left and right samples. Overall expression is higher on the left side, but some clusters have higher expression on the right side.

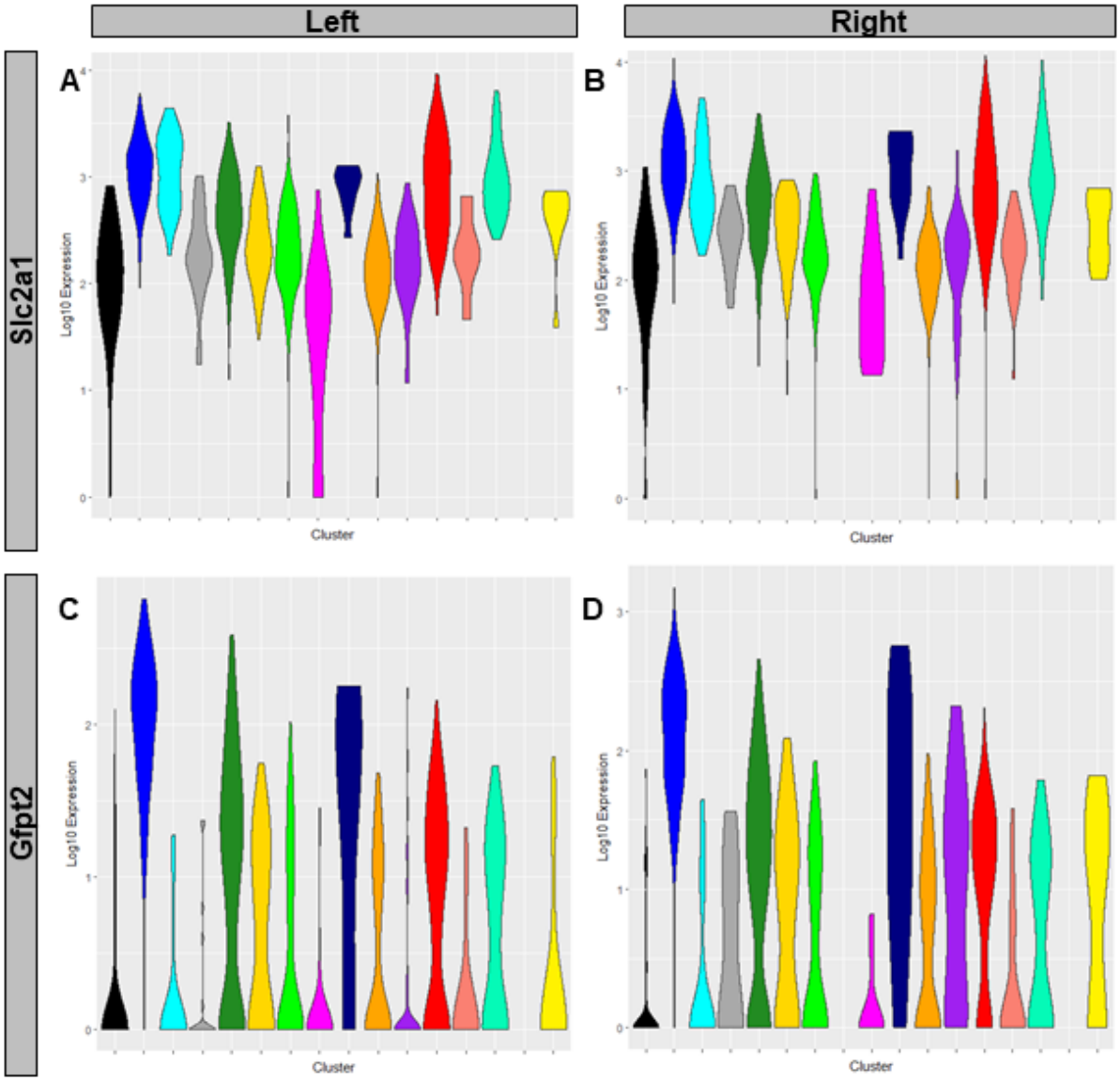

Fig. 4.15 – Expression of right side genes in different clusters - Expression pattern of identified “right” genes on individual clustters, Slc2a1 (A, B) and Gfpt2 (C, D), on manually dissect left and right samples. Overall expression is similar on both sides but some clusters have higher expression on the right side.

The availability of this scRNAseq dataset also provides a good opportunity to identify new markers of the first and second heart field. For this purpose, I took the expression of *Isl1*, as a marker of the SHF (fig. 4.16 – A), and *Hcn4* as a FHF marker (fig. 4.16 – B) as a starting point. In terms of the SHF, the ideal marker would have an expression as broad as Isl1 in the cardiac mesoderm but would not be expressed in the endoderm. Similarly to the approaches described previously, I looked for genes whose expression correlated with *Isl1* and *Hcn4*. It is expected for markers of the FHF to positively correlate with *Hcn4* and negatively correlate with Isl1. The inverse is expected for markers of the SHF. For the purpose of identifying new markers I considered only the top 5 positive and negatively correlated genes for each gene. (fig. 4.16 – C).

In terms of putative markers for the FHF a particularly promising candidate is *Fbxo32,* an F-box protein, as it is simultaneously positively correlated with Hcn4 and negatively correlated with *Isl1*. Indeed, *Fbxo32* expression pattern (fig. 4.17 – A) is a close match to *Hcn4*, albeit slightly broader. *Fbxo32* is also strongly correlated with *Cacna1d*, suggesting this gene may be an important regulator of cardiac function. *Csrp3* is another potential new marker for the FHF, with an expression pattern broader (fig. 4.17 – B) than both *Hcn4* and *Fbxo32*. Of the potential markers for the FHF, *Kcjn5*, a potassium channel involved in pacemaker activity, has the more restricted expression pattern (fig. 4.17 – C). While, *Kcnj5* may not be an ideal marker of the FHF as a whole, considering it marks a subset of Hcn4+ cells, it may represent the most specialised cardiomyocytes of the forest green cluster. Lastly, *Thsb4* also has a broad expression pattern as a potential FHF marker (fig. 4.17 – D) with the addition that has the highest expression of all the markers presented here.

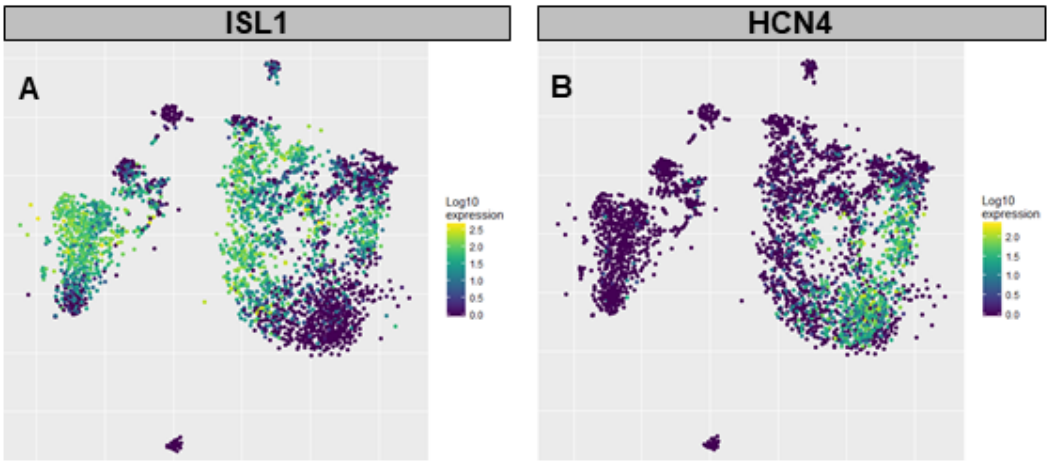

C

	Positive Correlations		Negative Correlations	
	Gene	Coefficient	Gene	Coefficient
HCN4	1700008O03Rik	0.6125364	Emb	-0.358262
	Tbx5	0.5929721	Prom1	-0.351333
	Csrp3	0.5699315	H3f3b	-0.3393737
	Fbxo32	0.5565579	Ifitm3	-0.323319
	Arhgap31	0.555747	Kit	-0.3231585
ISL1	Nkx2-6	0.414316	Emilin2	-0.4462221
	Frzb	0.4071427	Actn2	-0.4239265
	Nnat	0.3979134	Fbxo32	-0.4219635
	Fn1	0.3976727	Thbs4	-0.4196538
	Prdm1	0.3967072	Kcnj5	-0.4010588

Fig. 4.16 – Correlations with markers of the FHF and SHF – Expression pattern of Isl1 (A) and Hcn4 (B), markers of the second heart field and and first heart field respectivelly, on the scRNAseq cluster. (C) Table of genes positevely and negatively correlated with Hcn4 and Isl1, putative markers of the FHF and SHF.

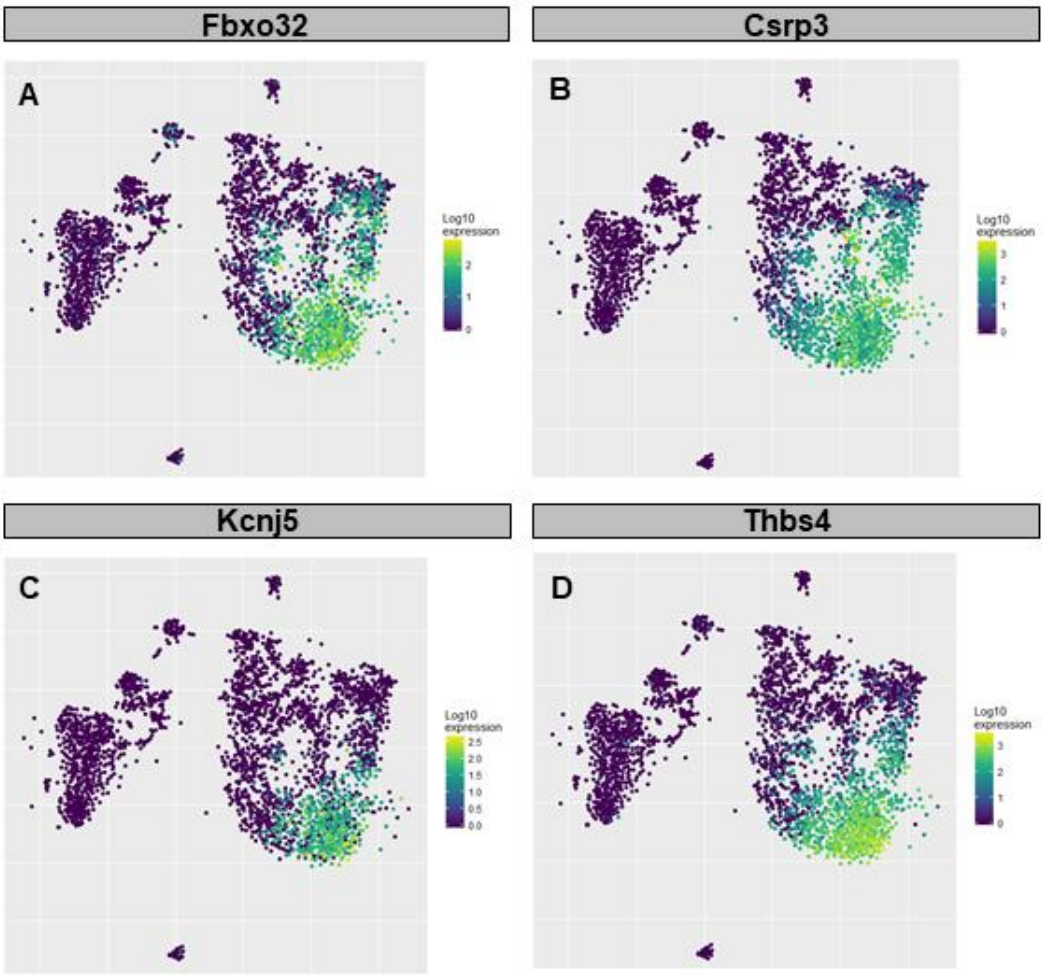

Fig. 4.17 – Expression pattern of potential FHF markers – Expression pattern of 4 potential new markers of the first heart field, Fbxo32 (A), Csrp3 (B), Kcnj5 (C), Thbs4 (D).

While the previous approach was useful in identifying new potential markers for the FHF, this has proven more challenging for the SHF. Because Isl1 is strongly expressed in the DE, the hits obtained such as *Prdm1* and *Prom1*, while having an expression pattern similar to *Isl1* (fig. 4.18 – A, B), are still expressed in the endoderm supercluster. In order to identify new candidate, I repeated the correlation analysis for *Hcn4*, but now restricting the analysis only to the mesoderm supercluster. With this analysis, I identified *Cdh11* as the top negatively correlated gene. *Cdh11* has been shown to be required for the development of the heart valves (*169*), an indication that Cdh11+ are part of the SHF. Furthermore, expression of *Cdh11* in this dataset overlaps well with the expression of *Isl1*, with the benefit of only being expressed in the mesoderm supercluster (fig. 4.18 – C), making it an ideal potential marker for the SHF. I then searched for genes that positively correlate with *Cdh11* in order to find new mesoderm exclusive markers of the SHF (fig. 4.18 – D). The top correlated marker was *Foxc2* (*170*), a well-known marker of a smaller subset of the SHF. The second highest correlated gene, *Haplnr1*, also has an expression pattern that overlaps with Isl1 in the mesoderm supercluster ((fig. 4.18 – E). However, this gene is also expressed in a subset of cells belonging to the cyan cluster, which while having an unclear tissue identity, may still belong to the endoderm supercluster. *Aplnr* is another potential new marker for the SHF. This gene is highly expressed in these developmental stages, and is restricted to the mesoderm supercluster ((fig. 4.18 – F), making it the potential best marker of the SHF.

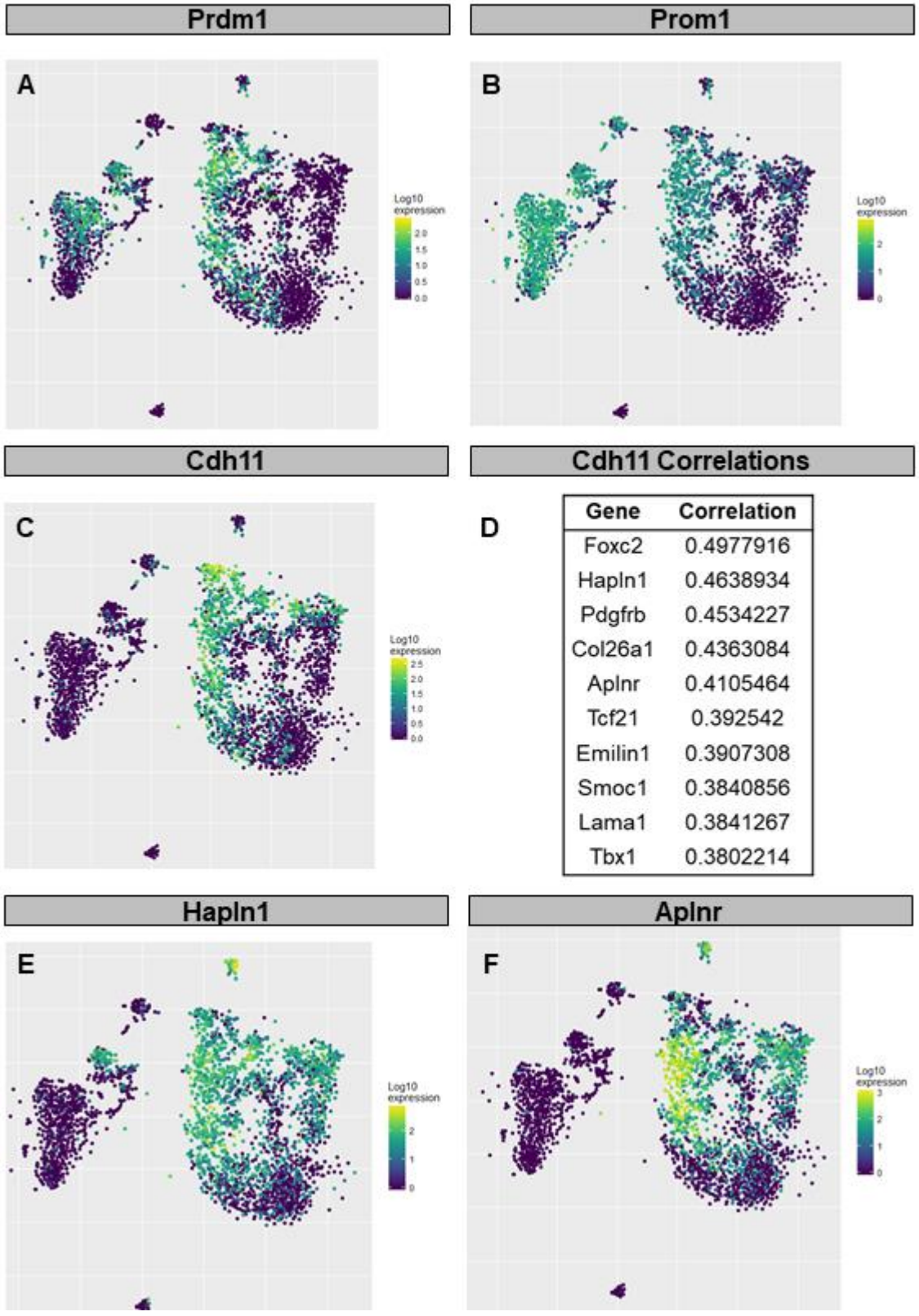

Fig. 4.18 – Expression pattern of potential SHF markers – (A, B) expression pattern of potential second heart field markers based on the correlation with Isl1 and Hcn4, on all clusters. (C) expression pattern of Cdh11, the top negatively correlated gene with

Hcn4 on the mesoderm supercluster alone. (D) list of genes positively correlated with Cdh11. (E, F) expression pattern of genes correlated with Cdh11 as potential mesoderm specific markers of the whole second heart field.

4.2.7 – First Cardiac Contractions in the Avian Embryo

While mouse is an excellent model to study heart development, studying other models may provide insights on how developmental processes evolved, which in turn may provide clues about the molecular mechanisms involved. In order to investigate whether the physiological mechanisms described in this chapter are conserved, I performed DIC imaging of live chick and quail embryos in order to investigate the onset of cardiac contractions. I also performed calcium imaging in chick embryos in order to investigate the physiological dynamics in avian embryos.

Unlike mouse, the first cardiac contractions in both chick and quail embryos can only be observed at stage 3 (fig. 4.19). This suggests that there is a delay in the maturation of cardiomyocytes compared to mouse, even though overall development is faster in avian embryos at this stage. The beat rate is also slower in avian embryo, which could be an indication of a different physiology or a consequence of the size of the tissue. The delay in the onset of cardiac contractions can be explained a delay in the onset of calcium transients and/or in sarcomere assembly. In order to investigate sarcomere assembly, I stained chick embryos with phalloidin in order to mark actin (fig. 4.20 – A-D). Unlike in mouse embryos, sarcomere assembly in chick embryos is only observable on stage 3 embryos, coincident with the onset of cardiac contractions. While it would be ideal to stain the embryos for other components of the contractile machinery, the antibodies did not work in chick embryos. In terms of calcium transients, the onset is similar to mouse. In chick, SACOs are also observable on stage 0 embryos (fig. 4.20 – E). Lateral propagation of calcium transients also starts at stage 1 (fig. 4.20 – F). This observation suggestion that the onset of calcium transients and sarcomere assembly are not regulated by the same mechanisms, and are likely to be decouple, at least to a certain extent. Unlike in mouse, lateral propagation of the

calcium transient is always from right-to-left. This suggests that the potential role of the left-right patterning pathway in the establishment of the calcium transients is different from mouse. This is particularly interesting as the mechanisms to establish left-right asymmetries are different in these two species.

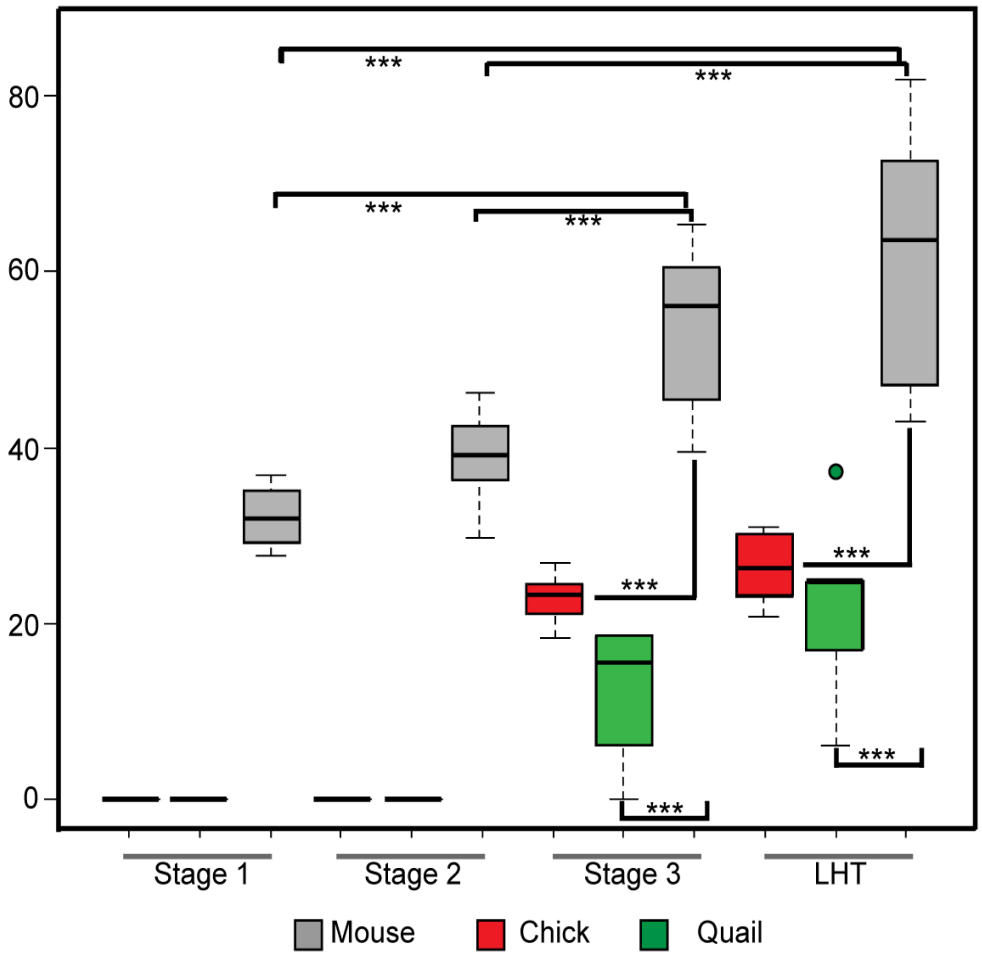

Fig. 4.19 – Beat rate in avian embryos – Boxplot of beat rate in chick and quail embryos (Chick: stage 1 n = 7, stage 2 n= 5, stage 3 n = 6, LHT n = 10; Quail: stage 1 = 4, stage 2 = 5, stage 3 = 5, LHT = 7), compared to mouse beat rates (presented on figure 4.4).

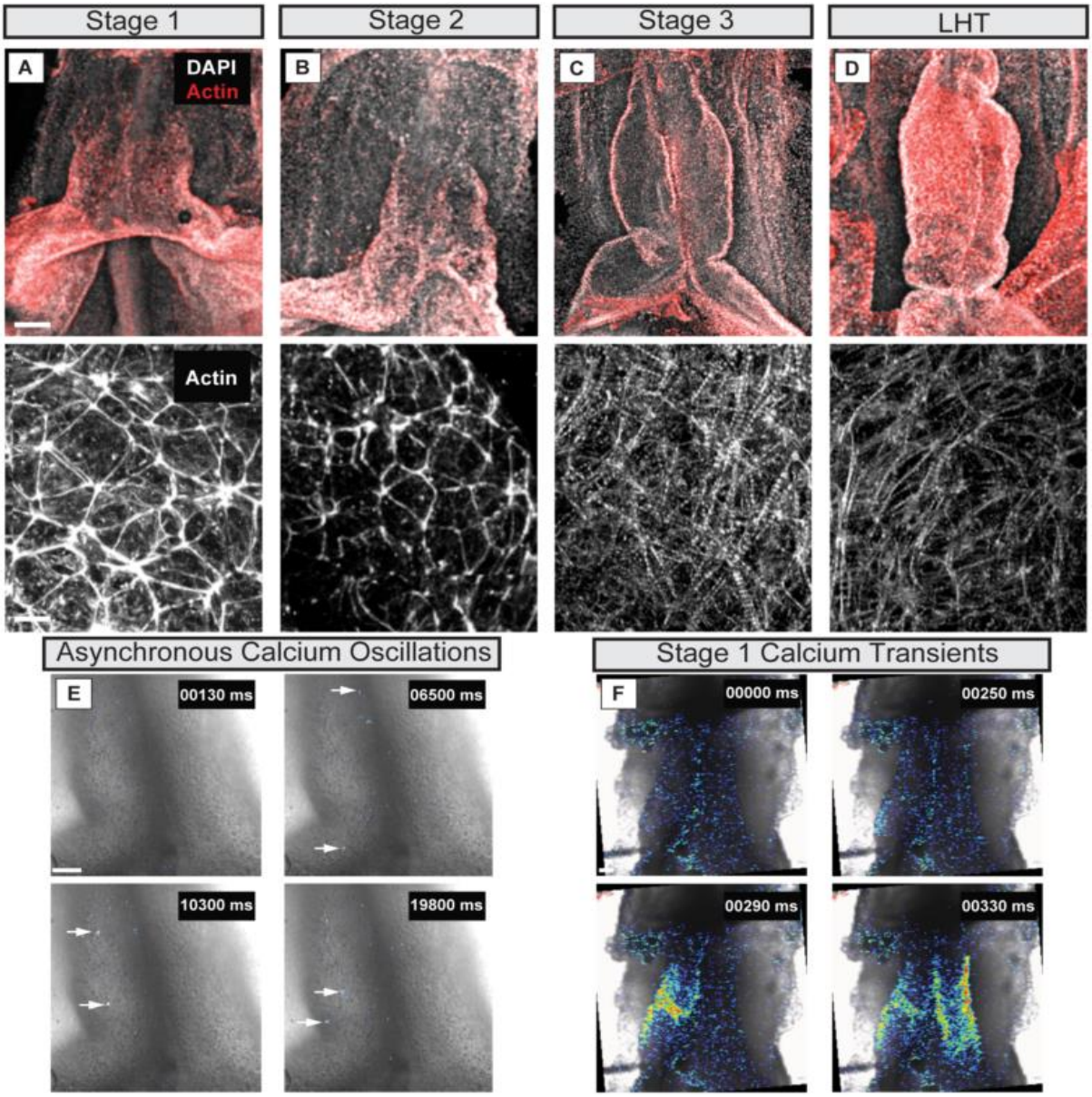

Fig. 4.20 – Characterisation of early stages of chick heart development – (A-D) Actin staining of chick embryos. Sarcomere assembly is only detected at stage 3. (E) calcium imaging of stage 0 chick embryos, showing SACOs (white arrows). (F) calcium imaging of stage 1 chick embryos. Scale bars = 100 µM.

4.3 – Discussion

Previous studies have attempted to investigate how cardiac function develops within the early embryo. Whilst these studies are informative they either rely on the dissociation and culture, over 12 to 70 hours, of embryonic cardiomyocytes to facilitate physiological measurements or, when performed in embryos, have limited resolution resulting in the loss of critical spatial and temporal information regarding Ca^{2+}-handling and downstream changes in gene expression and morphology. Furthermore, our data shows that culturing embryos for periods longer than 13 hours leads to a decrease in the rate of cardiac contractions (fig. 4.3), which could indicate a change in physiology from freshly dissected embryos. Even short 30 minutes cultures lead to an increase in arrhythmias (fig. 4.12). Using a staging method based on morphological landmarks (stages 0–3), we characterized in detail the *in vivo* progression of physiological activity during early heart development. The stage series defined correlates with gradual expression of several cardiac related genes and sarcomere assembly (fig. 4.3, 4.3, 4.6).

We observed spontaneous asynchronous Ca^{2+} oscillations (SACOs) at stage 0 in the developing cardiac mesoderm (fig. 4.6 - A), before any detectable cardiac contractions, which are maintained in a few cells at the later stages. SACOs appeared sporadically in individual cells within the forming cardiac crescent and did not appear to be synchronized or appear in any obvious pattern over the developmental time course studied here. At stage 1, periodic Ca^{2+} transients began to be propagated laterally through the cardiac crescent, and traversed the midline of the crescent where there were no visible contractions (fig. 4.6 - B). Unfortunately, the transition between SACOs and a full transient within a single embryo is not possible to capture with the

current methodology. This would require constant imaging of the embryos for longer period of times, which would cause photodamage. A potential way to overcome this limitation is to use lightsheet microscopy, which allows for faster frame rates and less exposure to light to observe the embryo. However, as the time of this transition cannot be predicted by cardiac morphology alone, it would likely be necessary to image a large number of embryos in to capture this transition in a small number of samples. There also seems to be a left-right bias in the directionality of this propagation, which could point to an involvement of the left-right pathway in this process (fig. 4.11). Treatment with Ivabradine also revealed that the two sides of the cardiac crescent respond differently (fig. 4.12), further supporting this hypothesis. This was a rapid and dynamic process occurring through stages 0–3 that involved sarcolemmal ion channel and exchanger function. NCX1 was exclusively required for SACOs at stage 0, whereas both NCX1 and LTCC appeared to play equally important roles at stage 1 and 2. NCX1 was no longer required from stage 3 onwards when the LTCC channels maintained Ca^{2+} transients. We observed no contribution of the SR in regulating Ca^{2+} transients within the cardiac crescent, as assessed by simultaneous blockade of RyR2 and InsP3. However, consistent with previous studies (*128, 129*), our data did show that the SR becomes functional at later stages during cardiac looping (~E8.5; fig. 4.9). The earliest stage we tested for SR contribution was stage 3, and therefore it is not possible to definitely conclude that there is no role for the SR at earlier stages or in the maintenance of SACOs, it seems likely this may represent a period in which SR Ca^{2+} filling is required before a threshold for Ca^{2+} release from the SR can occur, as has been proposed in the adult setting (*171*).

The observation of spontaneous asynchronous calcium oscillations (SACOs) within the forming cardiac crescent was a surprising finding that, to the best of my

knowledge, has not previously been reported in any type of excitable cell. The specific role of SACOs is currently unknown and I hypothesise that they are required in cells that need to optimally activate Ca^{2+}-dependent signalling (via the CAMKII pathway) in order to up-regulate genes necessary for further differentiation and morphogenesis. This would explain why SACOs are present much earlier than complete sarcomere assembly. An alternative hypothesis is that SACOs are a by-product of cells that are already committed to specific cardiac lineages and, therefore, arise with the expression of specific channels required for future function. This could explain the variation in duration and frequencies of SACOs observed within the same embryo high variation in the expression ion channels and pumps in the scRNAseq data (Table 4.3). I speculate that release of a Ca^{2+}-dependent signal from a 'pacemaker' cell may entrain neighbours to have synchronised transient periodicity. This is supported by the preliminary Ivabradine treatments, which blocks HCN channels, required for pacemaker activity, which leads to asynchrony between the left and right sides (fig. 4.12). To this end we observed highly variable Ca^{2+} periodicity but also regions containing cells of similar periodicity (fig. 4.6 - C). Since blockade of NCX1 prior to the formation of the cardiac crescent, leads to impaired cardiac differentiation it is also possible that SACOs may be present in mesoderm cells earlier than reported here. However, at the stage analysed here, SACOs to seem to be specific to the precursors of excitable tissues, since they are not observable in the endoderm in the same focal plane of the cardiac mesoderm.

Previous studies characterised functional expression of NCX from E8.5-E9.5 (post-LHT formation) in mouse (*122, 123*) coincident with cardiac looping and significantly later than the onset of the first heat beat described herein. NCX1 knock-out mice have been generated by multiple groups, with conflicting results in regards

to the phenotype, extent of mutant heart development and the stage at which embryonic lethality occurs (*172-175*). This suggests that loss of NCX1 may be compensated for at the level of early cardiomyocyte specification, differentiation and contraction. In mammals, there are three different Na+-Ca2+ exchangers (NCX1, NCX2 and NCX3), and it has been previously demonstrated that these three exchangers share similar physiological properties (*176, 177*). Furthermore, NCX1 has several splicing variants with exon 1 being mutually exclusive to exon 2 (*177, 178*). It is, therefore, possible that either a different NCX or an alternative splice variant will compensate for loss of the NCX1 variant targeted in the previous studies. Indeed, in all of the previous NCX1 generic loss-of-function studies, mutant mice were created by targeting exon 2, supporting the possibility that an alternately spliced variant may be able to compensate. Furthermore, precedent for genetic ablation being compensated for over the course of development exists, whereby patterning defects were muted over time (*179*). These findings are consistent with earlier findings in rodents demonstrating a requirement for elevated cytoplasmic calcium to drive cardiac myofibrillogenesis in developing cardiomyocytes (*180*). In order to ascertain the role of NCX1 in early heart development with more clarity, it would be advantageous to use a conditional knockout line in order to avoid compensatory mechanisms which may be present in the full knockout as well as possible off-target effects from drug treatments and the limitations imposed by the viability of embryos cultured *ex vivo.*

NCX1 can function in both forward (Ca^{2+} efflux from the cell) and reverse (Ca^{2+} influx into the cell) modes. Our data suggested that NCX1 in the early cardiac crescent was functioning in reverse mode, as KB-R7943, that is reported to specifically inhibit reverse mode NCX1 function (*181, 182*), recapitulated the results with CB-DMB and acted as a control for off-target effects of the latter. Whilst inhibition of NCX1 clearly

blocked SACOs in stage 0 cardiac crescents, the mechanism by which NCX1 could lead to periodic oscillations in Ca^{2+} is still unclear, and may it is likely to require oscillations in other ions, such as Na^{+}, and/or contribution of other sarcolemmal proteins, such as the Plasma membrane Ca^{2+} ATPase (PMCA), to regulate Ca^{2+} efflux while NCX1 is working in reverse mode. Due to the slow nature of SACOs, oscillations in energy production along with adenosine triphosphate levels could also be involved in SACO generation, especially with reduced SR function. This study could be further complemented by making use of fluorescent dyes to image the dynamics of other ions and *in vivo* electrophysiological analysis. Unfortunately, our scRNAseq analysis did not reveal any other channel or pump that correlates well with NCX1 (Table 4.3). This suggests that these processes may either be regulated by more ubiquitous proteins, or that there are different cell populations expressing different channels, originating different physiological dynamics. Although the existence of the NCX1 acting in reverse mode is contentious, and the precise function of KB-R7943 is still debated in the field, it is difficult to otherwise explain how inhibition of NCX1 can block SACOs. That said, regardless of mode of action, the observation that at stage 0 SACOs were abolished with both CB-DMB and KB-R7943 treatment, but persisted when treated with nifedipine, suggests that NCX1, and not the LTCC, plays a major role in Ca^{2+} transient generation within the early cardiac crescent.

As cardiomyocytes matured, transition to LTCC became the predominant mechanism for inward Ca^{2+} entry, as demonstrated by nifedipine-induced inhibition of beating at later stages. NCX1 expression was further maintained at high levels during more advanced stages (stage 0-LHT), suggesting a later role in ensuring Ca^{2+} removal via its forward mode of action. Of note, the early versus late roles for mammalian NCX1 and LTCC, respectively, are further supported by studies on *tre* zebrafish mentioned

above, whereby sarcomeric assembly defects in developing cardiomyocytes following loss of NCX1 function are not recapitulated by mutations in LTCC (*183*).

There is recent precedent for a role for Ca^{2+} in the establishment of other embryonic lineages; most notably Ca^{2+} signals are involved in the earliest steps of neurogenesis, including neural induction and the differentiation of neural progenitors into neurons (*184*). The appearance of Ca^{2+} transients in the embryonic heart prior to beating is consistent with the idea that Ca^{2+} signalling within early cardiac progenitors may be important to promote sufficient differentiation for subsequent contractile. We showed that pharmacological inhibition of NCX1 and dysregulation of Ca^{2+} handling from the outset had an adverse effect on early cardiomyocyte differentiation and led to impaired cardiogenesis in the embryo (fig. 4.10). Thus, an early induction of Ca^{2+}-handling preceding beating within cardiac muscle is pivotal for subsequent terminal differentiation and normal heart development. My preliminary analysis of the scRNAseq data suggest that Fbxo32 and Naca may be key regulators of early cardiac function, however further characterisation of the expression pattern and function of these genes is necessary. This could be achieved with *in-situ* hybridization to investigate the expression of the mRNA in the whole embryo, or ideally with antibody stainings as these provide more cellular resolution. The bioinformatic analysis presented in this chapter is also only a first attempt at uncovering overarching key players in the regulation of early cardiac function, clustering all the stages together. A more detailed analysis within each stage and comparing stages to one another would likely provide more specific information. However, while we collected an overall large number of cells, each individual stage as small number cells, not allowing a proper statistical analysis of this type.

Finally, my experiments in the chick embryo suggest that there may not be a complete conservation of the mechanisms mentioned above. While the onset of SACOs and the subsequent transition into calcium transients seems to be similar between mouse and chick, it appears that the chick embryo is different in two key aspects: the calcium transients always propagate right to left; sarcomere assembly, and cardiac contractions, are delayed until stage 3. The apparent difference in the propagation of the calcium transient may be due to the known differences in the left-right asymmetry mechanisms between mouse and chick. At the moment, it is difficult to explain the difference in the timing of sarcomere assembly, however since the onset of calcium transients seems to be similar between the two species, it is likely that sarcomere assembly and establishment of calcium transients are uncoupled and controlled by different molecular mechanisms. It is important to note that due to different size, optical properties and chemistries, it is not possible to directly compare mouse and chick embryos, especially protein stainings. A good example of this is the heterogeneity of phalloidin stainings in mouse embryos, which often makes it difficult to detect sarcomeres, even at the LHT stage. Future work should expand on the protocols used here and compare the two species with methods less susceptible to optical and chemical conditions such as electron microscopy to detect sarcomeres. Furthermore, chick and quail embryos seem to initiate cardiac contractions at stage 3, suggesting the existence of similar mechanisms between these two avian species. However, early development in mouse embryos is very different from other mammals which develop as a disk, therefore it is not possible to know if the mouse mechanisms is representative of mammalian development or if non-rodent species have a mechanism more similar to the avian embryos. For this purpose, it would be interesting to repeat the experiments mentioned in this chapter in rabbit embryos.

Chapter 5 – Examining Endodermal Contribution to Cardiac Development

5

Table of Contents

5.1 – Introduction

In the previous chapters I have described my work on the interplay between early cardiac physiology and cardiac development. The endoderm has been reported to have a close relationship with the cardiac mesoderm and be involved in the differentiation of cardiomyocytes. In this chapter I describe my preliminary work investigating the possible contribution of the pharyngeal endoderm to the formation of the heart.

5.1.1 – Mesoderm and Endoderm Origin

Gastrulation is a key step during embryonic development, leading to the formation of the different germ layers. The germ layers have been target of intensive research, and it is now possible to associate each organ in fully developed animals to specific germ layers. Regarding the number of germ layers, the animal kingdom can be divided in two groups - diploblastic, with 2 germ layers, and triploblastic, with 3 germ layers. Diploblastic animals are composed of endoderm and ectoderm tissues, with mesoderm being a germ layer exclusive to triploblastic animals. The mesoderm is usually considered an innovation of the Bilateria clade, making triploblasty the most common type of blastula, present in 30 out of 35 animal phyla alive today. Diploblasty is only present in simpler animals such as the member of the *cnidaria* and *ctephora* phyla (reviewed in (*185*)).

A great deal of research has given us insights into which tissues each germ layer ultimately forms and which markers can be used to identify these layers. Despite this knowledge, the precise evolution of these germ layers is still open to debate.

Considering the existence of diploblastic and triploblastic animals, there are two main hypotheses on how germ layers might have evolved. The first hypothesis states that triploblasty is the ancestral state and that diploblastic animals lost the ability to form mesoderm. The second, most likely and most accepted hypothesis, states that diploblasty is the ancestral state and mesoderm is an evolutionary novelty of triploblastic animals (*186*). Considering the second hypothesis the question then becomes whether the mesoderm evolved from the endoderm or the ectoderm. While there still is no definite answer to this question, evidence suggests that mesoderm has a strong relationship with the endoderm, and in fact may have evolved from this tissue, with both morphological and transcriptional evidence supporting this hypothesis.

In terms of morphological evidence, during amniote gastrulation the mesoderm originates next to endodermal pouches. Prior to the complete separation of these two germ layers, they also undergo a transitional state called mesendoderm (also known as endomesoderm). It is debatable whether the mesendoderm is a true progenitor state, with cells being able to form both endoderm and mesoderm cells, or simply a tissue composed of mixed population of endoderm and mesoderm cells, which have not segregated yet (*185*). Recent scRNAseq data suggests the former may indeed be the case (*60*).

At a transcriptional level, many transcription factors involved in some mesodermal lineages are also involved in the development of endodermal lineages. Some of these factors include the GATA transcription factors, especially Gata6 and Gata4, and Isl1. The expression of homologues for genes critical for mesoderm development, such as *GATA transcription factor, snailA, snailB twist, forkhead* and *mef2* has been investigated in cnidarians, more precisely in the sea anemone *Nematostella vectensis*. With the exception of *mef2c*, these genes are expressed in

the endoderm of *Nematostella*, supporting the idea that mesoderm has evolved from endoderm (*186*). Other studies have also found that *brachyury*, which is typically involved in mesoderm specification and cell movement during gastrulation, can actually induce endoderm formation in triploblastic animals, more precisely in ascidians and *Drosophila* tissues (*34*). Interestingly, the T protein in these species is missing a N-terminal motif, which seems to be required to supress endoderm induction. Furthermore, a transcriptomic analysis of *Caenorhabditis elegans*, *Xenopus tropicalis*, *Nematostella vectensis* and *Amphimedon queenlandica*, suggested that the endoderm is the oldest germ layer, with both the ectoderm and the mesoderm having evolved from ancestral endoderm cells (*187*). In summary, evolutionary evidence seems to suggest that the mesoderm has evolved from the endoderm, with these tissues retaining a close relationship during development, including at a transcriptional level (table 5.1).

5.1.2 – The Role of Endoderm During Cardiac Development

Besides the potential shared evolutionary history of these two germ layers, cross talk between the endoderm and the mesoderm has been reported in several contexts during embryonic development. These cross talks include signalling interactions between the cardiac mesoderm and the developing endoderm. For example, in zebrafish, Wnt signals from the cardiac mesoderm are permissive for the induction of liver development (*188*). In terms of heart development, the endoderm has been associated with differentiation of cardiomyocytes, endocardium, ventral folding and subsequent positioning of the heart.

Table 5.1 – Transcriptional similarity between early endodermal and mesodermal tissues – Some endodermal tissues have a high transcptional similarity with mesodermal tissues. An example of this similarity is the transcriptional similarity between the definitive endoderm (DE) and yolk sac endoderm (YSE) and the cardiac mesoderm in the mouse embryo at E8.0. More specifically, the DE and YSE share the same markers as the Second Heart Field (SHF), but to a lesser extent with the First Heart Field (FHF). Green – expressed; orange – expressed in some cells; red – not expressed.

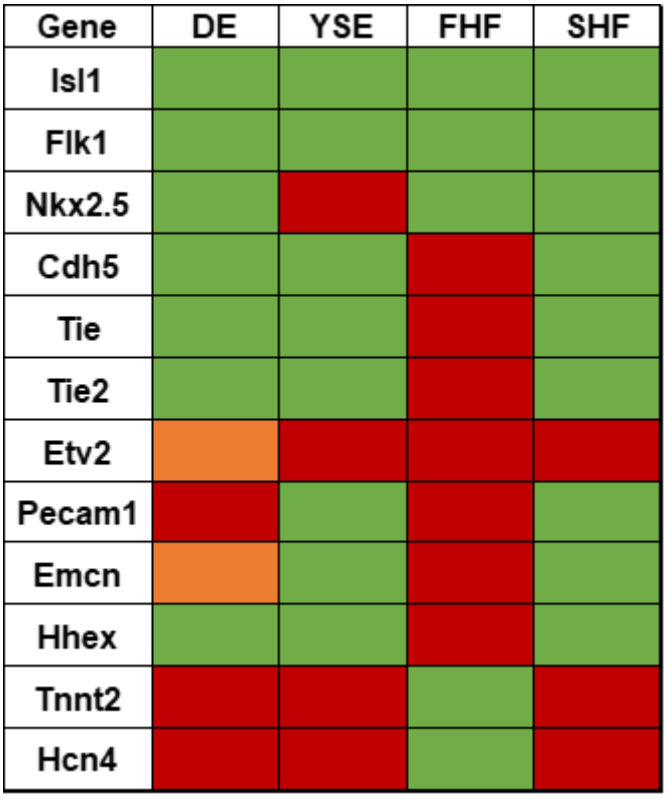

Much of the research involving the interplay between endoderm and cardiac mesoderm has focused on the early stages of cardiac development, prior to the formation of the linear heart tube. Initial experiments performed in chick embryos suggest an important role for the endoderm in the differentiation of cardiomyocytes in a stage dependent manner. Removing the endoderm prior to the formation of the cardiac crescent in HH5 chick embryos leads to a failure to form a heart. On the other hand, removal of the endoderm in HH8 chick embryos, either from both sides of the embryo or from just one side, does not impair cardiomyocyte differentiation but the cardiac crescent fails to fuse at the midline leading to *cardia bifida* (*189*). Cardiomyocyte differentiation seems to proceed under these conditions, however the beating rate of these cardiomyocytes is lower than normal. This suggest that the endoderm at this stage does while not entirely necessary for cardiomyocyte differentiation to proceed initially, it does seem to be required for the cardiomyocytes to reach a more functional differentiated state. Furthermore, during migration to the midline, endodermal progenitors migrate in close proximity with cardiac progenitors. Zebrafish embryos with mutations impairing the formation of endodermal progenitors also develop *cardia bifida* (*190-192*). It has been shown that rescuing the population of endodermal progenitors, mutants restores the formation of the cardiac tube (*193*), suggesting these defects are not due to the mutation affecting cardiomyocytes, but most likely due to the interaction between the endoderm and the mesoderm.

While the experiments described above do not provide detailed insights on the interaction between the two germ layers during cardiac development, experiments in mouse have clarified some details of this process. From these experiments, BMP2 has been identified as key molecule for early cardiac patterning. While BMP2 is expressed in several tissues at the time of the migration of the cardiac crescent to the

midline, such as in the splanchnic mesoderm, the definitive endoderm (DE) and the visceral endoderm (VE), recent experiments knocking-out BMP2 specifically in the VE has revealed a critical role in the positioning of the heart (*194*). Briefly, shortly after gastrulation, TGFβ signals from the VE induce cardiogenic potential in the epiblast and nascent mesoderm. Afterwards, BMPs from the endoderm induce cardiogenic lineage in the endoderm. Midline inhibitors of BMPs like noggin and chordin restrict this action to the more lateral regions. *In-vitro* experiments have also show that embryonic stem cells culture in the presence of VE-like cells promotes cardiomyocyte differentiation, leading to increased beat rates. Besides the importance of the endoderm in the differentiation of cardiomyocytes, signals from the endoderm have also been reported to be important for the differentiation of endothelial cells into endocardium.

The Pharyngeal Mesoderm (PhM) also has an important role for heart development, being involved in the formation of the Second Heart Field (SHF) (*48*). For this reason, due to proximity and molecular similarities, in particular the expression of Nkx2.5, the potential role of the pharyngeal endoderm (PhE) during cardiac development has also been investigated (*195*). Mesoderm-specific KO of Nkx2.5, using a Mesp1-Cre^{ERT} leads to several cardiac defects, such a smaller ventricle and later, septation defects. On the other hand, KO of Nkx2.5 in the endoderm, using a Foxa2-Cre^{ERT} driver, shows no overt cardiac defects, and mice live to adulthood. This result led the authors to suggest that PhE does not seem to play an important role during cardiac development. However, it should be noted that while KO of PhE Nkx2.5 leads to down-regulation of PhE markers, such as Nkx2.9, this does not affect the formation of the PhE itself, nor does it lead obvious craniofacial or larynx defects,

suggesting that KO of Nkx2.5 does not necessarily play a key role in the development and function of the PhE.

5.1.3 – Epithelial to Mesenchymal Transition

Over the course of this chapter I will be discussing the hypothesis that cells from the PhE physically contribute to the formation of the heart. The early DE and PhE are epithelial tissues, consisting of a single layer of cells, characterised by apical-basal polarity, several tight-junction and adherens junction proteins allowing cells to adhere to each other and form a stratified tissue. A recurrent theme during development is the ability of epithelial tissues to change their mechanical and adhesive properties, acquiring migratory properties. This process is termed epithelial-to-mesenchymal transition (EMT). Examples of developmental processes where EMT plays a key role includes the movements of cells through the primitive streak during gastrulation, neural crest migration, the formation of the sclerotome and delamination of the dermamyotome during somitogenesis, and the development of endocardial cushions and cardiac valves during heart development (reviewed in (*196*)).

During EMT, epithelial cells first downregulate adhesion molecules, which is accompanied by a loss of apical-basal polarity. This is followed by apical constriction and disassembly of the basement membrane, leading to a loss of epithelial integrity, allowing the cells to ingress and migrate away from the epithelial layer (*197*). EMT is one of the most studied cellular processes, not only for it's critical role during development, but also for the importance it plays during cancer metastasis (*198*). Due to interest in developing therapies to prevent EMT in malignant tumours, the molecular pathways involved in EMT are well understood.

The Snail family of transcription factors, such as Snail (Snai1) and Slug (Snai2), together with Twist are amongst the transcription factors more often associated with EMT (*199*). Nuclear localisation of these factors is usually indicative of EMT and associated with cadherin switch, i.e., a downregulation of e-cadherin and upregulation of n-cadherin (*197*). The activity of these transcription factors also leads to upregulation of membrane metalloproteases (MMPs), which are required for the degradation of the basement membrane. More recently, alternative pathways leading to EMT have been identified in several contexts, involving ZEB transcription factors or LEF1, without necessarily involving Snail factors (*199, 200*). Interestingly, even though these transcription factors involve different pathways, they lead to similar cellular changes as the Snail transcription factors, most notably the cadherin switch. Several pathways have been shown to lead to activation of the transcription factors mentioned above. Some examples of these pathways include the tyrosine kinase pathways (EGF and FGF), TGFβ, WNT, TNFα and Integrin pathways. Although some of these pathways have been strongly associated with specific EMT-related transcription factors (FGF with SNAI1, WNT with LEF1 and TGFβ with ZEB1/2), it is important to note that there can be a certain degree of interaction between these different pathways. For example, TNFα usually leads to the activation of NK-κB and subsequent EMT, however, EGF and FGF pathways, through AKT and TAK1, as well as TGFβ through TAK1 can also lead to the activation NK-κB (*199, 200*). Similarly, while ERK activity is mostly associated with TGFβ pathways, it can be achieved through FGF pathways, including in the mouse heart primordia (*201*) and chicken primitive streak (*202*). This redundancy in EMT, whereby several pathways can be used to achieve the same result, is indicative of the importance of this process during embryonic development.

5.2 – Results

5.2.1 – Morphological Integration Between Endoderm and Early Cardiac Mesoderm

It has long been recognised that the endoderm has a close relationship with the mesoderm during cardiac development. Signalling from the endoderm is facilitated by the close proximity of this tissue to the cardiac mesoderm. Furthermore, the definitive endoderm of the early embryo is almost genetically identical to the SHF cells. Due to these factors, we tested the hypothesis that endoderm cells can physically integrate into the cardiac mesoderm and contribute to heart formation. I examined, in the mouse embryo, endoderm cells in close proximity to the cardiac mesoderm at a higher detail using the Airy scan super-resolution mode on the Zeiss 880 confocal microscope.

At the early developmental stages, endodermal tissues are stratified epithelial tissues. At E8.0 mouse embryos (stage 0 to stage 2), while most of the definitive endoderm is a singe stratified layer of cells, the most central region (surrounding the midline), and overlying the cardiac crescent, consistently displays cells that look as if they are forming a pseudo-stratified tissue, similar to the morphological changes that cells undergo during EMT (fig. 5.1 – A, red arrow). During embryonic folding, the endoderm is internalised, forming the gut endoderm. We have also examined the aortic sac, a region of the outflow tract, meets the PhE at E8.5 (linear heart tube to looping stages). We found that, in this region, the endoderm is thicker and with a seemingly compromised epithelial stratification (fig. 5.1 – B). This region seems continuous to the endothelial cells of the heart and, similarly to the early stages, and

also displays cells that morphologically look as if they are undergoing EMT (fig. 5.1 – B, red arrow). For the rest of this these I will be referring to this region, consisting of the PhE and aortic sac, as Outflow Cap (OC). We also obtained a sectioned CS10 human embryo (fig. 5.1 – C), from Newcastle's Human Developmental Biology Resource, subjected to a Haematoxylin and Eosin staining. While difficult to precise define the exact stage of cardiac development, the morphology seems to indicate that the heart is between the linear heart tube and looping stages (fig. 5.1 – C'). By focusing on the OC region, it is possible to observe that, like mouse embryos, human embryos also display a thickening of the PhE in the OC region (fig. 5.1 – C''), where the tissue looks more disorganised (fig. 5.1 – C''').

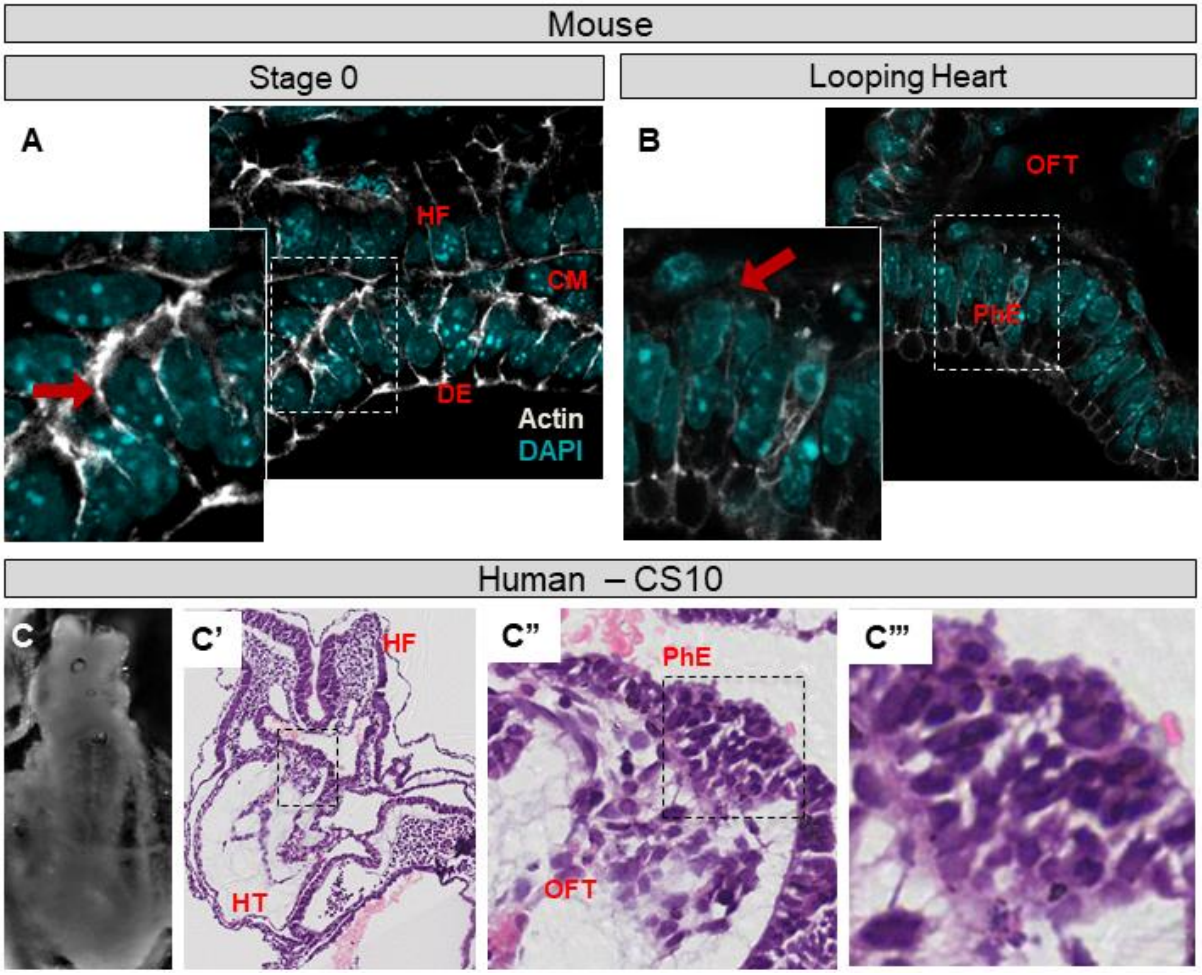

Fig. 5.1 – Morphology of early endodermal tissues – Super-resolution imaging of embryos stained for Actin (grey) and DAPI (cyan), at stage 0 (A) and the pharyngeal region at E8.5 (B). Red arrows point to regions not entirely stratified, resembling EMT. (C) Overview of a cs10 human embryo, stained for haematoxylin and eosin (C'-C'''). Dotted regions represent zoomed-in regions. HF- Head folds, CM – Cardiac mesoderm, DE – Definitive Endoderm, PhE – Pharyngeal Endoderm, OFT – Outflow Tract.

5.2.2 – DiI Analysis of Endoderm Cells

To further investigate the hypothesis proposed in this chapter, it is necessary to assess whether endoderm cells may indeed integrate into cardiac tissue and whether or not these cells are actively migrating out of endodermal sheets. In order to assess this, I performed three types of experiments: 1) live-imaging of whole stage 0 – stage 1, to investigate whether endoderm cells can migrate out of the epithelial layer; 2) DiI labelling in order to assess the short-term contribution to cardiac tissue; 3) Ttr-Cre lineage analysis, to analyse medium term contribution to the heart.

To perform live imaging of stage 0 – stage 1 cardiac crescents I performed DiI labelling of the endoderm overlaying the heart in Hhex-EGFP embryos (fig. 5.2). I used Hhex-EGFP because is a well characterised line in the Srinivas lab, and more importantly labels the DE in a salt-and-pepper fashion. However, Hhex-EGFP cannot be used alone because it is also expressed in endothelial cells, therefore it is difficult to pinpoint with absolute certainty when an endoderm cell is moving into the cardiac mesoderm layer. Hhex-EGFP was used because it provides some tissue context, which would be difficult to obtain with DiI and DIC alone. The DiI labelling was performed by holding the embryo with the anterior side of the embryo facing the bottom of the dish and realising DiI under the embryo with a thin glass needle. Due to different densities, the DiI will form a small cloud of dye. This way, DiI labelling is restricted to the superficial tissue of the embryo (fig. 5.2 – 0 min, red arrow), in this case the endoderm. Therefore, any cell that is internalised over the course of the imaging ought to be of endodermal nature. Imaging of stage 0 embryos revealed that cells in the definitive endoderm overlaying the heart can move into the cardiac region (fig. 5.2, white arrow). This process does not appear to happen frequently, as for the total

duration of the movie (5 hours), only one cell can be observed undergoing this transition. A limitation of live imaging is that the mouse embryo cannot be kept in culture for an extended period of time. In order to compliment the live-imaging experiments, I have also performed DiI labelling followed by rolling culture for 12 hours. Similarly, to the live-imaging experiments, at the end of the 12-hour period it is also possible to visualize internalised cells (fig. 5.3). Due to the longer culture period, it is usually possible to find more than one cell that has potentially left the endoderm layer, with cells occasionally migrating further into the cardiac cavity (fig. 5.3, dotted region).

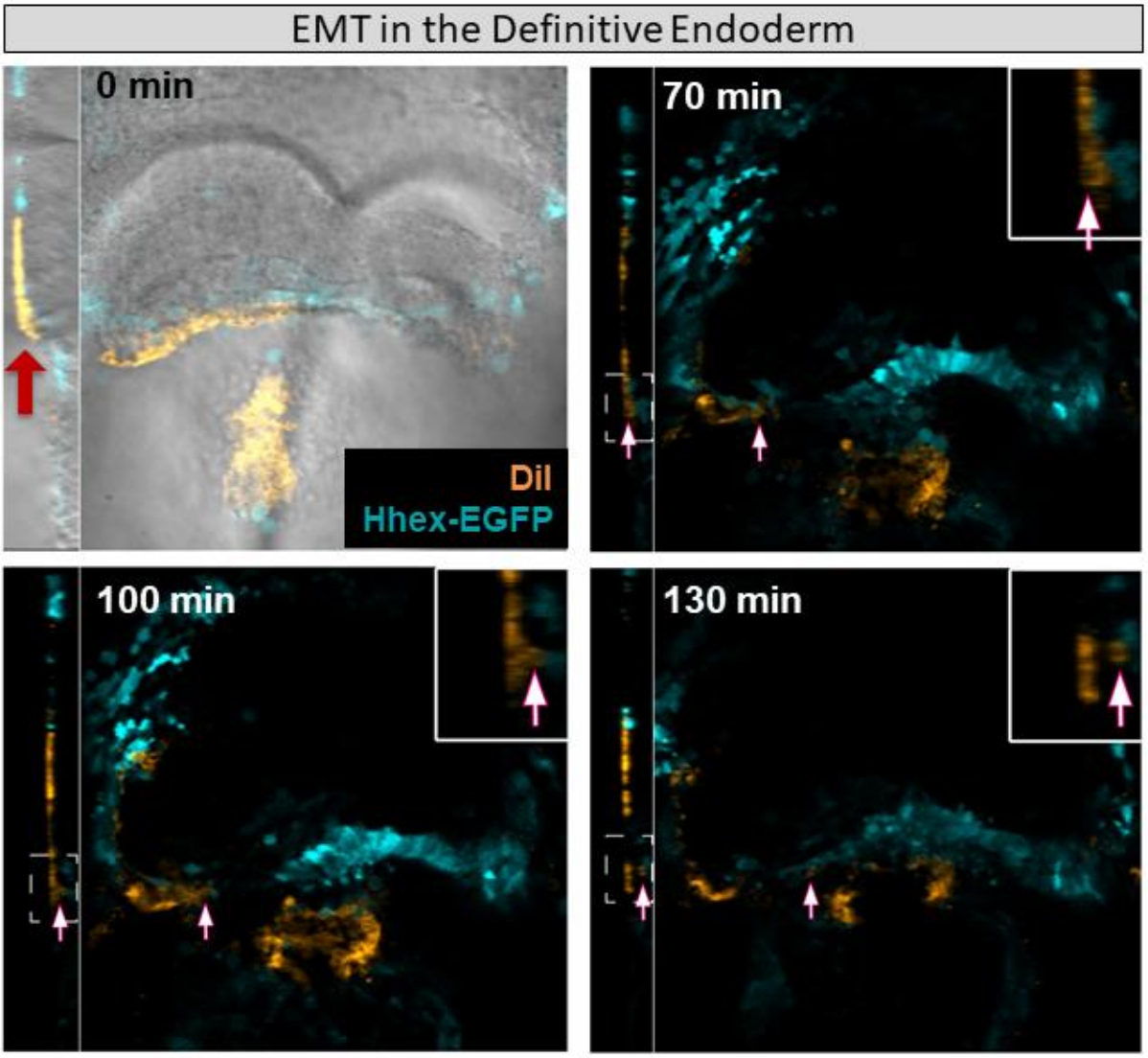

Fig. 5.2 – DiI staining and live-imaging of stage 0 Hhex-EGFP embryos – DiI labelling (orange) only stains the outer layer Hhex-EGFP (cyan) embryos (0 mins). Over the time lapse period a cell of the DE seemingly moves into the inner layer of the embryo (white arrow). Lateral box represents the YZ view. Dotted lines represent the zoomed-in region. A detailed section of Hhex-EGFP expression at E8.0 on annex 3.

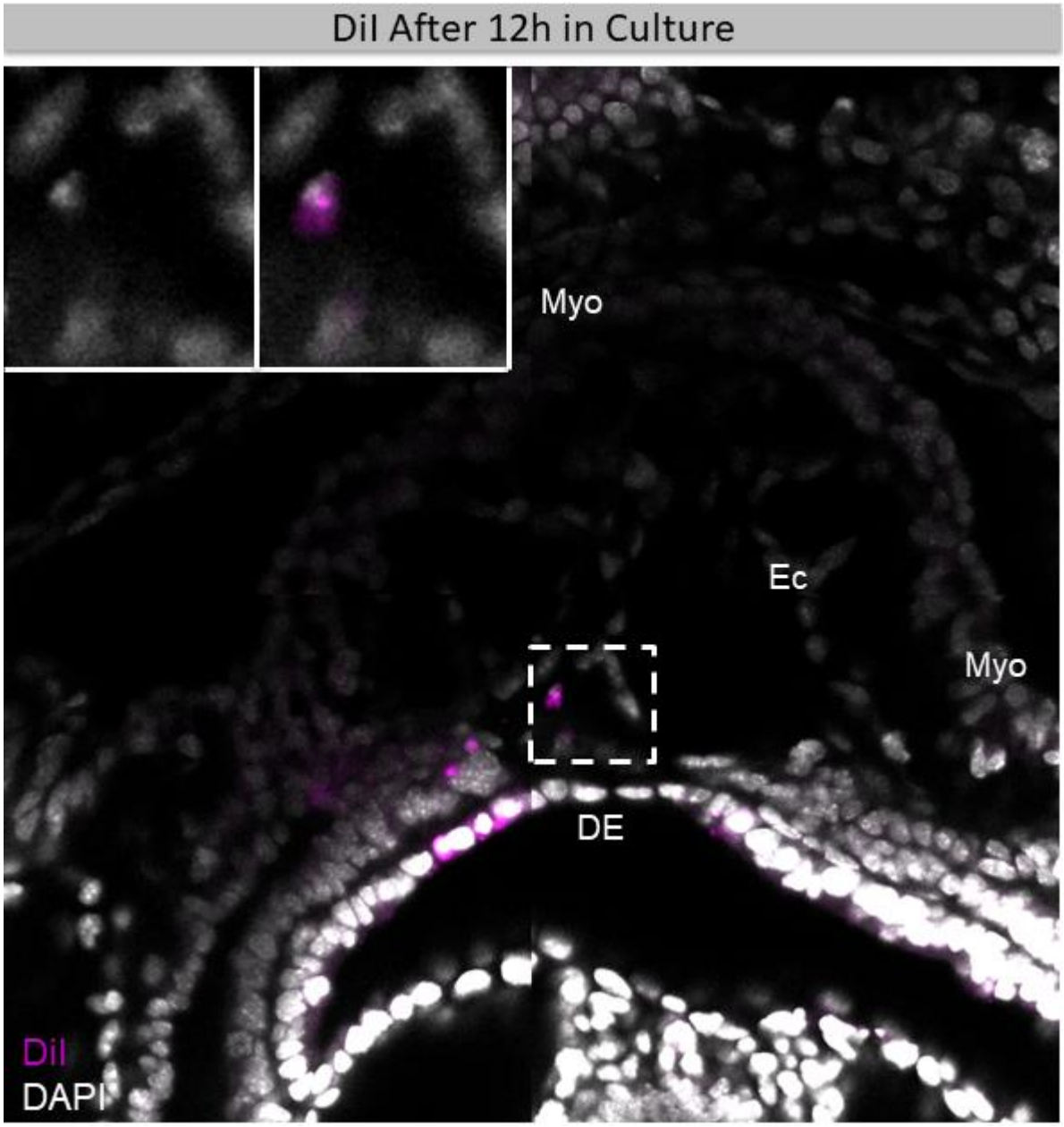

Fig. 5.3 – DiI in overnight cultured embryos – Stage 0 embryos labelled with DiI (magenta), cultured for a 12h period, and stained for DAPI (grey). After the culture period, embryos show internalised cells with DiI. Dotted line represents zoomed-in region, with a DiI+ cell. DE- Definitive Endoderm, Myo – Myocardium, Ec – Endocardium. N=6.

5.2.3 – Lineage analysis of Ttr-Cre/R26-EYFP cells

While DiI labelling and live-imaging experiments have been informative, they only provide short term insights into the fate of these endoderm cells. In order to investigate the long-term contribution of endoderm cells to the embryonic heart, genetic lineage experiments are required. As mentioned above, there are no known at this stage in development, as most suitable endodermal genes are also expressed in cardiac lineages, rendering it impossible to draw any meaningful conclusions from lineage analysis using such Cre drivers. In order to overcome this issue, I have used TTR-Cre to drive the expression of the ROSA26-EYFP transgene. TTR is expressed in the Visceral Endoderm (VE) in the early post-implantation mouse embryo, and while it is not expressed in the definitive endoderm in E8.5 mouse embryos, it has been reported that VE cells can integrate into the DE (*64*). Furthermore, this TTR-Cre line has been reported to not have any Cre expression by E8.5, even in the Yolk Sac (YS), where endogenous TTR expression is expected (*203*). Although, due to prior express of Cre in the VE, all yolk sac (YS) cells will have experienced Cre activity at an earlier time. This strategy then allows us to study the lineage of a limited number of DE cells that have been derived from the VE, while avoiding any confounding effect derived from expression of endoderm markers in the cardiac mesoderm.

I have analysed TTR-Cre/ROSA26-EYFP embryos at two stages of cardiac development – lopping stage at E8.5 and at E12.5 when the 4 chambers are already established. In both cases, embryos were first screened for EYFP expression in the YS (from here on referred as YS+ embryos), since all YS endoderm cells are EYFP+. From the imaging experiments described above, it seems reasonable to affirm that only a small proportion of endoderm cells seem to contribute to the heart. When

labelling cells using the before mentioned strategy the prediction is that some VE cells are going to contribute to the DE, as previously described, and subsequently some of these EYFP+ DE cells will contribute to the cardiac mesoderm. Therefore, since this strategy depends on two rare cellular events, the prediction is that not all YS+ embryos will show EYFP+ cells in the heart.

At E8.5 I looked for EYFP+ cells in the heart and in the OC region. As predicted, not all YS+ embryos showed EYFP+ cells in the heart, appearing only on 4/20 of YS+ embryos (fig. 5.4 – A). Furthermore, there is also a high variability of the number of cells in each heart, ranging from 1 cell to no more than 5 cells. While the number of embryos analysed is not high enough to say with confidence, these cells do not seem to localise to any particular region of the heart. Interestingly, and perhaps more surprising, only 8/20 of YS+ embryos show EYFP+ cells in the OC region, a DE tissue, with no more than 3 cells on each positive cap.

At E12.5, 4/16 of YS+ embryos had EYFP+ cells in the heart (fig. 5.4 – B, C), a similar ration to E8.5 embryos. Furthermore, at this stage these cells also do not seem to localise to any particular region of the heart, albeit they seem to localise more often to the outer layer of the heart. These cells often seem to form clusters, which could indicate a clonal origin (fig. 5.4 – B, C).

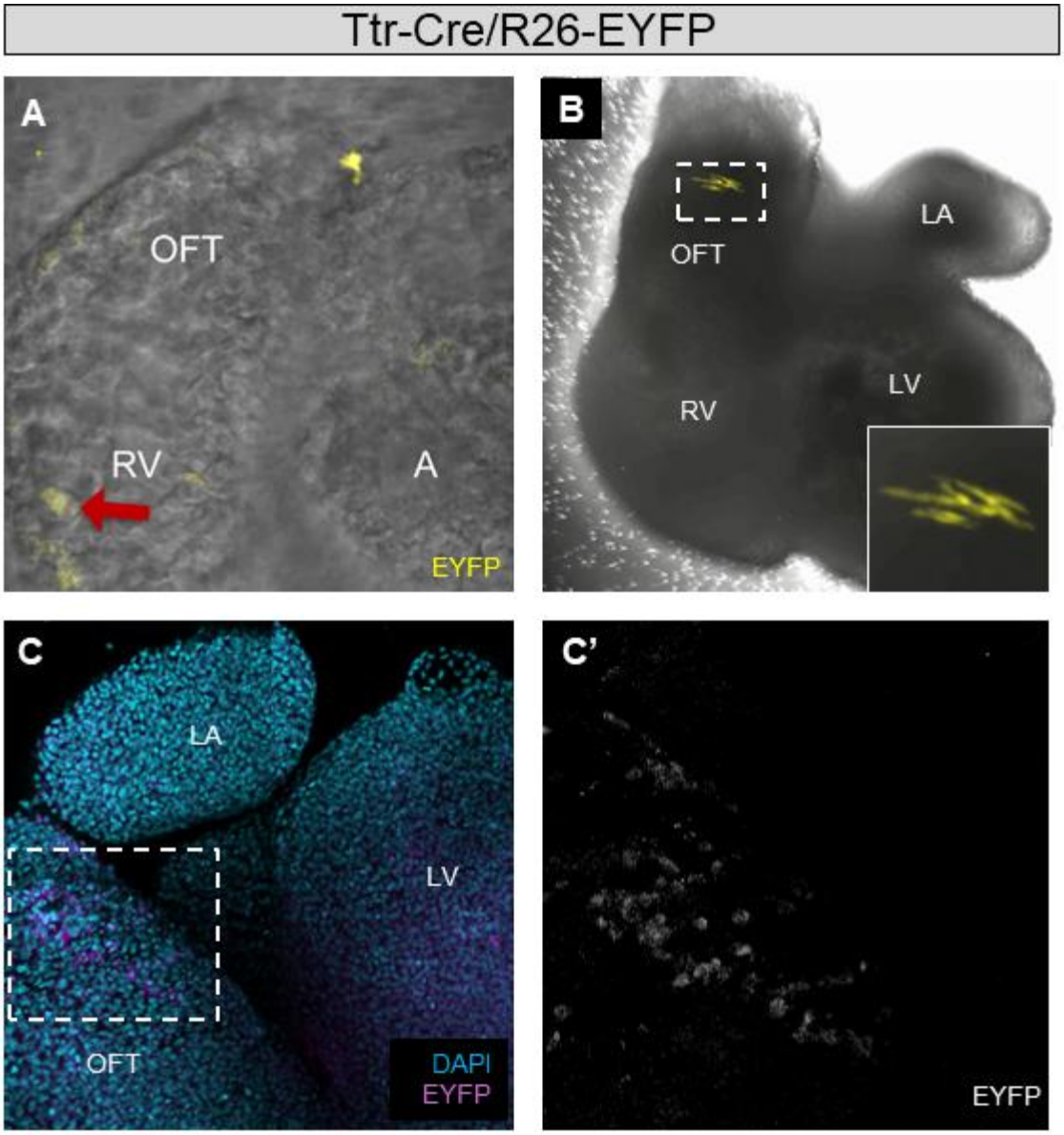

Fig. 5.4 – Ttr-Cre/R26-EYFP cells in the developing heart – Cells with EYFP expression driven by Cre under a Ttr promoter are detectable in developing hearts. EYFP (yellow) expression in live E8.5 (A) and E12.5 (B) hearts. (C, C') E12.5 heart stained for DAPI (cyan) and EYFP (C- magenta; C' – grey), stained with an αGFP antibody. Looping hearts never show more than a couple of positive cells in the heart (A, red arrow). E12.5 hearts (B, C) can show clusters of cells.

5.2.4 – Evidence for Endoderm EMT

In the previous section I described evidence which suggests that between E8.0 and E8.5, endoderm cells may integrate into the cardiac mesoderm and contribute to the formation of the heart. If endoderm cells are indeed leaving the epithelial layer, it is likely the cells are undergoing EMT. As described above there are several pathways that have been implicated in this process. To investigate whether or not EMT is occurring in the endoderm I have performed a series of immunostainings in the DE of E8.0 embryos for 3 transcription factors associated with 3 different EMT pathways: SNAI1, ZEB1 and LEF1.

At this stage, there seems to be a certain degree of tissue specific localisation of these 3 transcription factors. SNAI1 seems to be localised to endoderm layer but not to the myocardium or the cardiac endothelium (fig. 5.4 – A), ZEB1 is localised to the cardiac endothelium and myocardium (fig. 5.4 – B) and LEF1 is localised to the myocardium (fig. 5.4 – C). Interestingly, LEF1 and ZEB1 seem to be have a widespread expression in their respective tissues, while SNAI1 seems to be expressed, and localised to the nucleus, in only a few endoderm cells and it is not expressed throughout the whole tissue. These results are consistent with a SNAI1 mediated EMT is occurring in the endoderm.

FGF signalling and ERK activity has been associated with SNAI1 mediated EMT in both the mouse and chick primitive streak. To further test whether this pathway may be involved in endoderm EMT I performed immunostainings for FGFR1, FGFR2 and phosphorylated ERK (pERK). Both FGFR1 and FGFR2 are expressed in the definitive endoderm (fig. 5.6 – A, B), however FGFR2 also seems to be expressed in

the cardiac endothelium. Similarly, pERK is expressed in both the DE as well as the cardiac endothelium (fig. 5.6 – C).

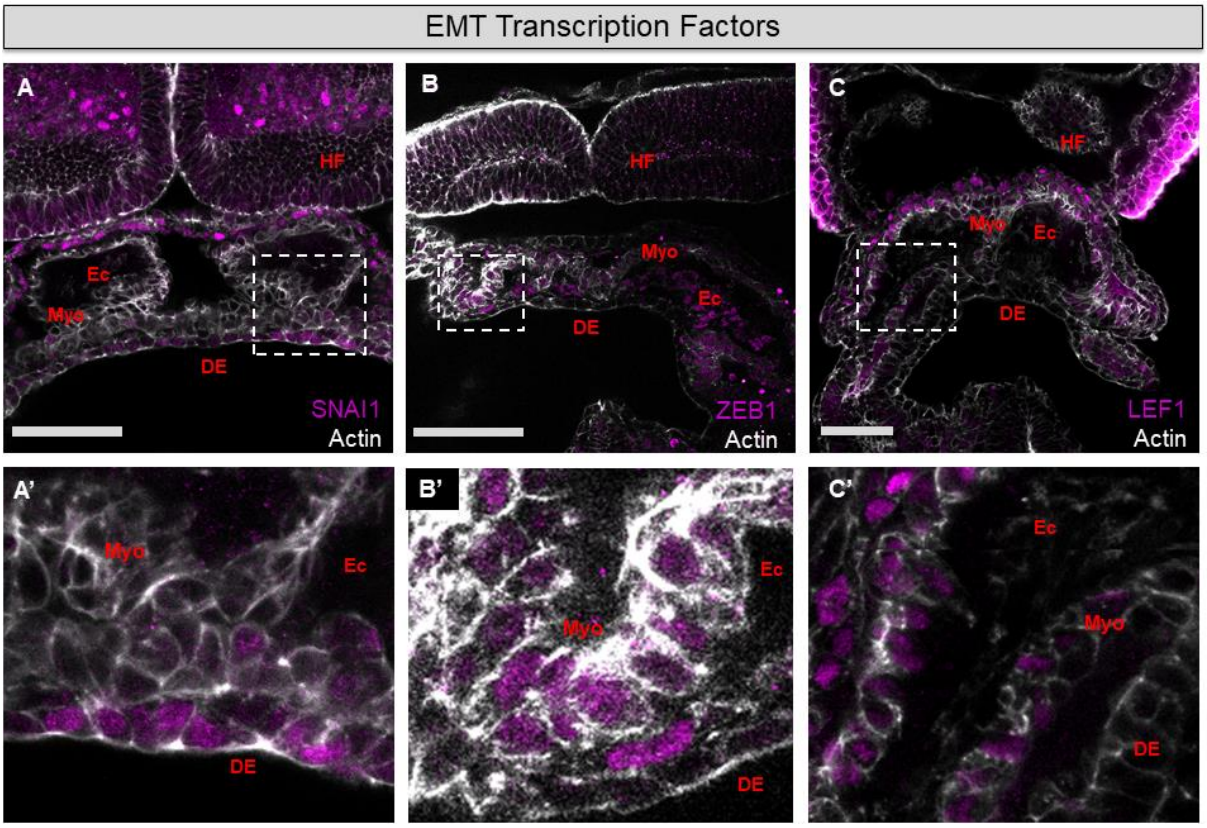

Fig. 5.5 – EMT transcription factors in the early developing heart – Stage 1 – 2 embryos stained for actin (grey) and transcription factors (magenta) of different EMT pathways, reveals complex regulation of this process in the different tissues. SNAI1 (A, A') appears to be expressed mainly the head mesoderm, splanchnic mesoderm and definitive endoderm (DE). Zeb1 (B, B') seems to be espresso mainly in the myocardium (Myo) and in the endocardium/cardiac endothelium (Ec). Lef1(C, C') is expressed mainly in the splanchnic mesoderm and myocardium. Dotted lines represent the zoomed-in regains. Scale bars = 100 µm.

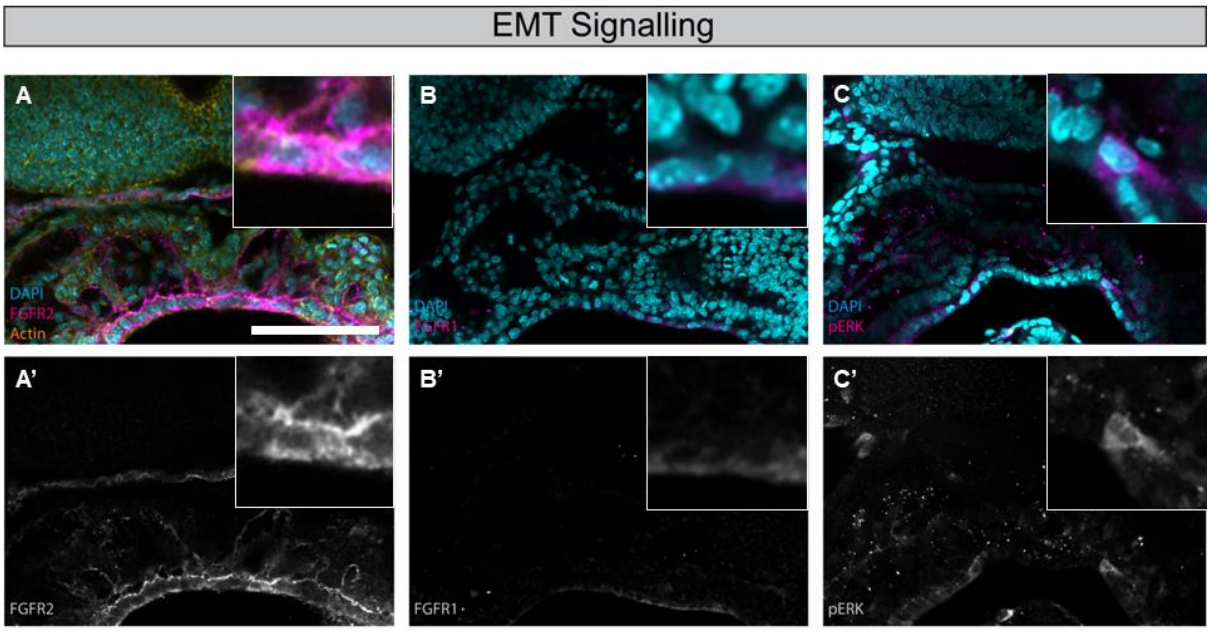

Fig. 5.6 – EMT signalling in the early developing heart – Stage 1 – 2 embryos stained FGFR2 (A, magenta; A', grey), FGFR1 (B, magenta; B', grey) and pERK (C, magenta; C', grey), key components of SNAI1 mediated EMT. All of these proteins are expressed in the DE. FGFR2 and pERK are also expressed in the cardiac endothelium.

Lastly, EMT is usually associated with changes in tissue architecture, most notably a cadherin switch and breakdown of the basement membrane. To investigate if the DE also undergoes these changes associated with EMT, I performed immunostainings for N-cadherin and E-cadherin (fig. 5.7) as markers of cadherin switch, and Laminin to visualise the basement membrane. EMT is usually associated with a downregulation of E-cadherin and upregulation of N-cadherin. While E-cadherin is still highly expressed in the DE (fig. 5.7 – B), N-cadherin is also expressed in this tissue, with some cells displaying slightly higher levels of expression (fig. 5.7 – A). Similarly, immunostaining for Laminin shows regions in the DE where there seems to be a breakdown of the basement membrane (fig. 5.8 – A', red arrow). These results are consistent with EMT occurring in the DE. While in this chapter I focused on the possibility of EMT occurring in the DE of E8.0 mouse embryos, staining for laminin in the OC region also shows a breakdown of laminin in the PhE (fig. 5.8 – B, red arrow). Furthermore, live imaging of the OC in Hhex-EGFP also suggests that EMT may be occurring in the PhE (fig. 5.9). It is then possible that endoderm EMT is a continuous process, from at least the cardiac crescent stages to the looping heart stages.

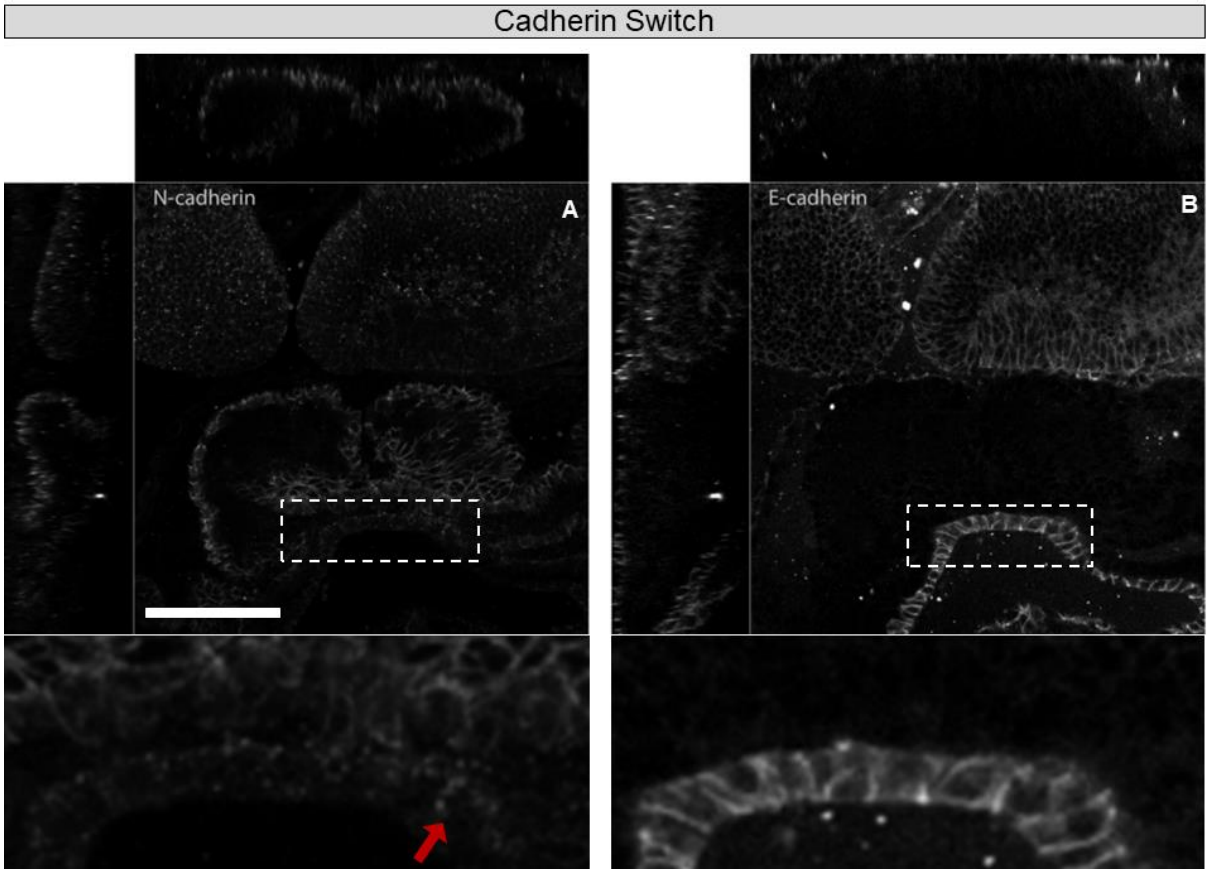

Fig. 5.7 – Cadherin switch in the definitive endoderm – During EMT epithelial cells usually undergo cadherin switch, from E-cadherin to N-cadherin. N-cadherin is widely expressed in the cardiac mesoderm, but also in the DE at lower levels (A, red arrow). E-cadherin is highly expressed in the Neurectoderm and in the DE (B). Scale bars = 100 µm.

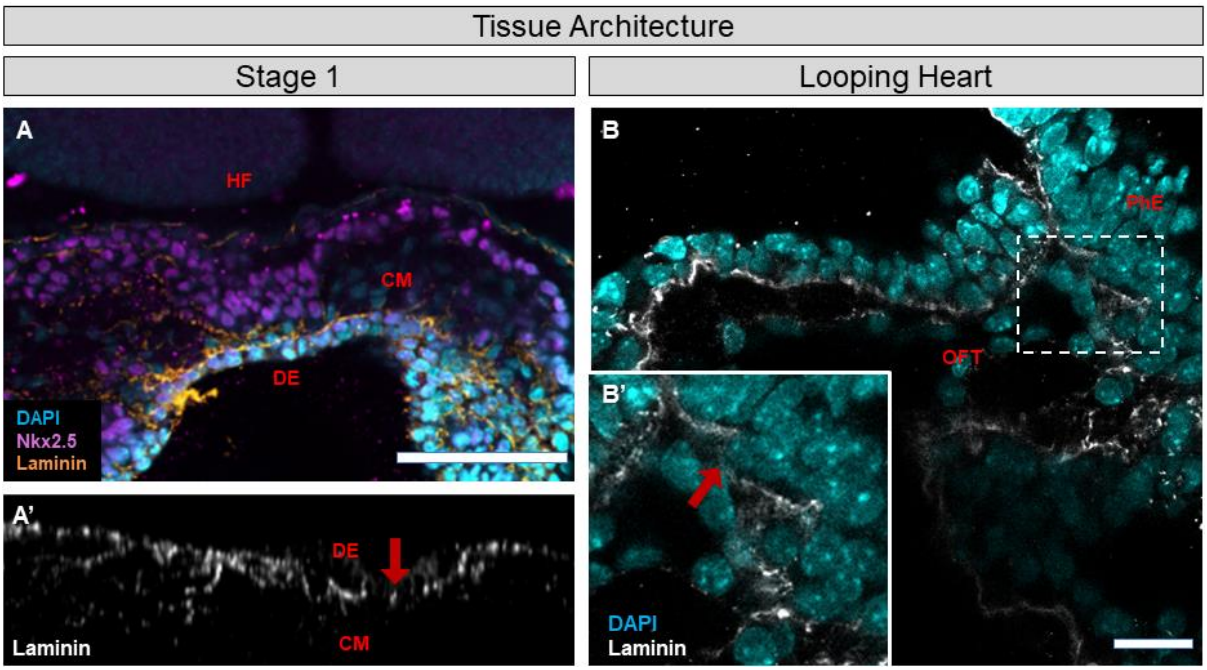

Fig. 5.8 – Laminin breakdown in endodermal tissues – Staining for laminin (A – orange, A', B – grey), reveals regions within the developing endoderm where laminin staining is not continuous (red arrows), consistent with EMT. A' – XZ view of A. Dotted line represents zoomed-in region. HF = head folds; CM = cardiac mesoderm; DE = definitive endoderm; PhE – pharyngeal endoderm; OFT – outflow tract. Scale bars = 100 µm.

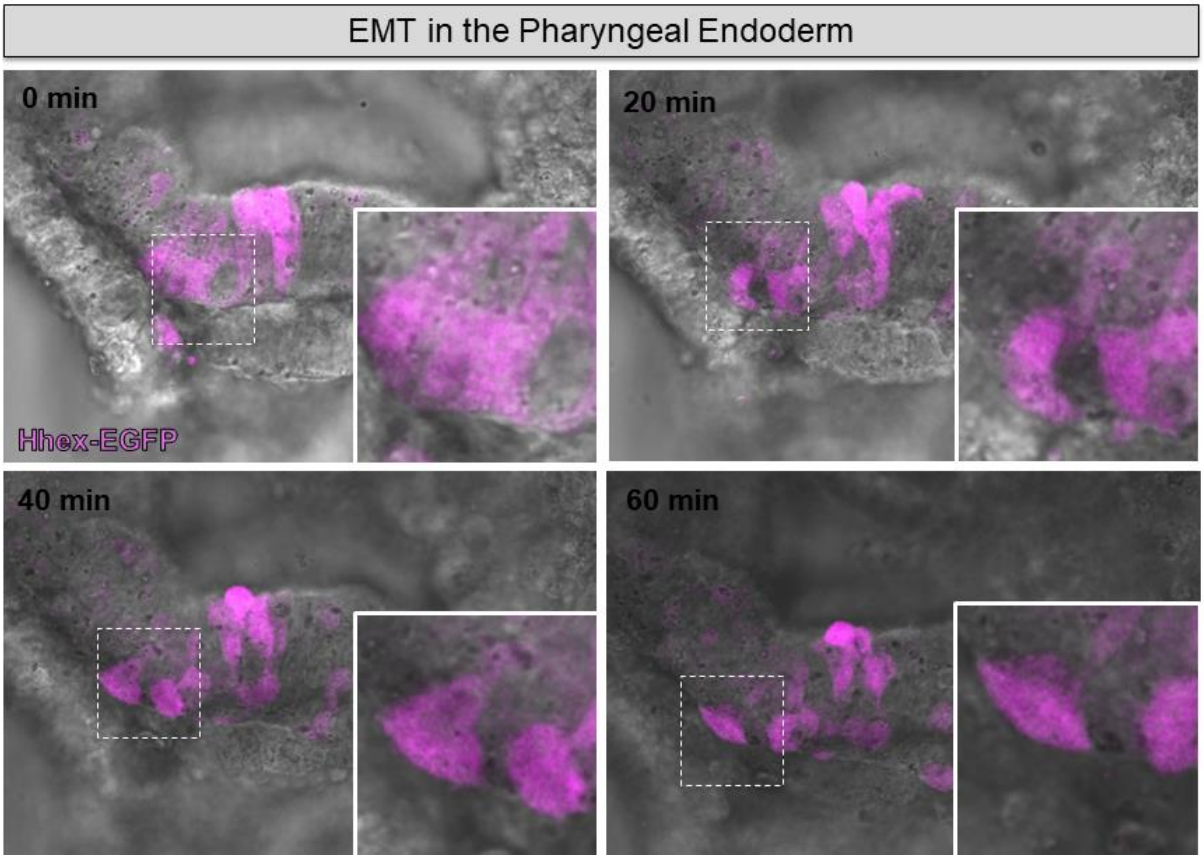

Fig. 5.9 – EMT in the pharyngeal endoderm – Live-imaging of pharyngeal explants of Hhex-GFP (magenta) embryos, reveals possible EMT occurring in the pharyngeal endoderm. Dotted lines represent zoomed-in region.

5.2.5 – Single Cell RNA Sequencing analysis of Endoderm Cells

In order to gain a better understanding on the identity Ttr-Cre/R26-EYFP and Hhex-GFP cells, in the heart and in the PhE, we performed scRNAseq analysis of these cells. Cells were collected from the heart and OC region of E8.5 embryos and the heart of E12.5 embryos. The collections were performed together with Dr. Richard Tyser and the bioinformatic analysis was performed by Dr. Antonio Scialdone from Dr. John Marioni group at EMBL-EBI, Hixton.

Hhex-GFP is expressed at high-levels in the endoderm and endothelial tissues at E8.5 and in the endocardium at E12.5. Clustering the cells using the tSNE method reveals both at E8.5 and E12.5, cells sorted by Hhex-GFP expression aggregate on different clusters based on their whole transcriptome (fig. 5.10 – A, B). Based on the expression of Hhex-GFP in the heart at these stages, it would be expected Hhex-GFP+ cells to be endocardial cells. Indeed, at E12.5 the largest clusters (blue cluster) is characterised by a number of markers usually associated with endocardial cells, such as Endomucin and Tie1 and Pecam. Interestingly, Gene Ontology (GO) analysis identifies the genes that characterise the green cluster as participating in the same processes as the genes that identify the blue clusters, which could indicate two major populations of endothelium cells in the heart at E12.5 embryos. GO analysis also suggests that the yellow cluster consists of cells involved in immune response, more precisely lymphocytes and leukocytes, and the brown clusters as cells involved in lung development, which indicates a certain degree of contamination during the dissection.

At E8.5, 85% of Hhex-GFP sorted cells are arranged on a single cluster (turquoise cluster), characterised by genes such as Isl1, Cldn6, Foxa2, Ttr and Ripply3, which are usually considered endodermal markers. Surprisingly, only 2% of

Hhex-GFP at E8.5 belong to the pink cluster, which is enriched for genes involved in early endothelial development, such as Sox17, Hhex and Tal1. Furthermore, the pink cluster is also the closest cluster to the E12.5 endocardium cluster (blue cluster), reinforcing the hypothesis that pink cells are the precursors to endocardial cells. The observation that only 2% of Hhex-GFP sorted from E8.5 hearts+ OC is surprising, as images the majority of Hhex-GFP cells in the heart ought to be endocardial cells, or at very least endocardial precursors.

In a different analysis, we compared E12.5 cardiac cells obtained from Ttr-Cre/R26-EYFP embryos (both EYFP+ and EYFP-), cells of stage 0 and stage 1 wild-type embryos (including cardiac mesoderm and DE cells), EYFP+ cells and Hhex-GFP cells from E8.5 hearts + OC region (from both Linear Heart Tube and Looping Heart stages) (fig. 5.10 – C, D). Interestingly, similarly to the previous analysis, only 3% of all cells belong to the cluster that seems to identify endocardial cells (black cluster) and most Hhex-GFP cells are arranged together in a cluster characterised by the expression of endoderm markers (turquoise cluster). Of the 6 cells sorted for EYFP at E8.5, only 5 showed detectable EYFP transcript (fig. 5.10 – D, blue cells, zoomed panel). These cells also express Ttr and in general show an endodermal signature, suggesting these cells are OC cells. Out of the 103 cells isolated from E12.5 hearts, only 5 expressed EYFP transcript. These cells do not express Ttr transcript, and the top expressed genes in these cells are related to cardiomyocyte function, such as actin and troponin subunits. Neither the E8.5 nor the E12.5 EYFP+ cells seem to show Cre expression, suggesting that the activation of the R26-EYFP transcript is not due to Cre expression at the stage these cells were collected, but form Cre expression at an earlier developmental stage, presumably in the endoderm at E5.5 to E7.5.

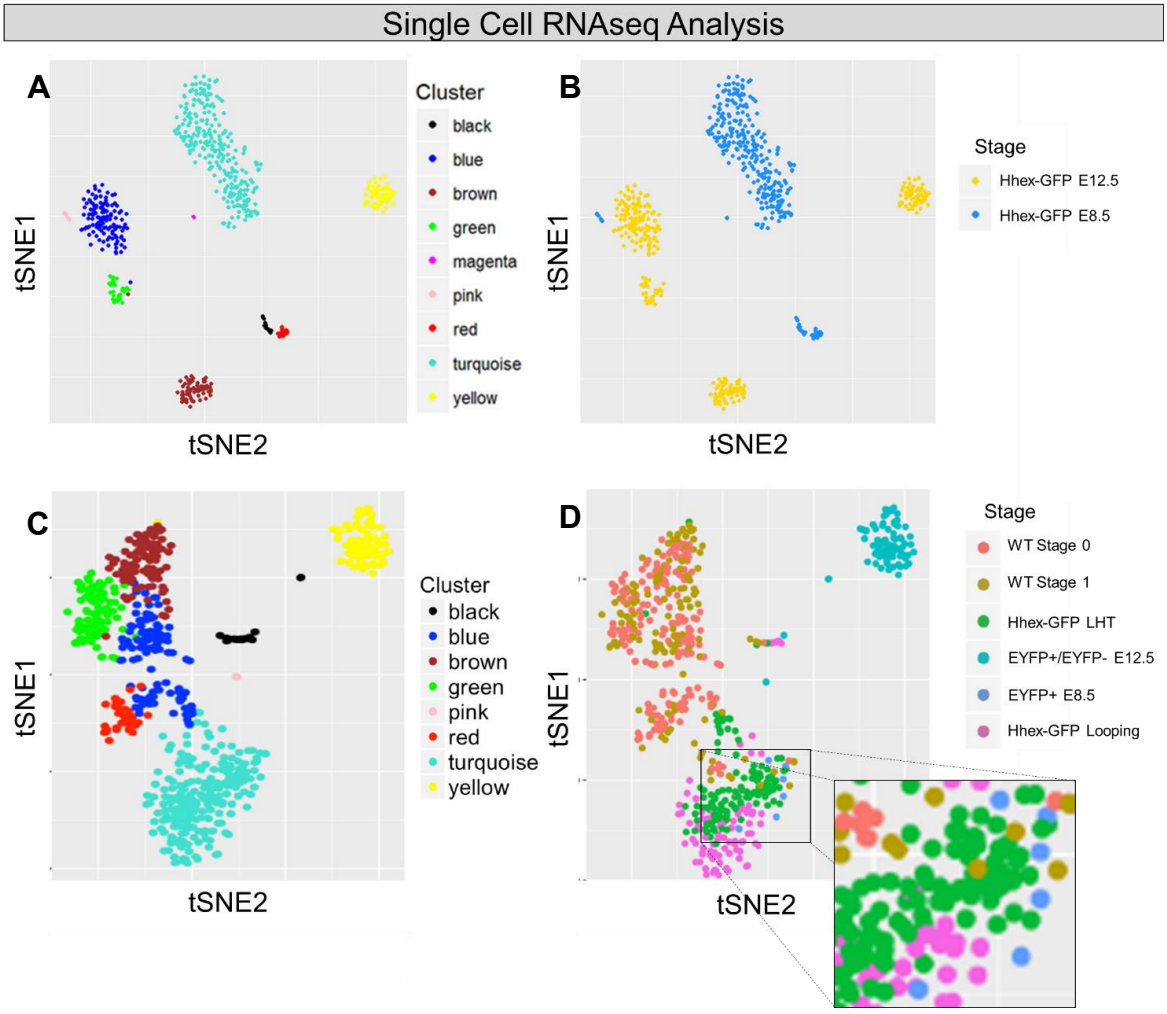

Fig. 5.10 – Single-cell analysis of WT, HHex-EGFP and Ttr-Cre/R26-EYFP cells – Clustering of scRNAseq data obtained from isolated hearts of E8.0, E8.5 and E12.5 embryos. Clustering was obtained from hierarchical clustering and graphical representation was obtained using the tSNE method.

5.3 – Discussion

In this chapter, I described preliminary experiments aimed at investigating the hypothesis that cells from the Pharyngeal Endoderm contribute to the formation of the heart. While the Pharyngeal Mesoderm has been shown to contribute to the second heart field, and vice versa, and the role of endoderm signalling during heart development has been addressed, the possibility of endoderm cells mixing with mesoderm cells during cardiac development has not been addressed.

From a transcriptional point of view, the OC is also the region within the PhE which shares more similarity with cardiac mesoderm, especially cells from the SHF and endothelial cells (fig. 6.2; Table 6.1). Transcription evidence also suggests that endoderm cells overlaying the heart at stage 0 are also distinct from the remaining endodermal layer, indicating these cells could be the progenitors to the PhE. This would also imply that at early stages of heart development, the PhE is also the endodermal tissue in closest contact to the heart, providing signals to the cardiac mesoderm to drive cardiomyocyte differentiation. While some studies have found that removal of the endoderm prior to the formation of the cardiac crescent impairs cardiomyocyte differentiation (*189*), this may be an indirect effect due to improper cardiac function. The likelihood of this hypothesis is supported by our own observations, described in Chapter 4, whereby impairing the function of NCX1, a calcium-sodium exchanger, leads to an abolishment of calcium oscillations in the early cardiac mesoderm and impairs subsequent cardiomyocyte differentiation. Furthermore, mutant embryos with endoderm KO of Nkx2.5 also do not show any endodermal defects (*195*), which could indicate that Nkx2.5 is not necessary for the

development of the PhE, or that the loss of Nkx2.5 may be compensated by other genes.

From a morphological perspective, both the early DE and PhE do not appear to be completely stratified epithelial layer of cells, with regions reminiscent of tissues where EMT occurs (fig. 5.1). Immunostainings for SNAI1 (fig. 5.5 - A) and Laminin (fig. 5.8), as well as live-imaging (fig. 5.2, 5.9) further support the hypothesis that EMT may be occurring in the DE and PhE. Embryos with mesodermal KO of Nkx2.5, using the Mesp1-Cre driver, although unreported by the authors, still seem to display Nkx2.5+ cells in the PhM, which could occur through EMT of the PhE, or alternatively mesoderm cells escaping recombination. It would be likely that PhE cells undergoing EMT would contribute solely to the PhM, as these two tissues are tightly interconnected during the development of the pharyngeal pouches. While this hypothesis remains untested and we did not investigate this possibility, experiments involving Ttr-Cre/R26-EYFP embryos suggest that these endoderm cells may also contribute to the heart. It should however be noted that Cre reporters are not perfect, and it is possibly for Cre under specific promoters to be expressed in cells that it ought not be expressed (*204*). Nevertheless, the morphology and behaviour of the potential endoderm-derived cells is similar to the mesoderm cells of the dorsal pericardial wall, which ultimately originate the SHF (*205, 206*), giving credence to the hypothesis that the PhE may indeed contribute to this cardiac tissue.

The experiments described here provide the first indication that endodermal cells may physically contribute to the heart. It is likely that these cells may be another source of SHF cells, however at this point it is only possible to speculate on the role of these cells in cardiac development. It is possible that these cells may be important for development of proper cardiac function, providing a source of signalling, similar to

the early endoderm. While the OC region also seems to be present in human embryos, it would be interesting to investigate whether endodermal contribution to the heart is conserved in all species. SHF cells are important for the development of most of the heart, therefore it is possible that having a second source of SHF cells may be important for the proper development of the 4 chambers, and that his process may not occur in animals with only 2 chambers, such as fish.

An inherent problem with studying the possible lineage and role of endoderm cells during cardiac development is the lack of specific genetic tools. For example, Foxa2 is not only expressed in the endoderm, endogenous expression of this gene, as well as lineage studies show that this gene is also expressed in endothelial cells, therefore it is not possible to completely certain that using the Foxa2-Cre driver mentioned above only has an effect on endodermal cells. To overcome this limitation, I opted to chemically label the endoderm with DiI. While DiI labelling can be useful to track cells, it is difficult to control what is labelled and at higher concentrations is toxic to the cells, potentially leading to experimental artefacts. Nevertheless, the fact that the results from the DiI further support the circumstantial evidence from the remaining experiments mentioned above, which are less likely to be artefacts. In order to properly study this process, it is necessary to identify specific markers for the OC region and generate mouse lines that would allow tracking these cells during development. A good candidate would be the use of a Nkx2.3-Cre, as this gene seems to be rather specific to the pharyngeal endoderm lineage during early development, however no such line has been studied to this date. Besides lineage studies, it would also be interesting to perform genetic cell ablation of PhE cells, in order to ensure that no compensation mechanism is occurring, to investigate whether these cells play any role during early heart development. For the purpose of identifying new early markers of

the PhE, we are also performing single-cell RNAseq of this tissue at E8.5. By combining this dataset with the dataset presented in chapter 4, it will make it possible to identify with confidence which potential markers are not expressed in the mesoderm. After identification of suitable markers, it will be necessary to create inducible Cre mouse lines, in order to conclusively track early endoderm cells without confounding effects from the mesoderm, which to the best of my knowledge has not been performed to date.

The experiments presented in this chapter suggest that a small number of endoderm cells may contribute to the SHF. It is possible that the small number of cells may be a result of the limitations of the experimental methods used here. It is conceivable that with a better endoderm marker would be possible to track more cells for a longer period of time. It is also possible that these cells may be a transient process, assuring that endoderm signalling can be maintained for a longer duration on discrete regions of the heart, finely tuning certain aspects of cardiac differentiation. It would also be interesting to take a Evo-devo approach and investigate if these observations can be replicated in other species. With the SHF having an important role in the formation on most heart chambers, I hypothesise that this process is exclusive to species with 4-chambers.

Finally, *in-vitro* cardiomyocyte differentiation seems to be promoted in the presence of endoderm cells (*207*). It would be interesting to investigate whether it is possible to obtain cardiac cells *in-vitro* from an endodermal lineage. This could be important for the development of better *in-vitro* models, whereby culturing cardiac mesoderm cells together with PhE-like cells may lead better self-organisation and more tissue variety in heart organoid models, which are still lagging behind in terms of complexity compared to other organoids (*208*).

Conclusion and Final Remarks

Throughout this thesis I have presented my work, performed in parallel with the work of others, in early heart development. The heart is the first organ to form during vertebrate development, the main developmental steps are well described and it possess an overt function in the form of cardiac contractions. This makes the heart an ideal organ to perform interdisciplinary developmental studies. In this thesis, I have discussed methodologies on how to image the early developing heart, the interplay between physiology and heart development, scRNAseq analysis of potential cardiac lineages and a possible contribution of the endoderm to the developing heart.

I believe that in order to properly understand developmental processes, it is necessary to visualise them in real-time. In chapter 3 of this thesis I described methodologies I developed to image early heart development process. These methods have been developed to image mouse embryos, but can be adapted to embryos of other species such as chick embryos. Especially useful in the context of this thesis was the method to perform live-imaging of cardiac tissue at E8.0 (fig. 3.1). This method was the main basis for the observation of the Ca^{2+} dynamics described in chapter 4. By imaging the cardiac crescent at well-defined stages, it was possible to determine that the heart starts to beat an earlier stage than previously appreciated (fig. 4.6). With this method and pharmacological inhibition, it was possible to ascertain that during the transition of the cardiac crescent to the linear heart tube, there are at least 3 different physiological mechanisms (fig. 4.9). The importance of live imaging is also shown in chapter 5, where I described the potential role of definitive endoderm EMT to contribute cells to the heart. While this is a preliminary study, and it is not clear the number of endoderm cells that may be contributing to the heart or what is their

biological importance, it does seem that live-imaging so far provides the best evidence of the process. It is important to appreciate that without a more detailed staging of early heart development these events can easily be missed, and perhaps the reason why this has not been described before, as traditionally researchers consider the cardiac crescent as a relatively homogeneous stage. The work present here is only a very small portion of what could be analysed regarding early cardiac physiology and cellular dynamics in the cardiac crescent. Future studies analysing other ions, such as sodium, imaging mitochondrial dynamics in the early cardiac studies could indicate further levels of heterogeneity in the early cardiac tissue. Furthermore, with emerging for lightsheet and super-resolution imaging, we may gain unprecedented knowledge of cellular dynamics in the developing heart.

Besides developing methods for imaging embryos in new ways it is also important to develop tool to extract quantitative measurements from the data. While, most inhibitor experiments described in chapter 4 have an overt effect, at least in some stages, the potential effects of inhibition of the HCN4 channel only become apparent when quantified with the tools presented in chapter 3. While most studies in developmental biology focus on overt phenotypes, mainly morphological, studying more temporary effects, with smaller phenotypical consequences may also provide us important clues on the regulation of developmental processes. This could be especially important, considering that many transgenic animals may have off-target effects, or may be compensated by the redundancy in developmental systems.

While live-imaging of developmental processes may provide insights into cellular dynamics and provide us indication about previously unappreciated cellular heterogeneity, it has to be complemented with detailed characterisation of gene expression. Until recently much of the focus of developmental genetics has been

mainly the description of key signalling pathways with striking phenotypes. Studying cellular heterogeneity was a cumbersome undertaking until the advent of single-cell RNA sequencing (scRNAseq). The importance of a more detailed analysis of developmental processes is also reflected on our scRNAseq analyses, presented mainly in chapter 4 but also in chapter 5. While, previous scRNAseq reports in the early embryonic heart, at E8.5, showed only 2 clusters of cells, by analysing a larger number of cells, at different stages of crescent maturation, we have identified several clusters of mesoderm cells at this stage in the mouse embryo (fig. 4.11). The bioinformatic analysis I performed, also suggests the potential existence of a couple pools of bipotent progenitor cells. Using scRNAseq datasets, more directed questions also prove useful to extract potential new information relevant for heart development, such as new markers of the first and second heart field, as well as new left-right asymmetry genes. The scRNAseq dataset also shows the importance of studying specific cell populations and small variations within the embryo, especially in left-right asymmetry, where some differences may be population specific. The scRNAseq datasets presented here can still also be further explored, and it will be interesting to combine this dataset with existing datasets in order to extract markers to study specific processes in heart development, or to study the regulation of specific pathways. Nevertheless, the single-cell RNAseq analysis performed here already suggests a high level of heterogeneity in the cardiac crescent, with cells divided in several clusters beyond the already defined heart fields, including heterogeneity in the expression of physiology-related genes, further supporting the observation from the live-imaging experiments. It is now necessary to validate the results from the scRNAseq, by analysing the expression profile of candidate genes via ISH or immunohistochemistry. A big gap in the experiments described in these thesis is how the cells and processes

that we observe in the early cardiac crescent relate to the adult cardiac tissues. Once the most interesting candidate genes relating to cellular heterogeneity are validated, it would be interesting to develop tools that allow the live-imaging and lineage-tracing of the different population of cells with more precision than the tools used so far. This may provide new insights into the differentiation of specialised cardiac tissues, which could help devise better protocols for the differentiation and applications of stem cells.

References

1. A. Breschi, T. R. Gingeras, R. Guigo, Comparative transcriptomics in human and mouse. *Nat Rev Genet* **18**, 425-440 (2017).
2. D. M. Church *et al.*, Lineage-specific biology revealed by a finished genome assembly of the mouse. *PLoS Biol* **7**, e1000112 (2009).
3. A. Griffiths, S. Wessler, R. Lewontin, S. Carroll, Introduction to Genetic Analysis. *W. H. Freeman* **9th Edition**, (2007).
4. A. Russ *et al.*, Random mutagenesis in the mouse as a tool in drug discovery. *Drug Discovery Today* **7**, (2002).
5. C. Wansleeben *et al.*, An ENU-Mutagenesis Screen in the Mouse: Identification of Novel Developmental Gene Functions. *PloS ONE* **6**, e19357 (2011).
6. D. Paquet *et al.*, Efficient introduction of specific homozygous and heterozygous mutations using CRISPR/Cas9. *Nature* **533**, 125-129 (2016).
7. A. Williams, J. Henao-Mejia, R. A. Flavell, Editing the Mouse Genome Using the CRISPR-Cas9 System. *Cold Spring Harb Protoc* **2016**, pdb top087536 (2016).
8. Y. Kojima, O. H. Tam, P. P. Tam, Timing of developmental events in the early mouse embryo. *Semin Cell Dev Biol* **34**, 65-75 (2014).
9. P. Thomas, R. Beddington, Anterior primitive endoderm may be responsible for patterning the anterior neural plate in the mouse embryos. *Current Biology* **6**, (1996).
10. S. Srinivas, T. Rodriguez, M. Clements, J. C. Smith, R. S. Beddington, Active cell migration drives the unilateral movements of the anterior visceral endoderm. *Development* **131**, 1157-1164 (2004).
11. M. J. Stower, S. Srinivas, Heading forwards: anterior visceral endoderm migration in patterning the mouse embryo. *Philos Trans R Soc Lond B Biol Sci* **369**, (2014).
12. S. J. Arnold, E. J. Robertson, Making a commitment: cell lineage allocation and axis patterning in the early mouse embryo. *Nat Rev Mol Cell Biol* **10**, 91-103 (2009).
13. B. Ciruna, J. Rossant, FGF Signaling Regulates Mesoderm Cell Fate Specification and Morphogenetic Movement at the Primitive Streak. *Developmental Cell* **1**, (2001).S
14. A. Moorman, S. Webb, N. A. Brown, W. Lamers, R. H. Anderson, Development of the Heart: (1) Formation of the Cardiac Chambers and Arterial Trunks. *Heart* **89**, (2003).C
15. M. Buckingham, S. Meilhac, S. Zaffran, Building the mammalian heart from two sources of myocardial cells. *Nat Rev Genet* **6**, 826-835 (2005).I
16. T. L. Creazzo, R. E. Godt, L. Leatherbury, S. J. Conway, M. L. Kirby, Role of Cardiac Neural Crest Cells in Cardiovascular Development. *Annu. Rev. Physiol.* **60**, (1998).E
17. B. G. Bruneau, The developmental genetics of congenital heart disease. *Nature* **451**, 943-948 (2008).N
18. P. Van Vliet, S. M. Wu, S. Zaffran, M. Puceat, Early cardiac development: a view from stem cells to embryos. *Cardiovasc Res* **96**, 352-362 (2012).C
19. J. M. Schleich, T. Abdulla, R. Summers, L. Houyel, An overview of cardiac morphogenesis. *Arch Cardiovasc Dis* **106**, 612-623 (2013).E
20. L. A. Samsa, B. Yang, J. Liu, Embryonic cardiac chamber maturation: Trabeculation, conduction, and cardiomyocyte proliferation. *Am J Med Genet C Semin Med Genet* **163C**, 157-168 (2013).
21. M. Lockhart, E. Wirrig, A. Phelps, A. Wessels, Extracellular matrix and heart development. *Birth Defects Res A Clin Mol Teratol* **91**, 535-550 (2011).I
22. L. Andres-Delgado, N. Mercader, Interplay between cardiac function and heart development. *Biochim Biophys Acta* **1863**, 1707-1716 (2016).S

23. M. Puceat, Embryological origin of the endocardium and derived valve progenitor cells: from developmental biology to stem cell-based valve repair. *Biochim Biophys Acta* **1833**, 917-922 (2013).
24. A. von Gise, W. T. Pu, Endocardial and epicardial epithelial to mesenchymal transitions in heart development and disease. *Circ Res* **110**, 1628-1645 (2012).S
25. Y. Ishii, J. Langberg, K. Rosborough, T. Mikawa, Endothelial cell lineages of the heart. *Cell Tissue Res* **335**, 67-73 (2009).H
26. I. S. Harris, B. L. Black, Development of the endocardium. *Pediatric cardiology* **31**, 391-399 (2010).I
27. R. Carmona *et al.*, The embryonic epicardium: an essential element of cardiac development. *J Cell Mol Med* **14**, 2066-2072 (2010).T
28. J. Schlueter, T. Brand, Epicardial Progenitor Cells in Cardiac Development and Regeneration. *Journal of Cardiovascular Translational Research* **5**, 641-653 (2012).
29. B. A. de Boer, G. van den Berg, P. A. de Boer, A. F. Moorman, J. M. Ruijter, Growth of the developing mouse heart: an interactive qualitative and quantitative 3D atlas. *Dev Biol* **368**, 203-213 (2012).
30. J. Schlueter, T. Brand, A right-sided pathway involving FGF8/Snai1 controls asymmetric development of the proepicardium in the chick embryo. *PNAS* **106**, 7485-7490 (2009).
31. B. Jensen, T. Wang, V. M. Christoffels, A. F. Moorman, Evolution and development of the building plan of the vertebrate heart. *Biochim Biophys Acta* **1833**, 783-794 (2013).
32. M. P. Santini, E. Forte, R. P. Harvey, J. C. Kovacic, Developmental origin and lineage plasticity of endogenous cardiac stem cells. *Development* **143**, 1242-1258 (2016).
33. R. S. P. Beddington, P. Rashbass, V. Wilson, Brachyury - a gene affecting mouse gastrulation and early organogenesis. *Development*, 157-165 (1992).
34. S. Marcellini, U. Technau, J. C. Smith, P. Lemaire, Evolution of Brachyury proteins: identification of a novel regulatory domain conserved within Bilateria. *Developmental Biology* **260**, 352-361 (2003).
35. I. Costello *et al.*, The T-box transcription factor Eomesodermin acts upstream of Mesp1 to specify cardiac mesoderm during mouse gastrulation. *Nat Cell Biol* **13**, 1084-1091 (2011).
36. S. S. Chan, H. H. W. Chan, M. Kyba, Heterogeneity of Mesp1+ mesoderm revealed by single-cell RNA-seq. *Biochem Biophys Res Commun* **474**, 469-475 (2016).
37. F. Lescroart *et al.*, Early lineage restriction in temporally distinct populations of Mesp1 progenitors during mammalian heart development. *Nat Cell Biol* **16**, 829-840 (2014).
38. S. Kitajima, A. Takagi, T. Inoue, Y. Saga, MesP1 and MesP2 are essential for the development of cardiac mesoderm. *Development* **127**, 3215-3226 (2000).
39. I. C. Scott, Life before Nkx2.5: cardiovascular progenitor cells: embryonic origins and development. *Curr Top Dev Biol* **100**, 1-31 (2012).
40. G. Nemer, M. Nemer, GATA4 in Heart Development and Disease. 599-616 (2010).
41. J. Schlesinger *et al.*, The cardiac transcription network modulated by Gata4, Mef2a, Nkx2.5, Srf, histone modifications, and microRNAs. *PLoS Genet* **7**, e1001313 (2011).
42. Z. Niu *et al.*, Serum response factor orchestrates nascent sarcomerogenesis and silences the biomineralization gene program in the heart. *Proc Natl Acad Sci U S A* **105**, 17824-17829 (2008).
43. A. Parlakian *et al.*, Targeted inactivation of serum response factor in the developing heart results in myocardial defects and embryonic lethality. *Mol Cell Biol* **24**, 5281-5289 (2004).
44. S. Arsenian, B. Weinhold, M. Oelgeschlager, U. Ruther, A. Nordheim, Serum response factor is essential for mesoderm formation during mouse embryogenesis. *The EMBO Journal* **17**, 6289-6299 (1998).
45. L. A. Dyer, M. L. Kirby, The role of secondary heart field in cardiac development. *Dev Biol* **336**, 137-144 (2009).

46. R. Ilagan *et al.*, Fgf8 is required for anterior heart field development. *Development* **133**, 2435-2445 (2006).
47. E. J. Park *et al.*, An FGF autocrine loop initiated in second heart field mesoderm regulates morphogenesis at the arterial pole of the heart. *Development* **135**, 3599-3610 (2008).
48. A. Francou *et al.*, Second heart field cardiac progenitor cells in the early mouse embryo. *Biochim Biophys Acta* **1833**, 795-798 (2013).
49. S. A. Ramsbottom *et al.*, Vangl2-regulated polarisation of second heart field-derived cells is required for outflow tract lengthening during cardiac development. *PLoS Genet* **10**, e1004871 (2014).
50. L. Xie *et al.*, Tbx5-hedgehog molecular networks are essential in the second heart field for atrial septation. *Dev Cell* **23**, 280-291 (2012).
51. M. T. Mommersteeg *et al.*, The sinus venosus progenitors separate and diversify from the first and second heart fields early in development. *Cardiovasc Res* **87**, 92-101 (2010).
52. X. Liang *et al.*, HCN4 dynamically marks the first heart field and conduction system precursors. *Circ Res* **113**, 399-407 (2013).
53. M. Bressan, G. Liu, T. Mikawa, Early mesodermal cues assign avian cardiac pacemaker fate potential in a tertiary heart field. *Science* **340**, 744-748 (2013).
54. S. J. Matkovich, J. R. Edwards, T. C. Grossenheider, C. de Guzman Strong, G. W. Dorn, 2nd, Epigenetic coordination of embryonic heart transcription by dynamically regulated long noncoding RNAs. *Proc Natl Acad Sci U S A* **111**, 12264-12269 (2014).
55. H. Wang *et al.*, Genome-wide analysis of alternative splicing during human heart development. *Sci Rep* **6**, 35520 (2016).
56. D. N. Barnette, M. VandeKopple, Y. Wu, D. A. Willoughby, J. Lincoln, RNA-seq analysis to identify novel roles of scleraxis during embryonic mouse heart valve remodeling. *PLoS One* **9**, e101425 (2014).
57. G. Peng *et al.*, Spatial Transcriptome for the Molecular Annotation of Lineage Fates and Cell Identity in Mid-gastrula Mouse Embryo. *Dev Cell* **36**, 681-697 (2016).
58. Z. Xue *et al.*, Genetic programs in human and mouse early embryos revealed by single-cell RNA sequencing. *Nature* **500**, 593-597 (2013).
59. S. Petropoulos *et al.*, Single-Cell RNA-Seq Reveals Lineage and X Chromosome Dynamics in Human Preimplantation Embryos. *Cell* **165**, 1012-1026 (2016).
60. J. Wen *et al.*, Single-cell analysis reveals lineage segregation in early post-implantation mouse embryos. *J Biol Chem* **292**, 9840-9854 (2017).
61. G. Li *et al.*, Transcriptomic Profiling Maps Anatomically Patterned Subpopulations among Single Embryonic Cardiac Cells. *Dev Cell* **39**, 491-507 (2016).
62. D. M. DeLaughter *et al.*, Single-Cell Resolution of Temporal Gene Expression during Heart Development. *Dev Cell* **39**, 480-490 (2016).
63. T. A. Rodriguez, E. S. Casey, R. M. Harland, J. C. Smith, R. S. Beddington, Distinct enhancer elements control Hex expression during gastrulation and early organogenesis. *Dev Biol* **234**, 304-316 (2001).
64. G. S. Kwon, M. Viotti, A. K. Hadjantonakis, The endoderm of the mouse embryo arises by dynamic widespread intercalation of embryonic and extraembryonic lineages. *Dev Cell* **15**, 509-520 (2008).
65. S. Srinivas *et al.*, Cre reporter strains produced by targeted insertion of EYFP and ECFP into the ROSA26 locus. *BMC Developmental Biology*, 1-4 (2001).
66. C. L. Murphy, J. M. Polak, Differentiating embryonic stem cells: GAPDH, but neither HPRT nor beta-tubulin is suitable as an internal standard for measuring RNA levels. *Tissue engineering* **8**, 551-559 (2002).
67. D. Ramskold *et al.*, Full-length mRNA-Seq from single-cell levels of RNA and individual circulating tumor cells. *Nature biotechnology* **30**, 777-782 (2012).

68. A. T. Lun, K. Bach, J. C. Marioni, Pooling across cells to normalize single-cell RNA sequencing data with many zero counts. *Genome Biol* **17**, 75 (2016).
69. A. T. Lun, D. J. McCarthy, J. C. Marioni, A step-by-step workflow for low-level analysis of single-cell RNA-seq data with Bioconductor. *F1000Research* **5**, 2122 (2016).
70. A. A. Kolodziejczyk *et al.*, Single Cell RNA-Sequencing of Pluripotent States Unlocks Modular Transcriptional Variation. *Cell stem cell* **17**, 471-485 (2015).
71. P. Langfelder, B. Zhang, S. Horvath, *Defining Clusters from a Hierarchical Cluster Tree: The Dynamic Tree Cut Package for R*. (2008), vol. 24, pp. 719-720.
72. W. H. De Vos *et al.*, Advanced light microscopy for biological space research. *Review of Scientific Instruments* **85**, (2014).
73. A. Du Toit, Advancing imaging. *Nat Rev Mol Cell Biol* **15**, (2014).
74. A. M. Sydor, K. J. Czymmek, E. M. Puchner, V. Mennella, Super-Resolution Microscopy: From Single Molecules to Supramolecular Assemblies. *Trends Cell Biol* **25**, 730-748 (2015).
75. S. G. Megason, S. Srinivas, M. E. Dickinson, A. K. Hadjantonakis, Microscopy to mechanism across the scales of development. *Curr Opin Genet Dev* **21**, 519-522 (2011).
76. J. Jonkman, C. M. Brown, Any Way You Slice It-A Comparison of Confocal Microscopy Techniques. *J Biomol Tech* **26**, 54-65 (2015).
77. B. Hockendorf, T. Thumberger, J. Wittbrodt, Quantitative analysis of embryogenesis: a perspective for light sheet microscopy. *Dev Cell* **23**, 1111-1120 (2012).
78. P. J. Keller, A. D. Schmidt, J. Wittbrodt, E. H. K. Stelzer, Reconstruction of Zebrafish Early Embryonic Development by Scanned Light Sheet Microscopy. *Science* **322**, (2008).
79. F. Amat, P. J. Keller, Towards comprehensive cell lineage reconstructions in complex organisms using light-sheet microscopy. *Dev Growth Differ* **55**, 563-578 (2013).
80. G. R. Mines, On circulating excitations in heart muscle and their possible relation to tachycardia and fibrillation. *Trans. R. Soc. Can* **8**, 43-52 (1914).
81. S. M. Hwang, T. Y. Kim, K. J. Lee, Complex-periodic spiral waves in confluent cardiac cell cultures induced by localized inhomogeneities. *Proc Natl Acad Sci U S A* **102**, 10363-10368 (2005).
82. R. M. Paredes, J. C. Etzler, L. T. Watts, W. Zheng, J. D. Lechleiter, Chemical calcium indicators. *Methods* **46**, 143-151 (2008).
83. J. T. Russell, Imaging calcium signals in vivo: a powerful tool in physiology and pharmacology. *British Journal of Pharmacology* **159**, (2010).
84. P. V. Koldenkova, T. Nagai, Genetically encoded Ca(2+) indicators: properties and evaluation. *Biochim Biophys Acta* **1833**, 1787-1797 (2013).
85. R. Massarwa, L. Niswander, In toto live imaging of mouse morphogenesis and new insights into neural tube closure. *Development* **140**, 226-236 (2013).
86. M. Weber, J. Huisken, In vivo imaging of cardiac development and function in zebrasfish using light sheet microscopy. *Swiss Med Wkly* **145**, (2015).
87. J. Ohn, H. Tsai, M. Liebling, Joint dynamic imaging of morphogenesis and function in the developing heart. *Organogenesis* **5**, 248-255 (2009).
88. F. Boselli, J. Vermot, Live imaging and modeling for shear stress quantification in the embryonic zebrafish heart. *Methods* **94**, 129-134 (2016).
89. P. Fei *et al.*, Cardiac Light-Sheet Fluorescent Microscopy for Multi-Scale and Rapid Imaging of Architecture and Function. *Sci Rep* **6**, 22489 (2016).
90. J. Pestel *et al.*, Real-time 3D visualization of cellular rearrangements during cardiac valve formation. *Development* **143**, 2217-2227 (2016).
91. A. L. Henning, M. X. Jiang, H. C. Yalcin, J. T. Butcher, Quantitative three-dimensional imaging of live avian embryonic morphogenesis via micro-computed tomography. *Dev Dyn* **240**, 1949-1957 (2011).
92. M. W. Jenkins, M. Watanabe, A. M. Rollins, Longitudinal Imaging of Heart Development With Optical Coherence Tomography. *IEEE J Sel Top Quantum Electron* **18**, 1166-1175 (2012).

93. W. J. Kowalski, K. Pekkan, J. P. Tinney, B. B. Keller, Investigating developmental cardiovascular biomechanics and the origins of congenital heart defects. *Front Physiol* **5**, 408 (2014).
94. K. Ivanovitch, S. Temino, M. Torres, Live imaging of heart tube development in mouse reveals alternating phases of cardiac differentiation and morphogenesis. *bioRxiv*, (2017).
95. A. Piliszek, G. S. Kwon, A. K. Hadjantonakis, Ex utero culture and live imaging of mouse embryos. *Methods Mol Biol* **770**, 243-257 (2011).
96. R. S. Udan, V. G. Piazza, C. W. Hsu, A. K. Hadjantonakis, M. E. Dickinson, Quantitative imaging of cell dynamics in mouse embryos using light-sheet microscopy. *Development* **141**, 4406-4414 (2014).
97. C. Bazan, D. Torres Barba, P. Blomgren, P. Paolini, Image processing techniques for assessing contractility in isolated neonatal cardiac myocytes. *Int J Biomed Imaging* **2011**, 729732 (2011).
98. E. Stein, Harmonic analysis real-variable methods, orthogonality, and oscillatory integrals. *Bulletin of the American Mathematical Society* **36**, 505-521 (1999).
99. B. Fongang, A. Kudlicki, Comparison between Timelines of Transcriptional Regulation in Mammals, Birds, and Teleost Fish Somitogenesis. *PLoS One* **11**, e0155802 (2016).
100. O. Barquero-Perez *et al.*, Cardiac Arrhythmia Spectral Analysis of Electrogram Signals Using Fourier Organization Analysis. *Computers in Cardiology* **36**, 336-336 (2009).
101. P. P. L. Tam, Postimplantation mouse development: whole embryo culture and micro-manipulation. *Int. J. Dev. Biol* **42**, 895-902 (1998).
102. R. S. Udan, M. E. Dickinson, Imaging mouse embryonic development. *Methods in enzymology* **476**, 329-349 (2010).
103. G. Guo *et al.*, Serum-Based Culture Conditions Provoke Gene Expression Variability in Mouse Embryonic Stem Cells as Revealed by Single-Cell Analysis. *Cell reports* **14**, 956-965 (2016).
104. V. K. Kalaskar, J. D. Lauderdale, Mouse embryonic development in a serum-free whole embryo culture system. *Journal of visualized experiments : JoVE*, (2014).
105. S. Srinivas, Imaging cell movements in egg-cylinder stage mouse embryos. *Cold Spring Harb Protoc* **2010**, pdb prot5539 (2010).
106. V. Navaratnam, M. H. Kaufman, J. N. Skepper, S. Barton, K. M. Guttridge, Differentiation of the myocardial rudiment of mouse embryos: an ultrastructural study including freeze-fracture replication. *J. Anat.* **146**, 65-85 (1986).
107. C. M. Goss, The first contractions of the heart in rat embryos. *The Anatomical Record* **70**, (1938).
108. S. Fujii, A. Hirota, K. Kamino, Optical signals from early embryonic chick heart stained with potential sensitive dyes: evidence for electrical activity. *J. Physiol.* **304**, 503-518 (1980).
109. D. Y. R. Stainier *et al.*, Mutation affecting the formation and function of the cardiovascular system in the zebrafish embryo. *Development* **123**, 285-292 (1996).
110. L. M. Duffey, Cardiogenesis and Observations of the First Heart Contractions in Certain Canids. *MSc Thesis, Kansas State College of Agriculture and Applied Science* (1953).
111. C. M. Goss, Development of the median coordinated ventricle from the lateral hearts in rat embryos with three to six somites. *The Anatomical Record* **112**, 761-796 (1952).
112. A. Hirota, K. Kamino, H. Komuro, T. Sakai, T. Yada, Early Events in Development of Electrical Activity and Contraction in Embryonic Rat Heart Assessed by Optical Recording. *J. Physiol.* **369**, 209-227 (1985).
113. K. Nishii, Y. Shibata, Mode and determination of the initial contraction stage in the mouse embryo heart. *Anat. Embryol* **211**, 95-100 (2006).
114. J. T. Granados-Riveron, J. D. Brook, The impact of mechanical forces in heart morphogenesis. *Circ Cardiovasc Genet* **5**, 132-142 (2012).
115. K. Y. Miyasaka *et al.*, Heartbeat regulates cardiogenesis by suppressing retinoic acid signaling via expression of miR-143. *Mech Dev* **128**, 18-28 (2011).
116. D. M. Bers, Cardiac excitation-contraction coupling. *Nature* **415**, (2002).

117. A. Fabiato, F. Fabiato, Use of chlorotetracycline fluorescence to demonstrate Ca2+-induced release of Ca2+ from the sarcoplasmic reticulum of skinned cardiac cells. *Nature* **281**, (1979).
118. S. J. Conway *et al.*, Role of Sodium-Calcium Exchanger (Ncx1) in Embryonic Heart Development. *Ann. N. Y. Acad. Sci.* **976**, 268-281 (2002).
119. S. Seki *et al.*, Fetal and postnatal development of Ca2+ transients and Ca2+ sparks in rat cardiomyocytes. *Cardiovascular Research* **58**, 535-548 (2003).
120. C. Seisenberger *et al.*, Functional embryonic cardiomyocytes after disruption of the L-type alpha1C (Cav1.2) calcium channel gene in the mouse. *J Biol Chem* **275**, 39193-39199 (2000).
121. L. L. Cribbs *et al.*, Identification fo the T-Type Calcium Channel (CaV3.1d) in the Developing Mouse Heart. *Circulation Research*, (2001).
122. K. K. Linask, M. Han, M. Artman, C. A. Ludwig, Sodium-Calcium Exchanger (NCX-1) and Calcium Modulation: NCX Protein Expression Patterns and Regulation of Early Heart Development. *Developmental Dynamics* **221**, 249-264 (2001).
123. H. Liang *et al.*, Electrophysiological Basis of the First Heart Beats. *Cell Physiol Biochem* **25**, 561-570 (2010).
124. T. Nakanishi, M. Seguchi, A. Takao, Development of the myocardial contractile system. *Experientia* **44**, (1988).
125. H. Takeshima *et al.*, Embryonic lethality and abnormal cardiac myocytes in mice lacking ryanodine receptor type 2. *The EMBO Journal* **17**, 3309-3316 (1998).
126. S. Viatchenko-Karpinski *et al.*, Intracellular Ca2+ oscillations drive spontaneous contraction in cardiomyocytes during early development. *Proc. Natl. Acad. Sci.* **96**, 8259-8264 (1999).
127. A. Mery *et al.*, Initiation of Embryonic Cardiac PAcemaker Activity by Inositol 1,4,5-Trisphosphate-dependent Calcium Signaling. *Molecular Biology of the Cell* **16**, 2414-2423 (2005).
128. P. Sasse *et al.*, Intracellular Ca2+ oscillations, a potential pacemaking mechanism in early embryonic heart cells. *J Gen Physiol* **130**, 133-144 (2007).
129. R. Rapila, T. Korhonen, P. Tavi, Excitation-contraction coupling of the mouse embryonic cardiomyocyte. *J Gen Physiol* **132**, 397-405 (2008).
130. Y. Komatsu, Y. Mishina, Establishment of left-right asymmetry in vertebrate development: the node in mouse embryos. *Cell Mol Life Sci* **70**, 4659-4666 (2013).
131. J. Gros, K. Feistel, C. Viebahn, M. Blum, C. Tabin, Cell Movements at Hensen's Node Establish Left/Right Asymmetric Gene Expression in the Chick. *Science* **324**, (2009).
132. A. Raya, J. C. Izpisua Belmonte, Left-right asymmetry in the vertebrate embryo: from early information to higher-level integration. *Nat Rev Genet* **7**, 283-293 (2006).
133. Y. Saijoh, M. Viotti, A. K. Hadjantonakis, Follow your gut: relaying information from the site of left-right symmetry breaking in the mouse. *Genesis* **52**, 503-514 (2014).
134. I. Dykes, Left Right Patterning, Evolution and Cardiac Development. *Journal of Cardiovascular Development and Disease* **1**, 52-72 (2014).
135. Y. Tao *et al.*, Pitx2, an atrial fibrillation predisposition gene, directly regulates ion transport and intercalated disc genes. *Circ Cardiovasc Genet* **7**, 23-32 (2014).
136. R. D. Nadadur *et al.*, Pitx2 modulates a Tbx5-dependent gene regulatory network to maintain atrial rhythm. *Science Translational Medicine* **8**, (2016).
137. E. S. Noel *et al.*, A Nodal-independent and tissue-intrinsic mechanism controls heart-looping chirality. *Nat Commun* **4**, 2754 (2013).
138. M. Kumai *et al.*, Loss of connexin45 causes a cushion defect in early cardiogenesis. *Development* **127**, 3501-3512 (2000).
139. G. A. Porter, S. A. Rivkees, Ontogeny of humoral heart rate regulation in the embryonic mouse. *Am J Physiol Regulatory Integrative Comp Physiol* **281**, 401-407 (2001).
140. M. H. Kaufman, V. Navaratnam, Early differentiation of the heart in mouse embryos. *J. Anat.* **133**, 235-246 (1981).

141. C. Biben, R. P. Harvey, Homeodomain factor Nkx2-5 controls left/right asymmetric expression of bHLH gene eHand during murine heart development. *Genes & Development* **11**, 1357-1369 (1997).
142. A. Secondo *et al.*, Molecular pharmacology of the amiloride analog 3-amino-6-chloro-5-[(4-chloro-benzyl)amino]-n-[[(2,4-dimethylbenzyl)-amino]iminom ethyl]-pyrazinecarboxamide (CB-DMB) as a pan inhibitor of the Na+-Ca2+ exchanger isoforms NCX1, NCX2, and NCX3 in stably transfected cells. *J Pharmacol Exp Ther* **331**, 212-221 (2009).
143. J. Kimura, T. Watano, M. Kawahara, E. Sakai, J. Yatabe, Direction-independent block of bi-directional Na+/Ca2+ exchange currnt by KB-R7943 in guinea-pig cardiac myocutes. *British Journal of Pharmacology* **128**, 969-974 (1999).
144. T. F. McDonald, S. Pelzer, W. Trautwein, D. J. Pelzer, Regulation and modulation of calcium channels in cardiac, skeletal, and smooth muscle cells. *Physiological Reviews* **74**, 365-507 (1994).
145. C. Garcia-Frigola, Y. Shi, S. M. Evans, Expression of the hyperpolarization-activated cyclic nucleotide-gated cation channel HCN4 during mouse heart development. *Gene Expression Patterns* **3**, 777-783 (2003).
146. A. Bucchi, A. Tognati, R. Milanesi, M. Baruscotti, D. DiFrancesco, Properties of ivabradine-induced block of HCN1 and HCN4 pacemaker channels. *J Physiol* **572**, 335-346 (2006).
147. C. Faust, A. Schumacher, B. Holdener, T. Magnuson, The *eed* mutation disrupts anterior mesoderm production in mice. *Development* **121**, 273-285 (1995).
148. C. Faust, K. A. Lawson, N. J. Schork, B. Thiel, T. Magnuson, The *Polycomb*-group gene *eed* is required for normal morphogenetic movements during gastrulation in the mouse embryo. *Development* **125**, 4495-4508 (1998).
149. W. Yu *et al.*, Depletion of polycomb repressive complex 2 core component EED impairs fetal hematopoiesis. *Cell Death Dis* **8**, e2744 (2017).
150. L. A. Moyle *et al.*, Ret function in muscle stem cells points to tyrosine kinase inhibitor therapy for facioscapulohumeral muscular dystrophy. *Elife* **5**, (2016).
151. D. Fonseca-Pereira *et al.*, The neurotrophic factor receptor RET drives haematopoietic stem cell survival and function. *Nature* **514**, 98-101 (2014).
152. S. Chakraborty *et al.*, Twist1 promotes heart valve cell proliferation and extracellular matrix gene expression during development in vivo and is expressed in human diseased aortic valves. *Dev Biol* **347**, 167-179 (2010).
153. J. W. Vincentz *et al.*, Twist1 controls a cell-specification switch governing cell fate decisions within the cardiac neural crest. *PLoS Genet* **9**, e1003405 (2013).
154. N. H. Shahrin, S. Diakiw, L. A. Dent, A. L. Brown, R. J. D'Andrea, Conditional knockout mice demonstrate function of Klf5 as a myeloid transcription factor. *Blood* **128**, 55-59 (2016).
155. S. Hayashi, I. Manabe, Y. Suzuki, F. Relaix, Y. Oishi, Klf5 regulates muscle differentiation by directly targeting muscle-specific genes in cooperation with MyoD in mice. *Elife* **5**, (2016).
156. M. Pajares *et al.*, Transcription factor NFE2L2/NRF2 is a regulator of macroautophagy genes. *Autophagy* **12**, 1902-1916 (2016).
157. G. H. Guibinga, F. Murray, N. Barron, HPRT-deficiency dysregulates cAMP-PKA signaling and phosphodiesterase 10A expression: mechanistic insight and potential target for Lesch-Nyhan Disease? *PLoS One* **8**, e63333 (2013).
158. J. van den Ameele *et al.*, Eomesodermin induces Mesp1 expression and cardiac differentiation from embryonic stem cells in the absence of Activin. *EMBO Rep* **13**, 355-362 (2012).
159. H. Watanabe *et al.*, HHEX promotes hepatic-lineage specification through the negative regulation of eomesodermin. *PLoS One* **9**, e90791 (2014).
160. S. J. Arnold *et al.*, The T-box transcription factor Eomes/Tbr2 regulates neurogenesis in the cortical subventricular zone. *Genes Dev* **22**, 2479-2484 (2008).
161. D. O'Carroll *et al.*, The polycomb-group gene Ezh2 is required for early mouse development. *Mol Cell Biol* **21**, 4330-4336 (2001).

162. X. P. Yang *et al.*, EZH2 is crucial for both differentiation of regulatory T cells and T effector cell expansion. *Sci Rep* **5**, 10643 (2015).
163. S. Stefanovic *et al.*, Interplay of Oct4 with Sox2 and Sox17: a molecular switch from stem cell pluripotency to specifying a cardiac fate. *J Cell Biol* **186**, 665-673 (2009).
164. H. Zhang *et al.*, Expression of podocalyxin separates the hematopoietic and vascular potentials of mouse embryonic stem cell-derived mesoderm. *Stem Cells* **32**, 191-203 (2014).
165. C. Y. Park *et al.*, skNAC, a Smyd1-interacting transcription factor, is involved in cardiac development and skeletal muscle growth and regeneration. *PNAS* **107**, (2010).
166. F. Sierro *et al.*, Disrupted cardiac development but normal hematopoiesis in mice deficient in the second CXCL12/SDF-1 receptor, CXCR7. *Proc Natl Acad Sci U S A* **104**, 14759-14764 (2007).
167. S. Yu, D. Crawford, T. Tsuchihashi, T. W. Behrens, D. Srivastava, The chemokine receptor CXCR7 functions to regulate cardiac valve remodeling. *Dev Dyn* **240**, 384-393 (2011).
168. S. Wanderling *et al.*, GRP94 Is Essential for Mesoderm Induction and Muscle Development Because It Regulates Insulin-like Growth Factor Secretion. *Molecular Biolofy of the Cell* **18**, 3764-3775 (2007).
169. J. Zhou *et al.*, Cadherin-11 expression patterns in heart valves associate with key functions during embryonic cushion formation, valve maturation and calcification. *Cells Tissues Organs* **198**, 300-310 (2013).
170. S. Seo, T. Kume, Forkhead transcription factors, Foxc1 and Foxc2, are required for the morphogenesis of the cardiac outflow tract. *Dev Biol* **296**, 421-436 (2006).
171. M. K. Stokke *et al.*, Ca(2+) wave probability is determined by the balance between SERCA2-dependent Ca(2+) reuptake and threshold SR Ca(2+) content. *Cardiovasc Res* **90**, 503-512 (2011).
172. K. Wakimoto *et al.*, Targeted disruption of Na+/Ca2+ exchanger gene leads to cardiomyocyte apoptosis and defects in heartbeat. *J Biol Chem* **275**, 36991-36998 (2000).
173. S. V. Koushik *et al.*, Targeted inactivation of the sodium-calcium exchanger (Ncx1) results in the lack of a heartbeat and abnormal myofibrillar organization. *The FASEB Journal*, (2001).
174. H. Reuter *et al.*, The Na+-Ca2+ Exchanger Is Essential for the Action of Cardiac Glycosides. *Circulation Research* **90**, 305-308 (2002).
175. C. Cho, S. Lee, H. Shin, K. D. Philipson, C. O. Lee, Partial rescue of the Na+*Ca2+ exchanger (NCX1) knock-out mouse by transgenic expression of NCX1. *Experimental and Molecular Medicine* **35**, 125-135 (2003).
176. B. Linck *et al.*, Functional comparison of the three isoforms of the Na+/Ca2+ exchanger (NCX1, NCX2, NCX3). *American Physiological Society*, (1998).
177. J. Lytton, Na+/Ca2+ exchangers: three mammalian gene families control Ca2+ transport. *Biochem J* **406**, 365-382 (2007).
178. B. D. Quednau, D. A. Nicoll, K. D. Philipson, Tissue specificity and alternative splicing of the Na+/Ca2+ exchanger isoforms NCX1, NCX2, and NCX3 in rat. *American Physiological Society*, (1997).
179. J. Bloomekatz, J. Grego-Bessa, I. Migeotte, K. V. Anderson, Pten regulates collective cell migration during specification of the anterior-posterior axis of the mouse embryo. *Dev Biol* **364**, 192-201 (2012).
180. S. E. Webb, A. L. Miller, Calcium signalling during embryonic development. *Nat Rev Mol Cell Biol* **4**, 539-551 (2003).
181. K. R. Hoyt, S. R. Arden, E. Aizenman, I. J. Reynolds, Reverse Na+/Ca2+ Exchange Contributes to Glutamate-Induced Intracellular Ca2+ Concentration Increases in Cultured Rat Forebrain Neuros. *Molecular Pharmacology* **53**, 742-749 (1997).
182. T. Iwamoto, Forefront of Na+/Ca2+ Exchanger Studies: Molecular Pharmacology of Na+/Ca2+ Exchange Inhibitors. *J Pharmacol Sci* **96**, 27-32 (2004).
183. A. M. Ebert *et al.*, Calcium extrusion is critical for cardiac morphogenesis and rhythm in embryonic zebrafish hearts. *Proc Natl Acad Sci U S A* **102**, 17705-17710 (2005).

184. C. Leclerc, I. Neant, M. Moreau, The calcium: an early signal that initiates the formation of the nervous system during embryogenesis. *Front Mol Neurosci* **5**, 3 (2012).
185. U. Technau, C. B. Scholz, Origin and evolution of endoderm and mesoderm. *Int. J. Dev. Biol* **47**, 531-539 (2003).
186. M. Q. Martindale, K. Pang, J. R. Finnerty, Investigating the origins of triploblasty: 'mesodermal' gene expression in a diploblastic animal, the sea anemone Nematostella vectensis (phylum, Cnidaria; class, Anthozoa). *Development* **131**, 2463-2474 (2004).
187. T. Hashimshony, M. Feder, M. Levin, B. K. Hall, I. Yanai, Spatiotemporal transcriptomics reveals the evolutionary history of the endoderm germ layer. *Nature* **519**, 219-222 (2015).
188. E. A. Ober, H. Verkade, H. A. Field, D. Y. Stainier, Mesodermal Wnt2b signalling positively regulates liver specification. *Nature* **442**, 688-691 (2006).
189. J. Lough, Y. Sugi, Endoderm and heart development. *Developmental Dynamics* **217**, 327-342 (2000).
190. J. F. Reiter *et al.*, Gata5 is required for the development of the heart and endoderm in zebrafish. *Genes & Development* **13**, 2983-2995 (1999).
191. J. Alexander, M. Rothenberg, G. L. Henry, D. Y. R. Stainier, casanova Plays an Early and Essential Role in Endoderm Formation in Zebrafish. *Developmental Biology* **215**, 343-357 (1999).
192. Y. Kikuchi *et al.*, The zebrafish bonnie and clyde gene encodes a Mix family homeodomain protein that regulates the generation of endodermal percursors. *Genes & Development* **14**, 1279-1289 (2000).
193. H. Fukui *et al.*, S1P-Yap1 signaling regulates endoderm formation required for cardiac precursor cell migration in zebrafish. *Dev Cell* **31**, 128-136 (2014).
194. M. Madabhushi, E. Lacy, Anterior visceral endoderm directs ventral morphogenesis and placement of head and heart via BMP2 expression. *Dev Cell* **21**, 907-919 (2011).
195. L. Zhang *et al.*, Mesodermal Nkx2.5 is necessary and sufficient for early second heart field development. *Dev Biol* **390**, 68-79 (2014).
196. Y. Nakaya, G. Sheng, EMT in developmental morphogenesis. *Cancer Lett* **341**, 9-15 (2013).
197. R. Levayer, T. Lecuit, Breaking down EMT. *Nat Cell Biol* **10**, (2008).
198. S. Lindsey, S. A. Langhans, Crosstalk of Oncogenic Signaling Pathways during Epithelial-Mesenchymal Transition. *Front Oncol* **4**, 358 (2014).
199. D. M. Gonzalez, D. Medici, Signaling mechanisms of the epithelial-mesenchymal transition. *Sci Signal* **7**, re8 (2014).
200. S. Lamouille, J. Xu, R. Derynck, Molecular mechanisms of epithelial-mesenchymal transition. *Nat Rev Mol Cell Biol* **15**, 178-196 (2014).
201. L. B. Corson, Y. Yamanaka, K. M. Lai, J. Rossant, Spatial and temporal patterns of ERK signaling during mouse embryogenesis. *Development* **130**, 4527-4537 (2003).
202. K. M. Hardy, T. A. Yatskievych, J. H. Konieczka, A. S. Bobbs, P. B. Antin, FGF signallin through RAS/MAPK and PI3K pathways regulates cell movement and gene expression in the chicken primitive streak without affect E-cadherin expression. *BMC Developmental Biology* **11**, (2011).
203. G. S. Kwon, A. K. Hadjantonakis, Transthyretin mouse transgenes direct RFP expression or Cre-mediated recombination throughout the visceral endoderm. *Genesis* **47**, 447-455 (2009).
204. C. S. Heffner *et al.*, Supporting conditional mouse mutagenesis with a comprehensive cre characterization resource. *Nat Commun* **3**, 1218 (2012).
205. K. L. Waldo *et al.*, Conotruncal myocardium arises from a secondary heart field. *Development* **128**, 3179-3188 (2001).
206. A. Francou, E. Saint-Michel, K. Mesbah, R. G. Kelly, TBX1 regulates epithelial polarity and dynamic basal filopodia in the second heart field. *Development* **141**, 4320-4331 (2014).
207. C. Mummery *et al.*, Differentiation of human embryonic stem cells to cardiomyocytes: role of coculture with visceral endoderm-like cells. *Circulation* **107**, 2733-2740 (2003).
208. H. K. Voges *et al.*, Development of a human cardiac organoid injury model reveals innate regenerative potential. *Development* **144**, 1118-1127 (2017).

Annex 1 - Secondary control for whole-mount immunostaings. Mouse embryo at the Linear Heart Tube stage stained with phalloidin (as positive internal control) and an alexa 555 secondary antibody

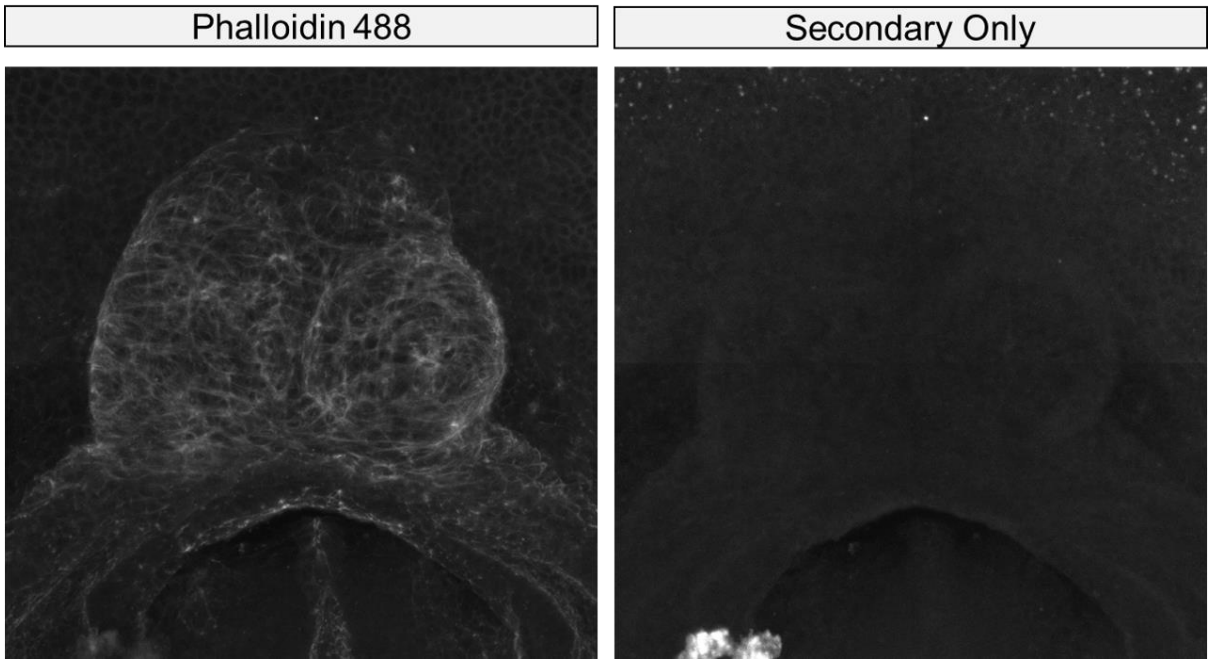

Annex 2 - Top 10 expressed genes from the scRNAseq clusters presented on chapter 4 (fig. 4.13)

	#1	#2	#3	#4	#5	#6	#7	#8	#9	#10
black	Hist1h1b	Hist1h4d	Basp1	Hist1h1e	Hist1h2ae	1700027J19Rik	Hist1h2ao	Ppp1r14b	Fam98b	Ube2m
blue	Igsf21	Nkx2-3	Trh	Kctd12b	Ppp1r16b	Dok5	Rab15	Foxa1	Gata3	Apela
cyan	Nuak2	Wnt8a	Rfx4	Nrcam	Pla2g7	Pax6	Stmn2	Hes3	Fgf15	Pim2
darkgrey	Acvrl1	Icam2	Esam	Grap	Nid1	Etv2	Elk3	Gata2	Fli1	Cd34
forestgreen	Kcnj5	Esrrg	Ppp1r3c	Dcaf12l1	Bmper	Cacna1d	Thbs4	Abtb2	Fbxo32	Sphkap
gold	Pgf	Mfap4	Col26a1	Tmem119	Fst	Eya1	Tbx1	Stra6	Foxc2	Nkd1
green	Wnt5a	Rgs4	Amph	Ap1s2	Nrp2	Sema3a	Mme	Sec24d	Prkaa2	Myocd
hotpink	Rab32	Edn1	Tmem144	Arhgap44	Art5	Tuft1	Fkbp14	Arl5c	9430038I01Rik	Fgf10
magenta	Fgf8	Ociad2	1700008O03Rik	Cfc1	Nkx2-5	Tpm2	Cdk2ap2	Hcfc1r1	Myl4	Mpped2
navy	Hkdc1	Hnf1b	Apom	Dkk1	Rbp4	Habp2	Fam20c	Cd55	Fgb	Dpp4
orange	Aldh1a2	Ptges	Scara3	Rdh10	Igfbpl1	Arg1	Aplnr	Prdm1	1700017B05Rik	Spon1
purple	Tnni3	Cited1	Tcap	Ramp1	Dcp1b	Myl1	Myl2	Hspb1	Crip1	Rrad
red	Pcdh18	Kitl	Hand1	Pcolce	Ccdc80	Lrrn4	Stard8	Nkd1	Hs6st2	Dlk1
salmon	Tspan32	Acp5	Ell2	Tspan33	Epor	Ikzf1	Slc16a10	Dmtn	Epb42	Alas2
turquoise	Slc40a1	Dlx5	Plcg2	Gjb3	Npnt	Tmem54	Lrp2	Grhl2	Kdf1	Zscan10
violet	Plppr5	Naa30	Abra	Tagln	Lhfpl1	Pus7l	Tdgf1	Wnt11	Mllt11	Mtus2
yellow	Six2	Col9a1	Sparcl1	Tgfbi	Lum	Olfml2a	Cyp26c1	Cped1	Rnf26	Smoc1

Annex 3 - Expression of Hhex-GFP+ embryo at Stage 0. Expression can be observed in several tissues, including the endocardium, the definitive and yolk sac endoderm.